Max-Planck-Institut für Polymerforschung
Max Planck Institute for Polymer Research

Advanced Polymer Nanocapsules with Enhanced Capabilities for Controlled-Release of Payloads

Dissertation
zur Erlangung des Grades
„Doktor der Naturwissenschaften“

am Fachbereich Chemie, Pharmazie und Geowissenschaften
der Johannes Gutenberg-Universität Mainz

Shahed Behzadi

geboren in Teheran, Iran

Mainz, Mai 2016

JOHANNES GUTENBERG
UNIVERSITÄT MAINZ

Dekan: Prof. Dr. Dirk Schneider

1. Berichterstatter: Prof. Dr. Katharina Landfester

2. Berichterstatter: Prof. Dr. Michael Maskos

Tag der Prüfung: 30.05.2016

Die als Dissertation vorgelegte Arbeit wurde in der Zeit von Mai 2013 bis Mai 2016 am Max-Planck-Institut für Polymerforschung in Mainz im Arbeitskreis von Prof. Dr. Katharina Landfester angefertigt.

Table of Contents

1. Introduction 1
2. Theoretical background 5
   2.1. Colloidal systems 5
      2.1.1. Van der Waals interactions 6
      2.1.2. Born repulsion 7
      2.1.3. Electrostatic forces 7
      2.1.4. Steric repulsion 8
      2.1.5. The total interaction potential curve 8
   2.2. Emulsions 10
      2.2.1. Definitions and classifications of emulsions 10
      2.2.2. Stability of emulsions 10
   2.3. Formation of capsules 12
      2.3.1. Phase separation induced by solvent evaporation 14
      2.3.2. Phase separation induced by polymerization 15
      2.3.3. Phase separation induced by interfacial polymerization 16
   2.4. Permeability mechanism 17
   2.5. Release from polymer capsules 18
      2.5.1. Diffusion model 20
   2.6. Factors influencing permeation 21
      2.6.1. Physicochemical properties of the polymer 21
      2.6.2. Physicochemical properties of the payload 22
3. Characterization methods 23
   3.1. Dynamic light scattering (DLS) 23
   3.2. Electron microscopy methods 24
      3.2.1. Scanning electron microscopy (SEM) 24

3.2.2. Transmission electron microscopy (TEM) 24
3.3. Ultraviolet-visible spectroscopy (UV-vis) 25
4. Results and Discussion 27
4.1. Osmotic pressure-dependent release profiles of payloads from nanocontainers by co-encapsulation of simple salts 27
4.1.1. Motivation 28
4.1.2. Preparation of polyurea nanocapsules 30
4.1.3. Release of the payloads 32
4.1.4. Responsible mechanism 35
4.1.5. Application for biomedicine and anticorrosion 40
4.1.6. Conclusions and Outlook 43
4.2. Controlled-release of hydrophilic payloads from reduction-responsive nanocapsules 45
4.2.1. Motivation 46
4.2.2. Preparation of polyurea nanocapsules 47
4.2.3. Characterization of polyurea shells 50
4.2.4. Reduction-responsive release of the payloads from the nanocapsules 53
4.2.5. Conclusions and Outlook 55
4.3. Triblock copolymers vs blends of diblock copolymers for nanocapsules addressed by three independent stimuli 56
4.3.1. Motivation 57
4.3.2. Preparation and characterization triblock terpolymers nanocapsules 59
4.3.3. Stimuli-responsive release of payload from triblock copolymers nanocapsules 61
4.3.4. Stimuli-responsive release of the payload from nanocapsules consisting of blends of diblock copolymers 65
4.3.5. Conclusions and outlook 73
4.4. The pro-active payload strategy significantly increases selective release from mesoporous nanocapsules 74
4.4.1. Motivation 75

4.4.2. Preparation of silica nanocapsules 77
4.4.3. Release of the payload and the pro-active payload 82
4.4.4. Conclusions and outlook 85
5. Experimental part 87
5.1. Experimental details for section 4.1 87
5.1.1. Materials 87
5.1.2. Characterization Methods 87
5.1.3. Preparation of the nanocapsules 88
5.1.4. Release Experiments 89
5.2. Experimental details for section 4.2 91
5.2.1. Materials 91
5.2.2. Characterization methods 91
5.2.3. Deprotonation of cystamine dihydrochloride 92
5.2.4. Preparation of the nanocapsules 93
5.2.5. Release experiments 94
5.2.6. Cystamine extraction 95
5.2.7. Quantification of disulfide-bond cleavage 95
5.3. Experimental details for section 4.3 96
5.3.1. Materials 96
5.3.2. Characterization methods 96
5.3.3. Exemplary Synthesis of PVFc-*b*-PMMA-*b*-PDMAEMA 98
5.3.4. Preparation of the nanocapsules 99
5.3.5. Release experiments 99
5.4. Experimental details for section 4.4 100
5.4.1. Materials 100
5.4.2. Characterization methods 100
5.4.3. Preparation of silica nanocapsules 100
5.4.4. Release experiments 101

5.4.5. Condensation of PEG dithiol with MBT 102
5.4.6. Cleavage of MBT molecules from PEG-MBT 102
6. Summary and Outlook 103
7. Zusammenfassung und Ausblick 107
References 110
Abbreviation and Characters 121
Acknowledgements 124
Appendix 125
Curriculum Vitae 127

1. Introduction

The past century has witnessed a tremendous progress of colloid science and the practical applications of colloid science display no signs of waning.[1, 2] Colloids form the basis of a variety of consumer goods, industrial, and high technology products. For instance, milk, toothpaste, and many paints are colloidal systems. Colloid science is the study of dispersions of one phase in another phase (*e.g.* oil in water of water in oil). The dispersed phase in colloidal systems can have dimension in the range few nanometers to a few tens of micrometers.[1-4]

The intersection of colloid science with nanoscience and polymer science has given rise to numerous ideas for manifold applications. On the one hand, nanomaterials present unique size- and material-dependent properties which make them interesting for applications such as drug delivery and anticorrosion.[5, 6] On the other hand, polymers can carry different functional groups which can fulfill a function on the molecular level. For instance, block copolymers, whose functional groups can be heterogeneously distributed along the polymer chain, yield fascinating functional structures in bulk or selective solvents.[7, 8] Additionally, unlike materials such as ceramics, metals, and glasses, polymers are permeable,[9, 10] a property which can be used to create systems where transport of molecules can take place between two environments separated by a polymer membrane. In colloid science, one of the most successful systems is the construction of core-shell compartments in the form of micro- to nano-scale capsules with a liquid core surrounded by a polymer shell.[11-14] Various guest substances (payloads) can be loaded and stored in capsules and thereby be protected against non-controlled interactions with the environment before controlled release is initiated.

Regardless of the application, controlled release of payloads is the dominating function of capsules. The term ‘‘controlled release’’ includes a range of different release profiles and mechanisms such as targeted release, triggered release, and sustained (or extended) release. To achieve efficient controlled release systems the two main points should be taken into account:

(i) The necessity to ensure that the non-controlled leakage of the payload does not occur in release medium.

(ii) The necessity to ensure that the shell materials adequately facilitate release of the payload in response to an external stimulus “just in time”.

The miniemulsion technique is known to be a versatile tool to prepare a wide range of polymer nanocapsules with either an oily or an aqueous core.[15, 16] The miniemulsion technique also offers the possibility to use a wide range of monomers/polymers and chemical reactions for the preparation of the polymer shell. Moreover, the miniemulsion process was already found to be useful for the encapsulation of diverse molecules in nanocapsules.[17-20] The objective of this thesis is to prepare polymer nanocapsules by the miniemulsion technique with improved capabilities for controlled-release of payloads. These nanocapsules consisting of stimuli-responsive units possess a remarkable release property only under the application of external triggers while preventing non-controlled leakage of the payload in release medium.

In this thesis, it will be shown that different release profiles can be programmed *via* the control of the osmotic pressure for various applications such as biomedicine or corrosion protection. The initial high release rate can be turned to an advantage for the acceleration of payloads release or one can take advantage of diminishing the burst release by changing the physicochemical properties of nanocapsule membranes for decreasing the rate of release. For example, the non-controlled leakage of hydrophilic payloads from nanocapsules can be efficiently hindered by increasing the shell thickness. The trigger release of payloads from nanocapsules in a very controlled fashion under certain environmental conditions can be then achieved by introducing stimulus-responsive groups into the shell. However, practical applications occur usually in complex environments. In some cases, capsules responsive to multiple stimuli are necessary for the triggered release of payloads. Therefore, novel triple stimuli-responsive nanocapsules that selectively respond to changes in temperature, pH value, and redox potential are prepared. To fulfil this goal, the triple responsive triblock terpolymer is

synthesized by sequential anionic polymerization. Finally, an efficient and straightforward strategy based on the encapsulation of a so called pro-active payload is established to hinder the non-controlled release of small payloads from mesoporous nanocapsules. A pro-active payload is defined as a compound that is converted to an active functional molecule in the environment where it is needed. The pro-active payload strategy can be combined with the use of stimulus-responsive materials to achieve selective release of cargo from mesoporous nanocapsules.

This thesis consists of five chapters, whose function and content will be briefly outlined here. The first chapter presents the general motivation for the whole thesis. Chapter 2 explains the fundamental of colloidal materials, especially polymer capsules. In addition, the basic foundations of release of a payload from a liquid core reservoir are laid out in this chapter. In Chapter 3, the different characterization methods primarily used in this thesis are theoretically described. Chapter 4 is divided into four sections exhibiting, discussing, and critically examining the results obtained in this thesis. In this chapter, each section corresponds to the topics described in the last paragraph and possesses an abstract following with a short introduction and motivation. The results are thoroughly explained and discussed. Finally, conclusions are made and an outlook is given. The experimental details for the experiments in chapter 4 can be found in chapter 5.

2. Theoretical background

2.1. Colloidal systems

Common in everyday life, colloids are the basis of a variety of consumer, industrial and high technological products from milk to sprays. Colloidal systems are heterophase mixtures that are composed of a dispersed phase (or discontinuous phase) distributed uniformly in a finely divided state in a dispersion medium (or continuous phase). The colloidal size range of the dispersed phase in the continuous phase is defined as extending over a range from a few nanometers to micrometers. The physical state of the dispersed and the continuous phase leads to one kind of classification of colloidal systems. Some of the most important types of colloidal systems are summarized in Table 2.1.

Table 2.1. Some typical colloidal systems.[1, 21]

Class	Continuous Phase	Dispersed Phase	Example
Sols or Colloidal suspensions	liquid	solid	Metallic hydroxide, paints
Emulsion	liquid	liquid	Milk
Foam	liquid	gas	Froths
Solid suspension or dispersion	solid	solid	Opal, Pigmented plastics
Solid Foam	solid	gas	Meerschaum
Gel	solid	liquid	Jellies
Solid Aerosol	gas	solid	Industrial smokes
Liquid Aerosol	gas	liquid	mist

Stability is one of the crucial aspects to be evaluated for their application, in terms of free energy of a colloidal dispersion. To understand the stability of colloidal particles, one must begin by discussing the origin and nature of intermolecular forces. Therefore, the individual forces will be shortly introduced, and then complete interaction potentials will be presented.

2.1.1. Van der Waals interactions

At short distances, molecules attract each other. The attractive forces arises from the interaction between fluctuating dipoles, induced by the motions of the outer electrons on the two molecules.[21] The free energy of attraction between a pair of atoms or molecules is proportional to the inverse sixth power of the separation distance (*d*):

$$\Delta G^{att} = -C_{AB}/d^6 \qquad (2.1)$$

The constant C_{AB} is related to the nature of the individual molecules, most importantly, the polarisability and dipole moment of the atoms or molecules.

In order to calculate the potential energy of interaction between two spherical particles of radius R_i, first it is assumed that every molecule in particle A interacts with each molecule of B. The total free energy of interaction is obtained by the sum of the contributions from all possible pairs of molecules, when the spheres are close ($d/R_i \ll 1$):[21]

$$\Delta G^{att} = -\frac{A_H}{6d}.\frac{R_1 R_2}{(R_1+R_2)} = -\frac{A_H R}{12d} \qquad (2.2)$$

where A_H is called the Hamaker constant. Its value is closely related to C_{AB}.

An important point can be understood via the comparison between both formulae. The energy of attraction between particles decreases much slower than that between single molecules. Therefore, one can expect a longer range of interaction between colloidal particles.

Because of attractive interaction between particles arising from van der Waals forces, colloids tend to aggregate. On the other hand, repulsive forces between particles prevent aggregation. These forces will be briefly presented below.

2.1.2. Born repulsion

At close distances, the electrons which are in non-bonding orbitals begin to interact and consequently, they repel each other. This repulsive force becomes infinite when the electron clouds of two atoms or molecules interpenetrate. The repulsive potential, that called the Born repulsion, at distance d is represented by:[2]

$$\Delta G^{rep} = B/d^{12} \qquad (2.3)$$

2.1.3. Electrostatic forces

Particles in the most colloidal dispersions in aqueous media carry an electric charge. The electric charge can arise from a variety of mechanisms like ionization of acidic or basic groups on the surface, different dissolution of ions from the surface of soluble crystal, or specific ion adsorption by adding a surfactant.

The concept of an electrical double layer, which was first introduced by Helmholtz, has been used to describe electrical potential in colloids.[22] Briefly, the Helmholtz model explains that the charge on a particle is distributed over its surface and is just balanced by the total charge in the double layer in which there is an excess of opposite charged ions. Mathematically, the electrical potential "ψ" in the solution dependent on the distance d is:

$$\psi = \psi_0 \exp(-\kappa d)\,, \kappa = \sqrt{\frac{2c_0 e^2}{\varepsilon \varepsilon_0 k_B T}} \qquad (2.4)$$

In this formula, κ includes all constants (c_0 as the ion concentration; $\varepsilon, \varepsilon_0$ the dielectric constants of bulk electrolyte solution under vacuum, respectively; and k_B the Boltzmann constant). At distance $(1/\kappa)$ the potential falls by a factor of $(1/e)$, this distance, which is loosely the thickness of double layer, is also called the Debye length (λ_D).

2.1.4. Steric repulsion

Polymers are present in many colloidal suspensions of particles. One effect of polymers is to provide colloidal stability by steric stabilization mechanism. Briefly, it involves an overlay of adsorbed or chemically attached polymer chains on the surface of the particles and the presence of the polymer layer gives rise to repulsion effect between particles. A simple analytical expression for the steric interaction energy between two polymer-coated particles of radius r is given by:[3]

$$\Delta G_{steric}^{rep} = 4\pi r K_B T \Gamma^2 N_A \frac{\vartheta_2^2}{V_1} (\frac{1}{2} - \chi)(1 - \frac{D}{2L_0})^2 \qquad (2.5)$$

When two particles approach each other, the polymer layer will touch as soon as the particle surface distance D become less than twice the layer thickness (L_0). At separation with $D \approx L_0$, the steric repulsion sharply rises and provides an effective stability. In this expression, the partial specific volume of the polymer chain and the molar volume of the solvent molecules are presented by ϑ_2 and V_1, respectively. The square of the surface coverage Γ also emphasizes the importance of high surface coverage for effective steric stabilization. For repulsive interactions a good solvent condition is needed, *i.e*. with the Flory-Huggins parameter$\chi < 0.5$. Finally, strong adsorptions and low free polymer concentration are also required to ensure strong repulsion.

2.1.5. The total interaction potential curve

The total free-energy difference between two particles can be obtained by adding the contributions mentioned above:

$$\Delta G = \Delta G^{att}\ (van\ der\ Waals) + \Delta G^{rep} (Born\ repultion)$$

$$+ \Delta G^{rep}\ (electrostatic) + \Delta G^{rep} (steric) \qquad (2.6)$$

To avoid complexity, instead of considering all these contributions at the same time, two simpler situations in which the long-range repulsive potential caused either by electrostatic or steric interaction are being explored. The combination of the Born repulsion, electrostatic interactions, and van der Waals interactions became known as DLVO (Derjaguin and Landau, Verwey and Overbeek) theory.[23, 24]

As Figure 2.1a shows, the Born repulsion prevents the particles from overlapping at short distances. In the DLVO curve, the primary minimum (*i.e.* I), which is caused by van der Waals attractions at close distances, is referred to as coagulation. If the particles reach this minimum, they are irreversibly agglomerated. The electrostatic repulsion also induces a primary maximum at larger distances (II). The height of the energy barrier determines the stability of the dispersion. Finally, the second minimum, which is referred as flocculation, is usually reversible aggregation. Figure 2.1b shows that with an increase in electrolyte concentration, the energy barrier of the system decrease. In fact, the electrolyte increasingly screens the charges of the particles, and the colloid consequently becomes unstable with lower energy barrier.

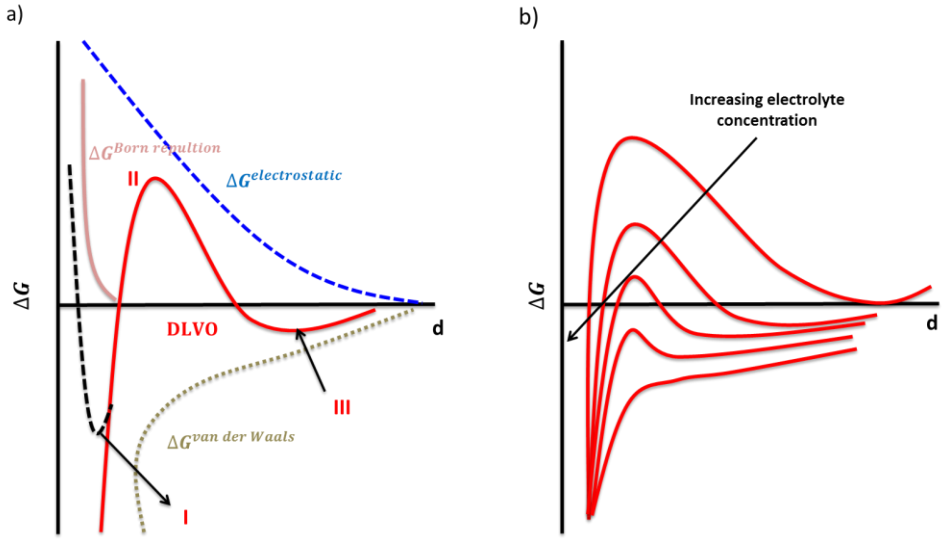

Figure 2.1. DLVO theory: (a) interaction potential of two particles with different distance according to DLVO theory. (b) Effect of electrolyte addition. The scheme is adapted from Napper.[25]

2.2. Emulsions

2.2.1. Definitions and classifications of emulsions

An emulsion is a dispersion and it consists of droplets of one liquid A (dispersed phase) in a liquid B (continuous phase), where the two liquids are immiscible.[1, 4] An emulsion can be classified according to its type or thermodynamic stability. According to its type, an emulsion is known as either oil-in-water (OW) or water-in-oil (WO). OW and WO are also called direct and inverse emulsion, respectively. Depending on the thermodynamic stability, emulsion systems can be microemulsion, macroemulsion, and miniemulsion. Microemulsions are thermodynamically stable systems and are formed by simple mixing without requiring high shear forces. The size of the droplets of the dispersed phase in microemulsions is smaller than 100 nm, usually 10 to 50 nm. Unlike microemulsions, macroemulsions are kinetically stable. Because of being kinetically stable, work has to be done (*e.g.* stirring or shaking) on the two liquids to form the emulsion. The size of dispersed droplets for macroemulsions is bigger than 1 µm.[1, 4]

Miniemulsions are kinetically stable systems, in which dispersed droplets ranging in size between 50 and 500 nm are formed by a high shear force applied to a system containing a mixture of two immiscible liquids with a certain amount of surfactant.[26, 27]

2.2.2. Stability of emulsions

To prepare a stable miniemulsion, dispersed droplets must be stabilized against molecular diffusion degradation (*i.e*. Ostwald ripening) and against coalescence by collisions, which will be introduced briefly below.

The process of collision and subsequent merge of two droplets is named coalescence.[1, 28] When two liquid droplets approach each other to a certain distance, the layer of the continuous phase liquid between them starts flattening until the formation of a parallel-sided film, and finally the burst of this thin film allows the material from the two droplets to combine and to form a larger

droplets with lower surface area (Figure 2.2 a). Coalescence process can be prevented by adding an appropriate surfactant that stabilizes droplets either electrostatically or sterically from each other.[15, 28]

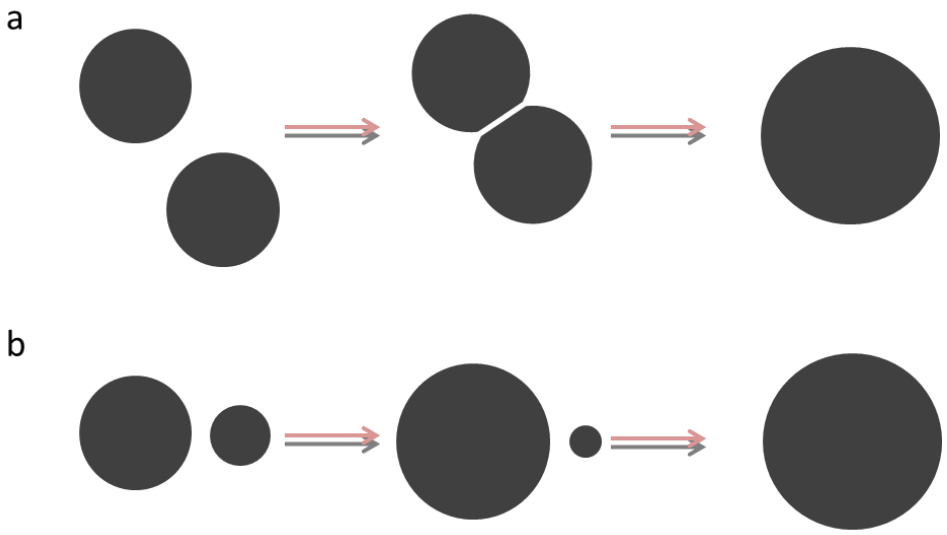

Figure 2.2. Schematic illustration of (a) Oswald ripening and (b) coalescence in miniemulsion system.

Ostwald ripening is another process of droplet destabilization in emulsion systems. The Laplace equation calculates the pressure difference (Δp) of a curved liquid/liquid interface via the ratio of the surface tension γ and radius of curvature r, as given below:

$$\Delta p = \frac{2\gamma}{r} \qquad (2.7)$$

According to the equation, smaller droplets have larger (Δp) than larger ones. The Laplace pressure difference between droplets of different sizes causes that material diffuses from smaller droplets to larger ones in order to reduce the total energy of the system (Figure 2.2 b). Ostwald ripening can be suppressed by a decrease in the size distribution of the droplets. Another method that is widely used is to add a component (2) (e.g. a hydrophobic agent in the case of an OW emulsion) in the dispersed droplets, which is insoluble in the continuous phase.

Thus, the chemical potential difference that arises from component 2 between the smaller and the larger droplets will be opposite in sign to the chemical potential difference associated with droplets of different sizes.

2.3. Formation of capsules

A simple theory for predicting the equilibrium configurations from a system including two immiscible liquid droplets (liquid-1 and liquid-3) brought into intimate contact when suspended in a third immiscible liquid has first been described by Torza and Mason.[29] The morphology of the system could be predicted by using the spreading coefficient S_i which depends on the interfacial tension of the oil and water phases. The spreading coefficient $S_i$is represented by the equation below:

$$S_i = \gamma_{jk} - (\gamma_{ij} + \gamma_{ik}) \qquad (2.8)$$

Where γ is the interfacial tension between component i, j, and k. The spreading coefficient can be calculated after measuring the different surface tensions. With the assumption that liquid 3 is significantly more hydrophilic than liquid 1, *i.e.*, $\gamma_{12} > \gamma_{23}$ it follows from the equation that $S_1 < 0$. Therefore, there are only three possible configurations. (Figure 2.3):

I. Complete engulfing (*i.e*. core-shell) when $S_2 < 0$ and $S_3 > 0$;
II. Partial engulfing when $S_2 < 0$ and $S_3 < 0$;
III. Non-engulfing when $S_2 > 0$ and $S_3 < 0$;

Although the aforementioned method was first proposed for systems in which materials are immiscible liquids, it can be also applied to systems consisting of low molecular weight polymers that can readily diffuse. [30] In the case of systems composed of polymers with high molecular weight, the system cannot always obtain the equilibrium morphologies. The main reason for that is a hindered phase separation of the materials of these systems. Hindered phase separation occurs when polymer chains undergo limitation in mobility because of their

great size, *i.e.*, restricted diffusion.[30, 31] In these cases, kinetic morphologies are formed once the free Gibbs energy G cannot be minimized because of a hindered phase separation. Therefore, the variation of free energy is considered as the driving force for the final configuration, which can be calculated by:

$$G = \sum_{i,j}^{n} \gamma_{ij} A_{ij} \qquad (2.9)$$

Where γ_{ij} is the surface tension of the phases i and j, while A_{ij} is the area of the interface. The configuration with minimal free energy changes is the thermodynamically final morphology.

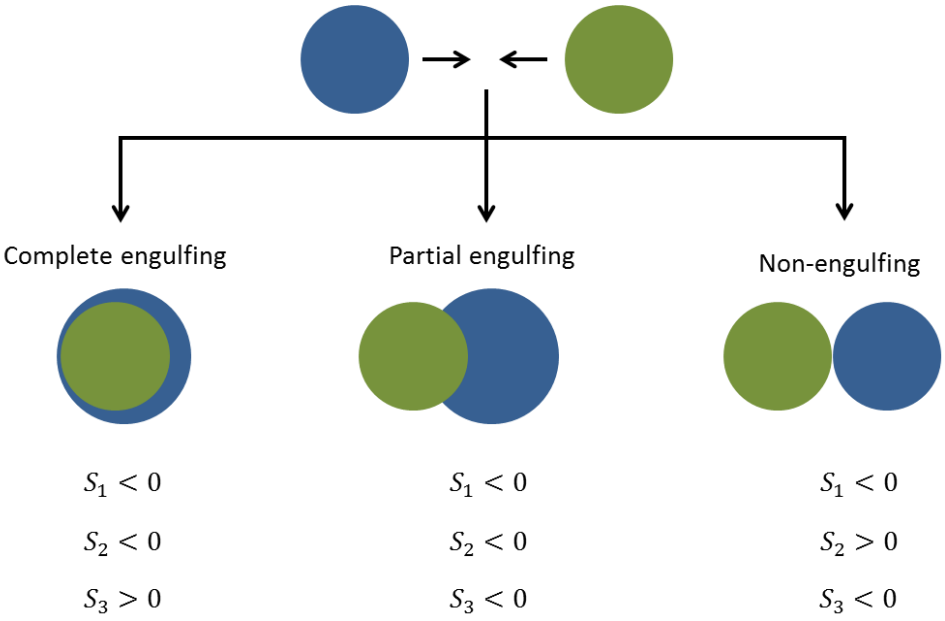

Figure 2.3. The spreading coefficients determine the final particle morphology. This scheme is adapted from Torza and Mason.[29]

In addition to the aforementioned parameters, the final morphology of a multiphase system depends on other factors such as the nature and amount of the polymers,[32, 33] the type and the amount of surfactant, [30, 34] the temperature of preparation process and its rate,[35, 36] reaction kinetics,[37] and etc.

In this dissertation, three techniques have been used for preparation of nanocapsule, namely polymerization-induced phase separation, interfacial polymerization, and solvent evaporation-induced phase separation. They are described in the following section.

2.3.1. Phase separation induced by solvent evaporation

The miniemulsion solvent evaporation technique is a facile method to form capsules based on the phase separation between a pre-synthesized polymer and a non-solvent for the polymer. [38, 39] Briefly, the pre-synthesized polymer and a non-solvent for the polymer are well mixed in a good solvent usually with a low boiling point. This mixture – which becomes the dispersed phase - is then mixed with another immiscible liquid (*e.g.* water) containing a surfactant (continuous phase). The whole system is then treated with ultrasonication to form small miniemulsion droplets. After slow evaporation of the good solvent, phase separation between the pre-synthesized polymer and the non-solvent takes place. If the interface polymer/continuous phase shows a lower interfacial tension then the "oil"/continuous phase interface,, the phase separation results in polymer chains moving to the interface of the droplets and solidifying to form a shell encompassing the non-solvent. *i.e*., the nanocapsules form. Figure 2.4 displays the preparation process of capsules using the solvent evaporation method in direct miniemulsion.

This method is especially interesting to fabricate capsules with various types of a polymer shell for encapsulating functional compounds for applications in biomedicine,[40] anticorrosion,[41] or optics (photon upconversion)[42] in the liquid core by simply dissolving them in the dispersed phase.

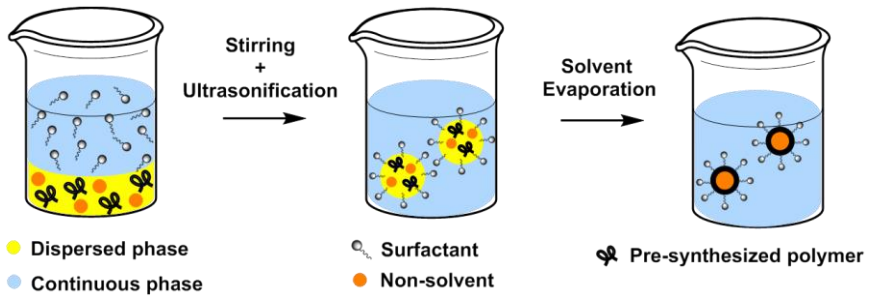

Figure 2.4. Schematic illustration of capsules formed via solvent evaporation in direct miniemulsion.

2.3.2. Phase separation induced by polymerization

The idea of miniemulsion polymerization is to initiate the polymerization in each of the small stabilized droplets of miniemulsion. In this method, capsules are formed because of the phase separation between solvent and the formed polymer.[43] Figure 2.5 shows the preparation process of capsules using the miniemulsion polymerization. The dispersed phase consists of monomer and initiator dissolved in hydrophobic oil whereas the continuous phase composed of a mixture of hydrophilic liquid and surfactant. When polymerization begins inside the miniemulsion droplets, the formed polymer becomes immiscible in the hydrophobic oil. Capsular morphology can form if the polymer chains are able to participate at the interface of the droplets, this requires the precise interfacial tension of polymer/oil, polymer/water and oil/water.

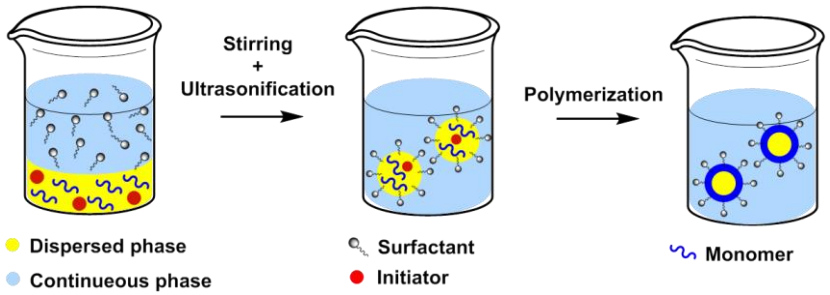

Figure 2.5. Schematic illustration of capsules formed via miniemulsion polymerization in direct systems.

There are numerous choices of monomers to generate polymer capsules by a variety of polymerization types ranging from radical[44] and anionic[45] polymerization to polyaddition[46] or polycondensation[47] methods. Capsules can be formed through tuning surface tensions of the participating interfaces in the system. For instance, by using more hydrophobic styrene, the copolymerization with hydrophilic monomers such as acrylic acid,[44] methacrylic acid,[48] or *N*-isopropylacrylamide (NIPAAm)[49] can lead to the formation of capsules.

2.3.3. Phase separation induced by interfacial polymerization

Another efficient approach to form polymer capsules is interfacial polymerization. This technique can be employed if the hydrophilic monomer is dissolved in the aqueous phase and the hydrophobic monomer is present in the organic phase, and these monomers meet and react at the interface of miniemulsion droplets (Figure 2.6). Different types of polymerization including interfacial radical copolymerization,[50, 51] anionic polymerization,[52] and interfacial polyaddition reactions[53, 54] are mostly applied to synthesize polymer capsules.

Good examples of polymer capsules prepared through interfacial polymerization are polyurea, polythiourea, and polyurethane capsules with an aqueous core prepared by polyaddition reactions in an inverse miniemulsion system. The control over the size of the capsules and the thickness of the shell can be achieved by altering the concentration of surfactant, the nature of monomers and their amounts.[16, 53-55]

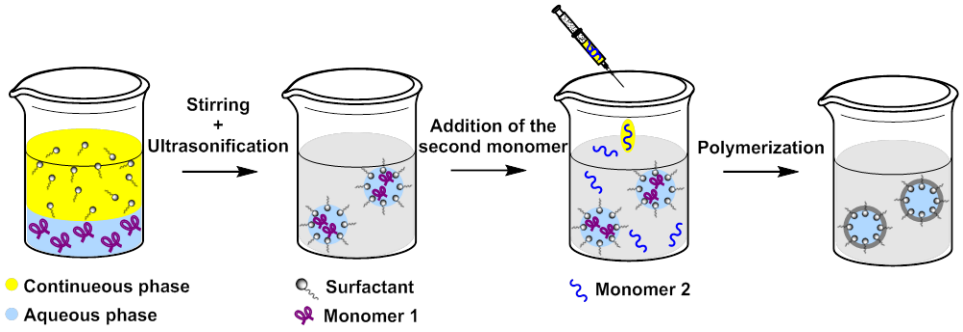

Figure 2.6. Schematic illustration of capsules formed via interfacial polymerization in miniemulsion.

2.4. Permeability mechanism

Permeation is a mass transport process where molecules (*i.e*. penetrants) diffuse through the polymer from either an 'exterior' environment to an 'interior' or vice versa. Mass transport through a polymer membrane can be simply explained by a three step process:

- Absorption of the penetrant at the membrane surface followed by dissolution of the penetrant in the polymer bulk.
- Diffusion of the penetrant through the membrane; where the concentration gradient between the 'interior' and 'exterior' environment is the driving force.
- Desorption from the surface of the polymer.

The permeability of a penetrant through a polymer membrane depends on two parameters: solubility and mobility (*i.e*. diffusion).[56] Both parameters are considered as thermodynamic processes. Individual molecules may adsorb, desorb, and diffuse in any direction, but the equilibrium condition is determined by thermodynamic energy consideration and consequently mass transport is driven by differences from the equilibrium in penetrant concentration. Mass transport of small molecules occur in polymers through the intrinsic porosity of the polymer bulk arising from the random nature of the polymer networks formed and the vibration of the molecular chains leading to sites into which small molecules can adsorb. Polymers can be manufactured deliberately as porous materials (*e.g.* foams or membranes) but even nominally solid, homogeneous polymers are likely to be porous to some degree owing to defects, inclusions and different phases, which leave pores, voids, and cracks capable of providing place for molecules.

The free volume concept has been extensively used to explain diffusion phenomena in macromolecules. The free volume is the volume of the polymer mass not actually occupied by the molecules.[57-59] Molecules will absorb more readily and will be more mobile in polymer matrixes with high free volumes than in polymers with low free volumes. The free volume

depends on the nature of the polymer and also on the physical state of the polymer, including molecular orientation and physical ageing effects.

2.5. Release from polymer capsules

The release of an active from a liquid core reservoir; for example capsule, is controlled by its permeation through the reservoir barrier (the shell) (*i.e*. release by membrane-moderated diffusion). The chemical nature of the shell dominates the permeation and consequently the release rate for reservoirs. Thus, it is necessary to differentiate between organic and inorganic reservoirs. This chapter does not describe permeation of inorganic matrix that was already reviewed by others.[60, 61] In the case of organic reservoirs (*i.e*. polymer capsules), the payload are diffusing through the free volume of the polymer membrane. The free volume theory implies that the release from a polymer membrane is related to both the kinetic energy and the likelihood of finding enough free volume for the diffusive agent.[57, 62] In the case of diffusion in a porous membrane with a random distribution of pores, the diffusion coefficient is proportional to the square of the free volume.[62]

Fick's first law is the fundamental law of diffusion. It explains that the flux is proportional to the concentration gradient ($\partial C/\partial X$):

$$F = -D\ (\partial C/\partial X) \qquad (2.10)$$

Flux is the rate of substance transferring across unit area in unit time.[10, 63] The first law can only be applied to diffusion in the steady state conditions, where the concentration does vary with time. It has been demonstrated that Fick's law predicts release rates of reservoir systems and will be zero order (*i.e*. constant) if the concentration is maintained constant with in the enclosure.[64, 65] The permeation characteristics of a reservoir system include more complicated variables. The relationship between these parameters and the release rate (*i.e*. flux) by assuming release under steady state condition can be expressed by corrected Fick's first law:

$$F = -DK(\partial C/\partial X) \qquad (2.11)$$

Where K (the partition coefficient) is the ratio of concentrations of the active in the core and the shell materials at equilibrium. The partition coefficient is a thermodynamic parameter describing the active-core-shell materials system which can be function of pressure, concentration, and temperature.[66] The magnitude of diffusion coefficient is dependent on the probability of a successful jump through a potential barrier separating on side from the next.[63] In the case of a non-ideal diffusion condition (*e.g.* reservoir systems), the probability can be largely reduced by the number of preventing parameters. The preventing parameters are described by porosity ε (the cross-sectional area available for diffusion), the tortuosity τ (the diffusive trajectory relative to the end-to-end), the active-to-pore size ratio λ $(= r_{active}/r_{pore})$, as well as interaction between the shell material and the active K_B.The relationship between the resulting diffusion coefficient D, called an apparent or effective diffusion coefficient,[67] and the free diffusion D_0 can be expressed as:

$$D = D_0 \frac{\varepsilon}{\tau} (1-\lambda)^2 K_B \qquad (2.12)$$

To clarify K_B, it is important to note a fraction of the active on the shell material can be immobilized by strong and specific interactions, such as coordinate interactions[64, 68] or hydrogen bonds,[68, 69] are described by K_B^{eq}. A shell material with a concentration of c_B binding sites will result in an immobilized fraction of actives and only the ''free'' fraction K_B is available for diffusion according to equations (2.12) and (2.13):[68]

$$K_B = (1 + K_B^{eq} c_B) \qquad (2.13)$$

As described above, the permeability constant P is defined as the product of the effective diffusion coefficient and the partition coefficient. It is well to note that sustained release, for a given reservoir system, can be controlled by modulating the diffusion coefficient (kinetic approach) and/or the partition coefficient (thermodynamic approach).

2.5.1. Diffusion model

The release kinetics has a time-dependent nature. On one hand, the core and the shell materials might undergo erosion or swelling, where the molecular mechanism during the time of release is not the transport of the payload. On the other hand, the concentration of the payload inside the reservoir varies during the time of release; in other words, diffusion does not follow a steady state condition.

A good starting point to find a simplistic approach for a release model is to refer the situation as Fickian diffusion. The total amount of diffusing substance entering or leaving the reservoir (M_t) is given by equation (2.14) derived by Crank.[63] The equation is valid when the materials constituting the core and the shell are stable against time, the reservoir is initially at a uniform concentration of an active (M_∞), and the surface concentration is maintained constant during release. Crank also considered a more realistic condition where the concentration variation of the active as well as its partition coefficient between the reservoir and the release media is taken into account. [63] The Fick's diffusion equation has been also solved for situations where the initial distribution of the active in the reservoir and the size of capsules are various:[70, 71]

$$\frac{M_t}{M_\infty} = 1 - \frac{6}{\pi^2}\sum_{n=1}^{\infty}\frac{1}{n^2}\exp(-Dn^2\pi^2 t/a^2) \qquad (2.14)$$

In the case where local variations in the release environment, *e.g.* sharp charge changes, interface transport or swelling, cannot be disregarded, one approach is to model such a behavior using a Langevin equation (eqn (2.15))[72] or the Fokker-Planck equation (eqn (2.16)),[73] where local variation are described as force acting on the active:[74]

$$\frac{\partial}{\partial t}X(r,t) = \frac{1}{\gamma}\nabla V(r) + \sqrt{2D}\Gamma(t) \qquad (2.15)$$

In the Langevin equation, the position of a particle at time t is defined as function of random forces $\Gamma(t)$. The term $\nabla V(x)$ also presents an additional force due to an external potential. If

the mean free path of the particle is low in comparison with the variation of the potential, it is possible to derive the Fokker–Planck equation (eqn (7)), where P presents the probability distribution:[72-74]

$$\frac{\partial}{\partial t}P(r,t) = \frac{1}{\gamma}\nabla[\nabla V(r)P] + D\nabla^2 P \qquad (2.16)$$

2.6. Factors influencing permeation

2.6.1. Physicochemical properties of the polymer

The chemical composition of the polymer membrane has a significant effect on diffusion properties of small molecules in the polymer membrane. Polymers with polar chemical groups have a stronger affinity for polar molecules, like water. In contrast, the affinity of polar molecules is much lower in non-polar molecules, for example polystyrene. In polar membranes, the diffusion coefficients of polar organic molecules increases with the absorbed concentration of molecules since there are strong interactions between the polymer chains and the molecules.[75, 76]Free volume is another intrinsic property of polymers. It can be considered as extremely small-size porosity arising from the gaps left between entangled polymer chains.[58] The absorption and diffusion of molecules in polymer membrane largely depend on the available free volume within the polymer. Free volume is proportional with the density and the physical state of the polymer. Amorphous regions in polymers are less ordered than crystalline ones and therefore the free volume is higher in these regions. Amorphous regions are more permeable and subsequently the sorption of molecules is higher than in crystalline regions of capsules membrane.[77-79] Different degree of crystallinity for capsules shell prepared from a specific type of polymer could be achieved by annealing the synthesized capsules in the appropriate medium,[78] by varying the molecular weight of the polymer used as shell-forming materials,[79] and by using cross-linkers.[80, 81]

2.6.2. Physicochemical properties of the payload

Beside the degree of the affinity between encapsulated molecules and polymer membranes- which was already discussed above- the molecule size of payloads plays an important role in the release of the molecules from capsules. Small molecules have higher diffusion coefficients than larger molecules. Larger molecules require larger space and hence have higher activation energies for diffusion. When a payload has a molecule size smaller than the monomer unit of the polymer and the interaction between these two is weak then diffusive process needs only a weak effect, such as limited rotational oscillation of a very few monomer units, in order to create enough space for the payload to move from one space to another. In contrast, when the payload has a size comparable to the monomer units it needs cooperative movements by several monomer units to make the penetration possible. It has been shown that the released fraction of payloads from capsules largely depends on the payloads molecular size.[80, 82, 83]

3. Characterization methods

The characterization methods used in this dissertation are explained here. The experimental details can be found in chapter 5.

3.1. Dynamic light scattering (DLS)

Dynamic light scattering (DLS) is an important device for characterizing the size of nanoparticles in solution. DLS is also a valuable tool for determining and measuring the agglomeration state of nanoparticles as a function of time or suspending solution. The principle of DLS is based on the effect of Brownian motion of particles, which is obtained by the intensity fluctuations of the scattered light. A detector measures the light from a laser beam passing through a solution and being scattered at colloids with scattering centers (*e.g.* macromolecules or particles). Then the fluctuation of the scattered light intensity as a function of time is analyzed. Larger particles diffuse slower than smaller ones which results in an intensity fluctuation that depends on the diffusion coefficients of the species in the sample. This recorded fluctuation can be converted in an autocorrelation function, which for monodisperse samples is described by a simple exponential decay:

$$g\ (t) = \ e^{(-Dq^2 t)} \qquad (2.17)$$

where D represents the diffusion coefficient, q is the wave vector, and t time. By calculating the diffusion coefficient of particles using the above autocorrelation function, the hydrodynamic radius (R_h) can be determined by the Stokes-Einstein equation:

$$R_h = \frac{K_B T}{6\pi\eta D} \qquad (2.18)$$

Here, k_B is the Boltzmann constant, T the temperature, η the dynamic viscosity of the system, and R_h the hydrodynamic radius of the dispersed particles.

3.2. Electron microscopy methods

The biggest advantage of electron microscopes over optical microscopes is that they have a higher resolution and capable of a higher magnification up to 10^6 times. This difference in magnification is associated with a physical limit imposed by the wavelength of the light compared to electrons. Here in this thesis, scanning and transmission electron microscopes are used to determine the specimens.

3.2.1. Scanning electron microscopy (SEM)

A scanning electron microscope (SEM) acquires micrographs of objects from several micrometers to a few nanometers. In SEM, the electrons are accelerated to the energy range between 0.5 keV and 30 keV and are converged by electromagnetic lenses to the surface of sample. The interaction between these electrons and the sample atoms produces secondary electrons that are recorded by one of the SEM detectors. The number of secondary electrons that is recorded depends on the angle at which beam hits the sample surface. The area appears brighter when the number of recorded secondary electrons is higher. This difference between the illuminations of sample's surfaces is responsible for the three-dimensional effect of SEM images.

Low voltage SEM imaging is as an efficient way to observe the surface morphology of polymer capsules without the need of an additional conductive coating.

3.2.2. Transmission electron microscopy (TEM)

In principle, the transmission electron microscopy (TEM) is a technique in which an accelerated electron beam transmits through the thin sample materials. The different interactions between the incident electrons and the sample atoms generate information about the structure of the sample. When the electrons hit the sample, many of them are not transmitted but scattered to a certain angle off the optical axis. Thicker structures and heavy atoms scatter more than those

of the thinner structures and lighter atoms, respectively. Therefore, thicker parts and areas with high electron density appear darker due to the fewer electrons that reach the viewing screen without being scattered off the optical. It is then possible to use TEM to observe the morphology of capsules due to the different density of the shell and core. TEM can be also used for visualization of different chemical structures on the surface of capsules after staining of the capsule shell with staining agent containing heavy metals.

3.3. Ultraviolet-visible spectroscopy (UV-vis)

Ultraviolet-visible spectroscopy is a technique to record the fraction of energy absorbed by molecules upon different wavelengths in the ultraviolet-visible spectral region. A UV-vis spectrum can be obtained by plotting absorbance (A) versus wavelength (λ). The concentration of an absorbing species in solution can be quantitatively determined since the absorbance of a solution is directly proportional to its concentration:

$$\mathrm{A} = \log\frac{I_0}{I} = \varepsilon \cdot c \cdot L \qquad (2.19)$$

Here, A presents absorbance, I_0 the intensity of the light at a given wavelength, I the transmitted intensity, ε molar absorptivity constant, c the concentration of absorbing species and L the path length through the sample.

4. Results and Discussion

4.1. Osmotic pressure-dependent release profiles of payloads from nanocontainers by co-encapsulation of simple salts [1]

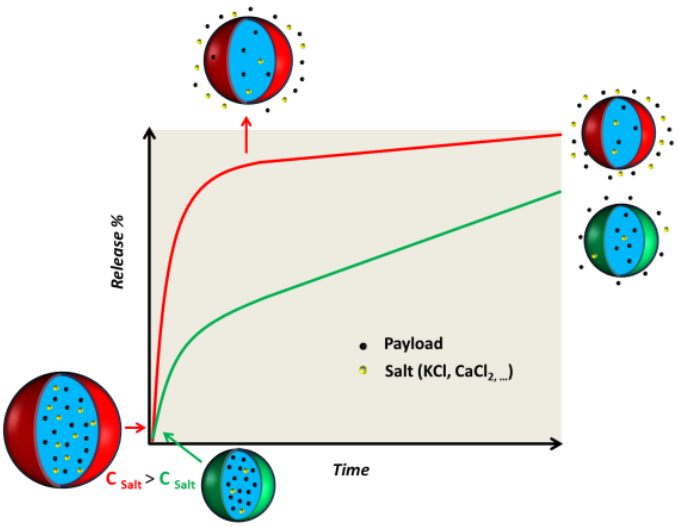

Nanocapsules with a hydrophilic core are particularly interesting for biomedical and anticorrosion applications since these nanocontainers allow encapsulating a wide range of hydrophilic payloads and controlling their release profiles. However, the burst release of hydrophilic payloads from the core due to osmotic pressure has been known as a major challenge for these capsules. Herein, we present an approach in which osmotic pressure generated by hydrophilic payloads in the core can be turned to an advantage for tuning the payloads release. In fact, we program the release of hydrophilic payloads from nanocontainers by co-encapsulating simple inorganic salts for adjusting the osmotic pressure. The latter either leads to a burst release at high concentration of co-encapsulated salts or a sustained release at lower concentrations. Osmotic pressure causes swelling of the nanocapsule´s shell and therefore sustained release profiles can be adjusted by crosslinking it. The approach presented allows for programing release of payloads by co-encapsulating inexpensive salts inside nanocontainers without the help of stimuli-responsive materials.

[1] Parts of this section are submitted to Nanoscale under the title “Osmotic pressure-dependent release profiles of payloads from nanocontainers by co-encapsulation of simple salts”.

4.1.1. Motivation

Osmotic pressure is a crucial phenomenon in nature.[84, 85] The cell maintains concentration of solutes via osmotic pressure[84] and plants rely on it to absorb water and maintain cell rigidity.[85] The control of osmotic pressure is important for medical care and water purification to avoid breakdown of the cell membrane (lysis), for storage of red blood cells,[86] for dialysis in artificial kidneys[87], to control osmotic dehydration in food preservation,[88] and to apply reverse osmosis for water desalination.[89] In recent decades, miniaturized devices consisting of a thin membrane have found applications in many areas of science and technology.[11, 90, 91]

As explained in section 2, micro- to nano-scale capsules are well-known controlled release systems. The use of these capsules for medical and technical purposes has rapidly been expanded.[13, 92-94] Regardless of the application, controlled release of payload is the dominating function of capsules. The term ''controlled release'' includes a range of different release profiles and mechanisms such as targeted release,[95] triggered release,[96] and sustained (or extended) release.[97] Modification of the membrane's physiochemical properties is of utmost importance to achieve a desired release profile.[98-100] Considerable efforts have been devoted to achieve these types of release profiles by modifying the physiochemical properties of the membrane. These efforts include the use of novel stimuli-responsive functional groups.[17, 101, 102] In the case of sustained release, the desired lifetime of release highly depends on the targeted applications. As an example, the desired life-time of release for pharmaceutical applications is roughly one day whereas for coatings it can be thousands of days.[93, 103]

However, to avoid synthetic complexity, there is a huge interest in simple strategies for the release of the payload in a controlled fashion. The overall release of the payload is explained as a sum of two contributions - these are burst and (slow) diffusive release.[104] Osmotic pressure can be used as a trigger for burst release profiles.[105] For drug delivery systems, burst release profiles were achieved *via* osmotic pressure for various types of macroscopic ($D \sim 6$ mm) capsules with an asymmetric membrane.[106, 107] As another example, the release properties of

microcapsules were controlled by osmotic pressure generated by either the dissolution of the encapsulated materials[108-111] or the addition of an osmotic agent in the release media.[112-114] It is believed that osmotic pressure imposes stress on the membrane of microcapsules that largely accelerate the release of payloads once the membrane bursts.[108, 111-113, 115, 116] However, membrane rupture arising from osmotic pressure is detrimental for some applications. Indeed, the initial high release rate may lead to drug concentrations near or above the toxic level *in vivo*.[105, 117] Preventing a burst profile is therefore crucial, especially with low molecular weight payloads (*e.g.* drugs) which are more likely to display burst release due to high osmotic pressure and their small size.[118-120] Crosslinking [121, 122] and increasing of the shell thickness[82, 123] are expected to have an influence on the shell permeation and subsequently suppress the release of the payloads from the NCs despite of an osmotic pressure difference. A major problem in osmotically driven release systems is the lack of control over the ratio of burst and diffusive contributions. The control over these properties plays a key role for advanced applications. A very simple model predicts that the burst release is proportional to osmotic pressure and the quadratic functions of size and membrane thickness.[124-126]

The deformation of capsules by osmotic pressure can be measured and predicted. This feature allowed Kim et al. to use microcapsules prepared *via* microfluidics to calculate the osmotic strength of solutions by measuring the buckling of these microcapsules.[127] Since nanocapsules (NCs), as their name suggests, are very small and have a thin membrane, the release profile can be tuned more effectively by controlling the osmotic pressure. However, how the release profiles can be tuned as a function of osmotic pressure remains unclear.

We aim at programming the release profile of NCs from burst release to sustained release by using the osmotic pressure as a trigger and without the use of other stimuli-responsive materials. To fulfill this goal, we prepared NCs containing a dye and low to high concentrations of salts. Firstly, we quantified the influence of co-encapsulated salts on the release profile of a dye when the salt concentration changed. A detailed insight on the correlation between the released fraction of the dye and the co-encapsulated salts was obtained.

4.1.2. Preparation of polyurea nanocapsules

The formation of polyurea shells was performed through a polyaddition reaction between the primary amino groups (-NH_2) of hydrophilic 1,4-diaminobutane and the isocyanate group (-NCO) of 2,4-toluene diisocyanate (TDI) that occurs at the interface of miniemulsion droplets.[16] Polyurea NCs with an average hydrodynamic diameter of 318 ± 98 nm containing the payloads were obtained (see Figure 4.1a and Table 4.1). After the synthesis, the obtained polyurea NCs were transferred in an aqueous solution of surfactant (0.3 wt.%). In all cases, no precipitation, coagulation, or flocculation of the NCs was observed. To study the influence of osmotic pressure on the release of payloads from the NCs, the dye 2-nitrophenol sodium salt and different concentration of salts (potassium chloride (KCl) or calcium chloride ($CaCl_2$)) were co-encapsulated. The concentration of $CaCl_2$ was calculated to produce an equal osmolarity to the corresponding KCl concentrations so that the influence of the nature of salt on the release could be eliminated. It is widely accepted that the thermodynamically-controlled morphology of colloids depends on the interfacial tensions between the continuous and dispersed phases in the presence of a surfactant.[128, 129] The TEM and SEM images showed evidence of a core-shell structure for the NCs (see Figure 4.1b-c). In the SEM and TEM images, the collapse of NCs is due to the shrinkage of specimens caused by the vacuum chamber of the electron microscopes.

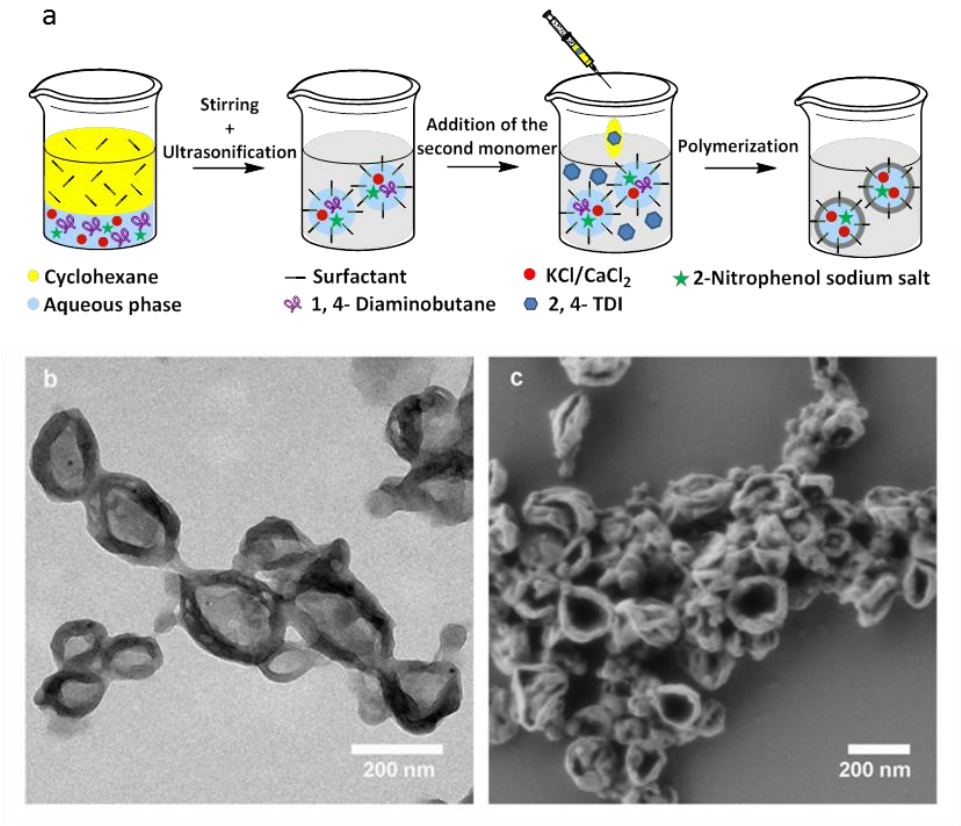

Figure 4.1. Schematics for the preparation of the NCs by interfacial polyaddition reaction in inverse miniemulsion (a). TEM (b) and SEM (c) micrographs of the NCs containing 2-nitrophenol sodium salts (sample NPD, Table 4.1).

Table 4.1. Composition of the dispersed phase for the dispersion of nanocapsules used in the experiments. NP means nanocapsules and D is added for samples containing 2-nitrophenol sodium salt (dye). X refers to the addition of diethylentriamine (crosslinker) and $[salt]_c$ indicates that the concentration of encapsulated salt in aqueous dispersed phase is equal to "*c*".

Entry	1,4-diaminobutane [mg]	diethylentriamine [mg]	KCl [mol·L^{-1}]	$CaCl_2$ [mol·L^{-1}]	2-nitrophenol sodium salt [mg]
NPD	88	-	-	-	23
$NPD[KCl]_{0.1}$	88	-	0.1	-	23
$NPD[KCl]_{0.25}$	88	-	0.25	-	23
$NPD[KCl]_{0.5}$	88	-	0.5	-	23
$NPD[KCl]_1$	88	-	1	-	23
$NPD[KCl]_2$	88	-	2	-	23
$NPD[KCl]_3$	88	-	3	-	23
$NPD[KCl]_4$	88	-	4	-	23
$NPD[CaCl_2]_{0.067}$	88	-	-	0.067	23
$NPD[CaCl_2]_{0.167}$	88	-	-	0.167	23
$NPD[CaCl_2]_{0.33}$	88	-	-	0.33	23
$NPD[CaCl_2]_{0.67}$	88	-	-	0.67	23
$NPD[CaCl_2]_{1.3}$	88	-	-	1.3	23
$NPD[CaCl_2]_2$	88	-	-	2	23
$NPD[CaCl_2]_{2.67}$	88	-	-	2.67	23
NP	88	-	-	-	-
NPX	76	14		-	-
$NPDX[KCl]_1$	76	14	1	-	23
$NP[KCl]_1$	88	-	1	-	-
$NPX[KCl]_1$	76	14	1	-	-

4.1.3. Release of the payloads

A detailed insight concerning the correlation between the releases of the payloads, the dye, and the salts, was obtained by measuring the release of both payloads. The release profile of 2-nitrophenol sodium salt was determined by monitoring the concentration of the dye with time

in the aqueous SDS solution of dialyzed dispersions of NCs. The absorption of the dye could be clearly distinguished and the release could therefore be measured using UV-spectroscopy (see Figure 5.1). The concentration of the salts with time in the release media was measured by ICP-OES (see Figure 5.2). The release profile of the dye depends on the concentration of co-encapsulated salt (see Figure 4.2a). With an increase in the KCl concentration, the fraction of released dye increased from 54 (sample NPD) to 73% (sample NPD$[KCl]_4$) after 24 h. The results also indicate that the release rate in the first hour undoubtedly depends on the KCl concentration. A comparison between the release curves reveals a 92% increase in the release of the dye after 1 h. As expected, the results with co-encapsulation of $CaCl_2$ instead of KCl exhibited the same propensity as osmotic pressure is a colligative property. This is exemplified for the sample NPD$[CaCl_2]_{0.67}$ where the concentration of $CaCl_2$ in the dispersed phase is equal to the osmolarity in sample NPD$[KCl]_1$ (see Figure 4.3a). Regardless of the salt types, the molar concentration of co-encapsulated salt played a controlling role in the dye release. Parallel to monitoring the release profile of the dye, the concentrations of KCl and $CaCl_2$ in the release media were measured. The released fraction of the salts out of NCs with initial internal osmolarity at t = 1 and 24 h can be observed in Figure 4.2b. The release properties of the salts, including the initial release and released fractions, were also dependent on the concentration of salts. For example, a 42% increase in the released fraction of KCl was observed when the KCl concentration in the dispersed aqueous phase was raised from 0.1 M to 4 M. The differences between release profiles of the dye and KCl with an initial concentration in the dispersed phase of 0.1 M (sample NPD$[KCl]_{0.1}$) emphasize the importance of payload nature, including its molecular size and possible interaction with the shell of the NCs (see Figure 4.3b). The overall and the burst release of KCl are higher than that of the dye. The release rate of KCl is faster than that of the dye because KCl has a lower molecular weight (~ 78 $g \cdot mol^{-1}$) than the dye (~ 161 $g \cdot mol^{-1}$).

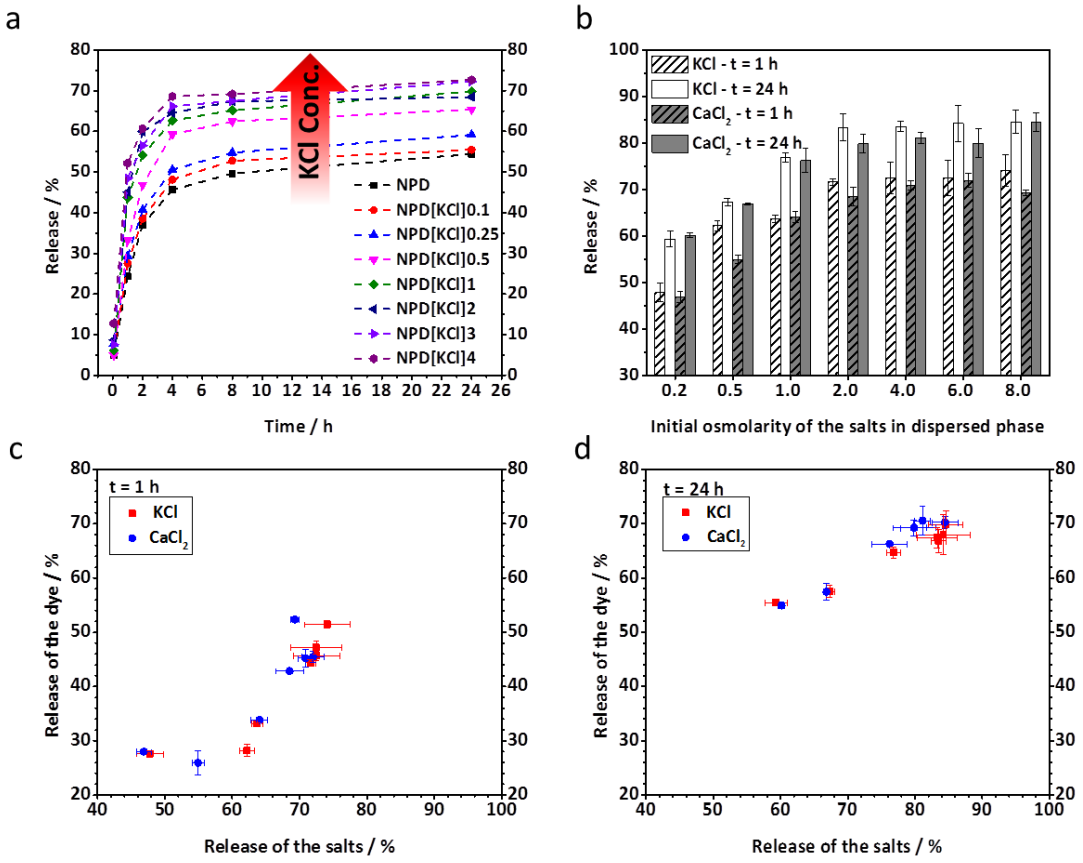

Figure 4.2. Temporal release profiles of the dye from NCs consisting of KCl at concentrations between 0 and 4 M in the dispersed phase (a). Release of KCl and $CaCl_2$ out of NCs at 1 and 24 h. The salts induced initial osmolarity in the dispersed aqueous phase between 0.2 and 8 $Osmol \cdot L^{-1}$ (b). Correlation between the released fraction of dye and salts at 1 (c) and 24 h (d).

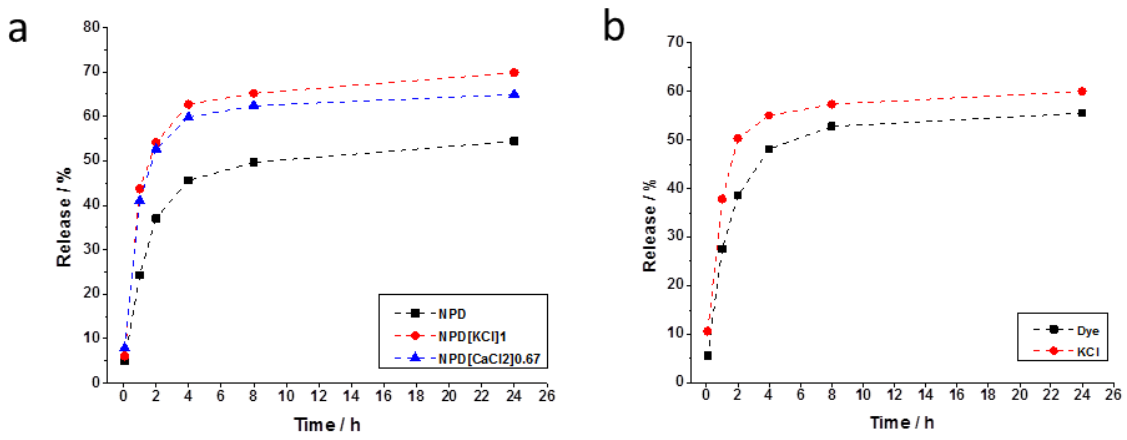

Figure 4.3. Release profiles of (a) the dye versus time for NPD, NPD$[KCl]_1$, and NPD$[CaCl_2]_{0.67}$ and (b) the dye and KCl versus time for sample NPD$[KCl]_{0.1}$ where the dye and KCl were encapsulated at concentration 0.1 M in the dispersed aqueous phase.

Measuring the release of the dye and of the salt provided the possibility to determine the correlation type between the release of the dye with the osmotic pressure generated by the salt. The correlation is shown at t = 1 and 24 h (Figure 4.2c-d). The results show a non-linear correlation between the released amount of dye and the initial salt's concentration in the dispersed phase. At a salt concentration below 0.25 M, there was hardly any observable increase in the dye release whereas the release was sharply increased at intermediate salt concentration, *i.e.* between 0.25 and 1 M. Upon a further increase of the concentration of salt, there was no significant increase of the dye´s release on the salt concentration anymore. The maximum release of the dye was almost achieved. It can be concluded that a fast release of the dye is triggered with an initial salt concentration in the dispersed phase between 0.25 and 1 M.

4.1.4. Responsible mechanism

The phenomenon of osmotic pressure has been fully described by Van 't Hoff [130] and is defined as pressure differences between interior and exterior environments of systems separated/enclosed by a membrane. Accordingly, an osmotic substance, *e.g.* water, has the

propensity to move through a semi-permeable membrane into the solution containing a solute (*e.g.* salt) until the osmotic pressure differences become equilibrated. This can change the size of the system, causing it to swell. In extreme cases, disintegration of polymer systems by imposing significant stress on the membrane was reported.[111-113, 115, 116] The osmotic pressure π_{osm} is related to the concentration of solutes,

$$\pi_{osm} = i\emptyset cRT \qquad (4.1)$$

where *i* is number of ions produced by solute dissociation, Φ is osmotic coefficient of solute, *c* is the molar concentration of the solute, R is the gas constant, and *T* is the absolute temperature. The salt concentration can therefore be used to tune a range of π_{osm} and consequently the release profile. The osmotic pressure inside a NC's core varies from ~ 0.46 to 19.7 MPa (for more details see Table 4.2) with an increase in the initial concentration of KCl in the dispersed phase from 0.1 to 4 M.

Table 4.2. Osmotic pressure inside the NCs containing KCl with initial concentration in dispersed phase between 0.1 and 4 M.

Entry	KCl [mol·L^{-1}]	Osmotic Coefficient (ϕ)	The number of ions (i)	Osmotic pressure (π) [MPa]
NPD[KCl]$_{0.1}$	0.1	0.927	2	0.46
NPD[KCl]$_{0.25}$	0.25	0.913	2	1.15
NPD[KCl]$_{0.5}$	0.5	0.900	2	2.23
NPD[KCl]$_1$	1	0.898	2	4.45
NPD[KCl]$_2$	2	0.912	2	9.04
NPD[KCl]$_3$	3	0.950	2	14.2
NPD[KCl]$_4$	4	0.990	2	19.7

We hypothesized that the co-encapsulation of salt and subsequently generated osmotic pressure were responsible for the observed differences in the dye release, and the underlying mechanism was the swelling of NCs as shown in Figure 4.4a. NCs fabricated with

diethylentriamine were synthesized to obtain NCs with crosslinked shells (Table 4.1). Crosslinking is expected to have an effect on the shell rigidity[121] and consequently hinder the release by obstructing the swelling of the NCs despite of an osmotic pressure difference. A comparison between the release properties of KCl-loaded NCs with and without crosslinker showed a decrease of the initial release and of the released fraction of the dye (Figure 4.4b). The results showed that the initial burst release generated by co-encapsulation of salts was largely hindered by crosslinking. To investigate the contribution of the swelling effect to the release profile, DLS measurements were carried out for different NCs after dilution (X = 40) of the aqueous dispersion of these NCs at time interval t = 0 min and t = 240 min (Figure 4.4c). One of the interesting properties of the NCs loaded with KCl is that they deswell (sample NP$[KCl]_1$). The swelling of the NCs caused by the salt osmotic pressure was therefore confirmed by the observed reversible deswelling. The deswelling can be explained by the fact that the shell is permeable towards the co-encapsulated salts. The NC's size increases (by 40 nm in diameter) because of a flux of water into the inner core to reduce the osmotic pressure. The swelling of the shell induced an increase of permeability of the shell for both dye and salt. When the salt is released, the shell started to deswell and the permeability decreased. Afterwards, the salt concentrations both outside and inside the NCs are equalized and the NCs hence start to deswell (see Figure 4.4c). The polydispersity index of sample NP and sample NP[KCl]1 were measured to be 0.09 and 0.12 after dilution of the aqueous dispersion of these NCs at t = 240 min, respectively. Because the hydrodynamic average diameters (see Figure 3c) and polydispersity index of samples NP and NP$[KCl]_1$ at t = 240 min are not significantly different, it can be concluded that the size distribution of the NCs does not depend on the concentration of co-encapsulated salt. Moreover, roughly unchanged sizes for sample NPX$[KCl]_1$ (Figure 4.4c) explain why the addition of diethylentriamine in sample NPDX$[KCl]_1$ hinders the increase in the dye release when the salt is co-encapsulated (Figure 4.4b). Diethylentriamine leads to crosslinking between the polymer chains in the NC's shell by providing an additional secondary amine group and therefore hampers the increase of size induced by osmotic

pressure. As a consequence, less increase in the release of the dye was observed for sample NPDX[KCl]$_1$ in comparison with sample NPD[KCl]$_1$ at t = 1 and 24 h.

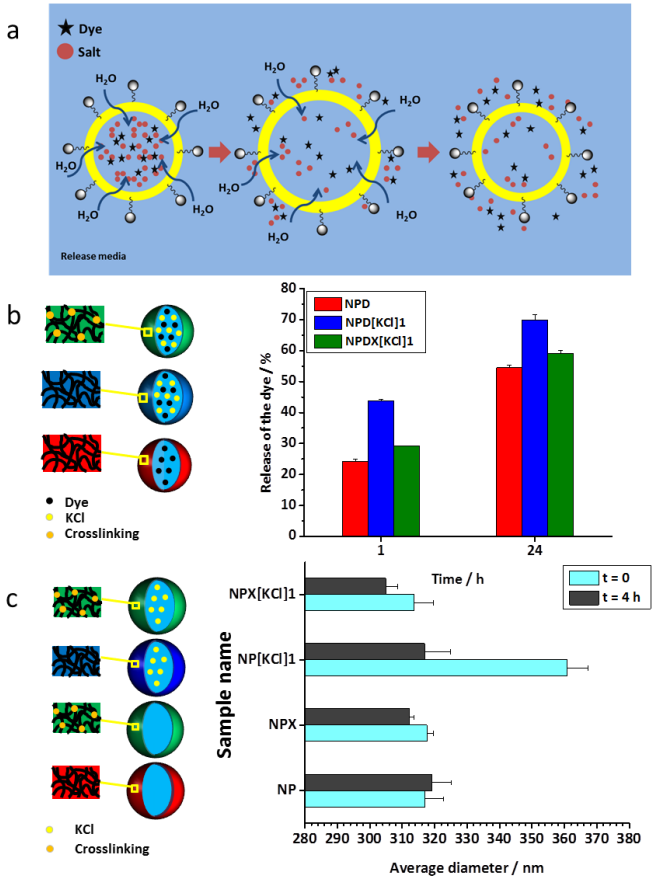

Figure 4.4. (a) Schematic illustration of the release of the dye from NCs induced by osmotic pressure. I: The osmotic pressure between the inner core and the release medium is equalized with the flux of water through the shell. II: Swelling of NCs leads to an increase in the dye and the salt release. III: Payloads release results in decreasing the osmotic pressure inside the core and the subsequent deswelling of NCs. (b) Release of the dye from KCl-loaded NCs in the absence (NPD[KCl]$_1$) and the presence (NPDX[KCl]$_1$) of the crosslinker at t =1 and 24 h. (c) Hydrodynamic average diameters of the non-loaded NCs (NP), non-loaded crosslinked NCs (NPX), NCs loaded with KCl (NPX[KCl]$_1$), and crosslinked NCs loaded with KCl (NPX[KCl]$_1$) at t = 0 and 4 h. The values of these hydrodynamic average diameters were determined by the extrapolation of value for q = 0 (zero angle).

Young's modulus of capsules shell can be estimated based on the fact that capsules swell owing to excess osmotic pressure of the aqueous core. If the capsule swells from the initial radius (r_0) to final radius(r), then Young's modulus can be estimated by:[110, 131]

$$r \approx r_0\left(1+\frac{r}{4h}\,\frac{i\,\emptyset\,c\,RT\,(1-\nu)}{E}\right) \qquad (4.2)$$

where h is the shell thickness, E is the Young's modulus of the polymer and ν is the Poisson ratio. The shell thickness of sample NPDX$[KCl]_1$ was measured to be 37 nm from TEM images and r (*i.e.* the radius of swollen capsules) and r_0 (*i.e.* the radius of deswollen capsules) were estimated to be 180 and 158 nm by using DLS measurements for sample NPDX$[KCl]_1$ (Figure 4.4c). The Poisson ratio of bulk polyurea is 0.49.[55-56] Using equation (4.2), the Young's modulus of the polyurea shell was then calculated to be 18.9 MPa –a value close to the 27 MPa reported for an aliphatic-aromatic polyurea in bulk.[57] However, when discussing the mechanical properties of the polyurea shells, one has to consider the peculiar stress-strain response of bulk polyurea. For stresses up to about 7 MPa, corresponding to strains of about 10%, polyurea shows a linear elastic response with the above Young's modulus. Beyond that stress value, it behaves much softer with an almost plateau-like stress-strain curve, that allows to reach large strains of several 100% before reaching the failure stress.[57] A change of radius from 158 nm to 180 nm corresponds to a strain of 30%, which implies that in fact linear elastic regime was already slightly exceeded in that experiment and the use of equation (4.2) will underestimate the Young's modulus of the shells for smaller strains. The plane stress σ in the shell of a spherical capsule due to an osmotic pressure difference π across it is given as:[58]

$$\sigma = \frac{\pi r}{2h} \qquad (4.3)$$

where *r* is the capsule radius and *h* is the shell thickness. For a shell thickness of 36 nm and a capsule radius of 158 nm, we obtain a stress values of 5.1 MPa for the NPD$[KCl]_{0.25}$, which is within the linear elastic regime (< 7 MPa), where polyurea reacts relatively stiff (steep slope in stress-strain curve). For the NPD$[KCl]_{0.5}$ sample the stress reaches 9.9 MPa, which is beyond the

linear elastic regime, where the response of polyurea becomes much softer (plateau-like stress-strain curve). This transition in mechanical response may be responsible for the disproportionate increase in release observed in Figure 4.2a between NPD[KCl]$_{0.25}$ and NPD[KCl]$_{0.5}$. As soon as the stress within the shell is exceeding around 7 MPa, small further increases in stress will lead to large strains, which in turn should lead to increased permeability. This kind of material response of polyurea should have two effects on the release properties: first, by adjusting the size of the particles, one can easily tune the osmotic pressure at which transition between the two regimes and therefore the maximum boost in release occurs. According to equation (4.3), nanocapsule with mean diameter of 500 nm can resist a 100 times higher osmotic pressure that is needed to rupture microcapsules consisting of the same shell-forming materials with mean diameter of 50 µm. Second, capsules may be more stable against rupture by osmotic stress than expected from equation (4.3) and a given failure stress obtained from a stress-strain curve. For large osmotic pressures, capsule shells will experience large strains, which may lead to a large permeability and possibly to a fast enough reduction in osmotic pressure before rupture can occur.

4.1.5. Application for biomedicine and anticorrosion

Finally, we illustrated how this approach can be applied to induce either triggered release or sustained release profiles through two different applications, which are encapsulation of potassium thiocyanate (KSCN) for anticorrosion and Foscarnet as drug for biomedical application (Table 4.3). KSCN in contact with ferric ions produces a solution, which is red due to the formation of a thiocyanate iron complex. The reaction can therefore be used for monitoring iron oxidation. The burst release of KSCN was therefore triggered by encapsulating a solution of KSCN at a concentration of 1 M (see Figure 4.5). When the concentration of KSCN was increased, a larger burst release after 1 h was observed, which was characterized by an increase of release from 53% to 84% of released KSCN compared to the initial amount of KSCN in the dispersions. Moreover, the released KSCN after 24 h for sample NP[KSCN]$_1$ was raised 38% in comparison with the sample containing KSCN with the initial concentration of 0.1M

(NP[KSCN]$_1$). Reducing the burst release is also possible although it is not suitable for sensing application. Indeed, the addition of crosslinker reduced the intensity of the initial release generated by osmotic pressure (NPX[KSCN]$_1$). The NCs with KSCN can then be used as optical sensors for the detection of corrosion. Indeed, the color turned from pale yellow-white to red when a solution of ferric ions was added to the dispersion of the nanocontainers (see Figure 4.6). The nanocontainers can be embedded in a protective coating deposited on metals, as was previously reported for other types of nanocontainers containing corrosion inhibitors.[132, 133]

Table 4.3. Composition of the dispersed phase for the dispersion of nanocapsules used in the experiments. NP means nanocapsules and X refers to the addition of diethylentriamine (crosslinker) and [salt]$_c$ indicates that the concentration of encapsulated salt in aqueous dispersed phase is equal to "*c*".

Entry	1,4-diaminobutane [mg]	diethylentriamine [mg]	KSCN [mol·L^{-1}]	Foscarnet [mol·L^{-1}]
NP[KSCN]$_{0.1}$	88	-	0.1	-
NP[KSCN]$_1$	88	-	1	-
NPX[KSCN]$_1$	76	14	1	-
NP[Foscarnet]$_{0.1}$	88	-	-	0.1
NPX[Foscarnet]$_{0.1}$	76	14	-	0.1

The control of initial burst release is necessary for many biomedical applications. For instance, Foscarnet, which is an antiviral drug, blocks the pyrophosphate binding site of the viral DNA polymerase at a concentration that does not influence cellular polymerases [134]. However, the poor and variable absorption of Foscarnet via oral administration, because of a limited capacity or saturation of the phosphate transport system exiting in the intestinal brush-border membrane and its decomposition in acidic solution, limits its usage.[135] The encapsulation of Foscarnet can overcome the aforementioned limitations if the initial burst release is avoided. Using a crosslinker decreased the part of initial burst of Foscarnet from 65% to 47%. Additionally, the amount of released Foscarnet from the NCs after 24 h for sample NPX[Foscarnet]$_{0.1}$ was decreased by 10% relative to sample NP[Foscarnet]$_{0.1}$ as a consequence

of the crosslinker addition (Table S1 and Figure 4.5). Such a change in release properties can be considered as a step forward to achieve the release of a drug at a predetermined rate in order to maintain a constant drug concentration for a specific period of time release.

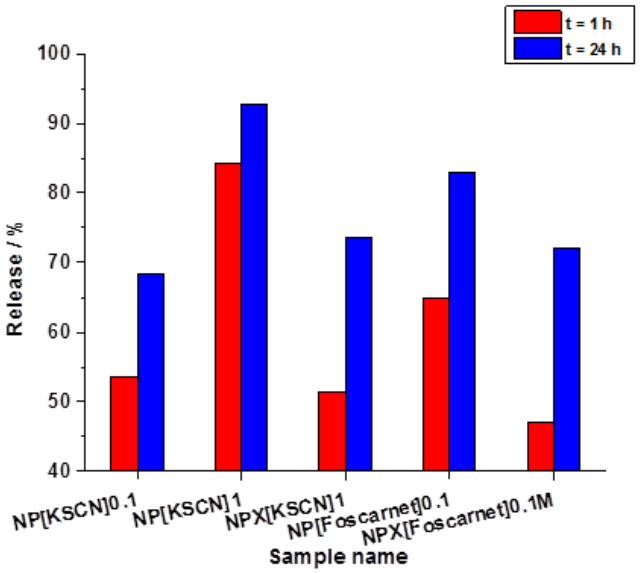

Figure 4.5. Released amount of KSCN and Foscarnet from NCs. 0.1 and 1 indicate the molar concentration of the payload and X refers to the addition of crosslinker in the dispersed aqueous phase.

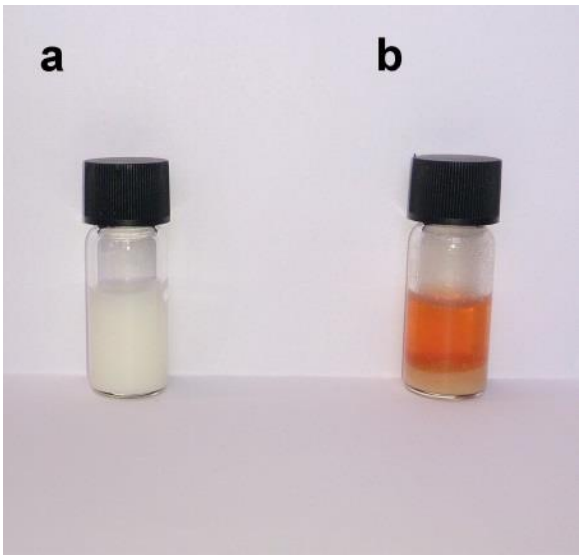

Figure 4.6. Photograph of the dispersion of nanocontainers with encapsulated KSCN before (a) and after (b) addition of a solution of ferric ions.

4.1.6. Conclusions and Outlook

In conclusion, the release of hydrophilic payloads from NCs was controlled by varying the osmotic pressure in the core. To investigate the effect of osmotic pressure on the ratio of initial burst release to diffusive release, we determined the release profiles for different payloads. The results indicate that the initial release of the payloads from NCs were significantly dependent on the concentration of osmotic pressure agents. The analysis showed a non-linear correlation between the release of the dye and the concentration of the co-encapsulated salts. Further measurements revealed that the responsible mechanism for the observed differences between the release profiles of the dye from the NCs loaded with osmotic pressure generating species (*i.e.* the salts) and non-loaded ones is the swelling of NCs. Note that the concentration of the dye was kept as low as 0.1 M so that its influence on osmotic pressure is not significant. The addition of a small amount of crosslinker showed that it is possible to hamper the initial burst release generated by osmotic pressure. This study shows that different release profiles can be programmed *via* the control of osmotic pressure for various applications such as biomedicine or corrosion protection. Burst release can be turned to an advantage for the acceleration of

payloads release or one can take advantage of diminishing the burst release by changing the physicochemical properties of NC membranes for decreasing release kinetics.

4.2. Controlled-release of hydrophilic payloads from reduction-responsive nanocapsules[2]

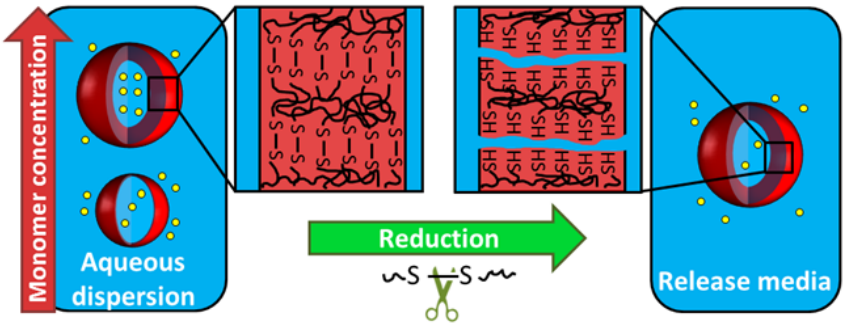

The previous section described an approach in which osmotic pressure generated by the payload can be turned to an advantage for the acceleration of payload release. However, the initial high release rate of payloads arising from osmotic pressure can be harmful for some applications such as drug delivery where the burst release rate may result in drug concentrations above the toxic level *in vivo*. The preparation of nanocapsules consisting of an aqueous core by the miniemulsion technique is a versatile method for the encapsulation of diverse molecules including drugs, nucleic acids, peptides, and proteins. However, a major challenge associated with the preparation of these nanocapsules is the initial high release rate (*i.e.* non-controlled leakage) of hydrophilic payloads from the core due to osmotic pressure. In this section, we present an approach for the preparation of polymer nanocapsules that suppress the non-controlled leakage of payloads and respond to chemical reduction that triggers release of encapsulated payloads. The non-controlled leakage of hydrophilic payloads from the nanocapsules is hindered by increasing the shell thickness. These nanocapsules consisting of reduction-responsive units possess a remarkable release property only under reductive condition while cease non-controlled leakage of the payload in the aqueous release medium. The described nanocapsules can be applied for biomedical and anticorrosion applications in which triggered release of hydrophilic payloads is suitable.

[2] Parts of this section will be submitted to Nanoscale under the title "Controlled-release of hydrophilic payloads from reduction-responsive nanocapsules".

4.2.1. Motivation

As explained in section 2, polymer nanocapsules can be prepared with strategies based on the miniemulsion technique, which allows the formation of nanocapsules with either hydrophobic (oily) or hydrophilic (aqueous) core. The core dictates the polarity and hydrophobicity of payloads that can be encapsulated.[12, 13, 16, 136, 137] The miniemulsion technique also offers the possibility to use a wide range of monomers/polymers and chemical reactions for the preparation of the polymer shell (please see section 2.3). Thus, miniemulsion can be used for synthesizing polymer shells bearing specific physicochemical properties that are essential for controlled release.[136-138] Diverse molecules including drugs, nucleic acids, peptides, and proteins were successfully encapsulated by the miniemulsion technique in nanocapsules consisting of an aqueous core prepared.[12, 55, 139, 140] However, the major challenge associated with the preparation of these capsules is the leakage of encapsulated payloads due to osmotic pressure. Osmotic pressure imposes stress on the shell of capsules and thus accelerates the initial release of payloads (For more details please see section 4.1.1).[105, 108, 111, 113, 127] For biomedical applications, the leakage or high initial release rate of payloads may lead to drug concentrations near or above the toxic level *in vivo*.[105] Therefore, preventing leakage and burst profile is critical, especially with low molecular weight payloads (*e.g.* drugs) which are more likely to exhibit burst release due to their small size.

Some studies have already shown the influence of increased shell thickness on the release profile for polymer capsules formed by different methods, including interfacial polymerization.[82, 123, 141] On one hand, a significant increase of shell thickness can hinder the leakage of payloads from capsules. On the other hand, it can largely slow down the release kinetics and thereby hampers a precisely targeted delivery of payloads in desired time. It is therefore beneficial to introduce responsive groups into the thick shell in order to trigger release of payloads in a very controlled fashion under certain environmental conditions. Among all available reactions to trigger the release of payloads, oxidations and reductions play a unique role because they are very common in nature.[142, 143] They are associated with stress

conditions[144] and signaling cascade[145] in cells such as for instance cancer cells[146]. Recently, glutathione-responsive nanocontainers have been developed for targeted intracellular drug and gene delivery.[147-151] In fact, the cleavage of disulfide bonds incorporated in a polymer shell by glutathione existing in intracellular compartments leads to an increase in the permeability of the polymer shell. Thus, the release of pharmacological payloads from the carriers was facilitated.[147-155] The reduction of disulfide bonds can also be used the protection of metallic systems against corrosion due to the decrease of the electrochemical potential when corrosion occurs.[19]

In the present study, we aim at analyzing the redox-induced release of hydrophilic payloads from nanocapsules with potential applications in self-healing materials and drug delivery. To achieve this objective, we prepared nanocapsules consisting of an aqueous core and a polyurea shell. Polyurea was selected as the shell material due to its high mechanical resistance[156] and its biocompatibility.[156, 157] In the following, we first address the problem of leakage of the payload from the nanocapsules and then monitor the triggered release from their cores upon application of a reducing agent.

4.2.2. Preparation of polyurea nanocapsules

Polyurea nanocapsules were synthesized by a polyaddition reaction between the primary amino groups of the hydrophilic cystamine and the isocyanate groups of 2,4-toluene diisocyanate (TDI) occurring at the interface of miniemulsion droplets (Table 4.4 and Figure 4.7a).[16] TEM images evidenced the core-shell structure of the nanocapsules (Figure 4.7b-e). The collapse of nanocapsules, visible in these images, was caused by the vacuum in the chamber of the electron microscope. After the synthesis, the obtained polyurea nanocapsules were transferred to an aqueous solution of the SDS surfactant. No aggregation of the nanocapsules was observed. The molar ratio of cystamine to TDI was 1:1.5 for all samples. Nanocapsules were synthesized with the same procedure without dye to avoid unwanted influence of the dye (emission wavelength 625 nm) on DLS measurements (Table 4.4). In this chapter, the

nanocapsules without dye are designated with a"-d". The obtained nanocapsules containing water displayed an average hydrodynamic diameter between 254 and 444 nm when the concentration of monomers in the cyclohexane dispersion increased from 4.9 to 39.3 $g{\cdot}L^{-1}$ (Table 4.4). The shell thickness of the nanocapsules could not be properly measured by using TEM images since the nanocapsules shrank due to the vacuum of the electron microscope chamber. However, the observed increment in the diameter of the samples (Table 4.4) can be correlated to an increase of the shell thickness by the facts that the amount of aqueous core was kept constant for different samples.

Table 4.4. Concentration of cystamine and 2,4-toluene diisocyanate in the cyclohexane dispersion of nanocapsules, average hydrodynamic diameter of miniemulsion droplets and nanocapsules in their cyclohexane dispersion, and the theoretical shell thickness of the shell.

Entry	Cystamine [$g{\cdot}L^{-1}$]	2,4-toluene diisocyanate [$g{\cdot}L^{-1}$]	Hydrodynamic diameter [nm] [a]	Polydispersity index [b]	shell thickness [nm]
NPC1-d	1.8	3.1	252	0.2	4
NPC2-d	3.7	5.2	278	0.28	9
NPC3-d	7.3	12.3	324	0.15	18
NPC4-d	14.7	24.6	444	0.23	37

[a] as measured by DLS; [b] determined at 90°

As a comparison, the thickness of the shell could be estimated from the polymer amounts used for the formation of the shell. Theoretical core radius (r_c) is calculated by using Equation 4.4 where R represents average hydrodynamic radius measured by DLS. In this equation, V_c is the total volume of core used in the aqueous phase for the preparation of nanocapsules and the shell volume (V_p) is calculated by Equation 4.5:

$$\frac{V_p}{V_c} = \frac{R^3}{r_c^3} - 1 \qquad (4.4)$$

$$v_p = \frac{m_{Cys} + m_{TDI} + m_S}{\rho_p} \qquad (4.5)$$

where m_{Cys}, m_{TDI}, and m_S are the amount of cystamine (mg), 2,4-TDI (mg), and surfactant used for the p reparation of nanocapsules, respectively.

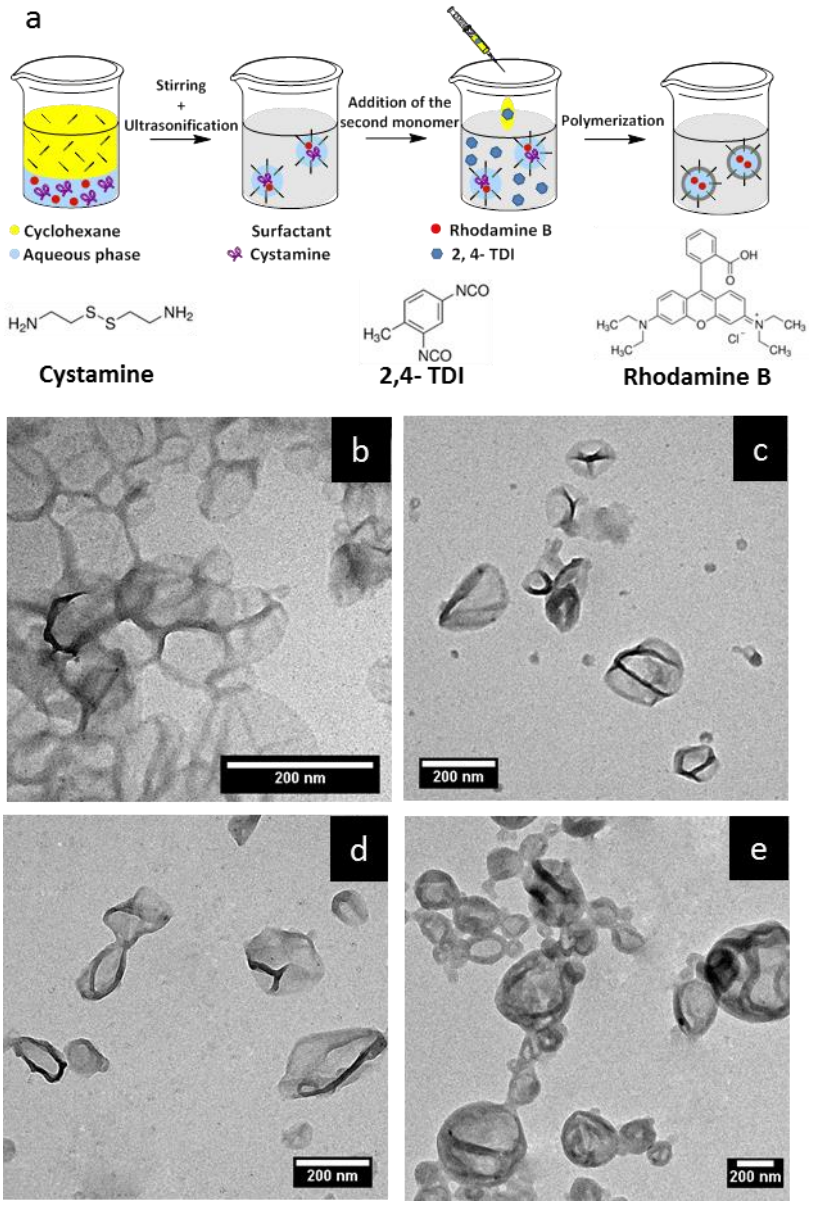

Figure 4.7. (a) Schematic illustration of the preparation of nanocapsules by interfacial polymerization in inverse miniemulsion. TEM micrograph of sample NPC1 (b), NPC2 (c), NPC3 (d), and NPC4 (e).

For aliphatic-aromatic polyurea, bulk density is reported to be between 1.0 and 1.2 g·cm^{-1}.[158] In equation 4.5, we assumed ρ_p to be 1.0 g·cm^{-1}. The theoretical shell thickness was calculated by subtracting the average hydrodynamic radius from the theoretical core radius. These calculations displayed that the shell thickness increased from 4 nm to 36 nm when the concentration of monomers in the cyclohexane dispersion increased from 4.9 to 39.3 g L^{-1} (Table 4.4).

4.2.3. Characterization of polyurea shells

The formation of the polyurea shell with cystamine is likely, but it is not guaranteed that the cystamine is fully incorporated into the shell since polyurea shell can also to a limited amount be formed by reaction of the TDI with its hydrolyzed form (however, the reaction of TDI with amino groups is much faster (1000 times) than with water).[159-161] Fourier transform infrared spectroscopy (FTIR) was performed on the cyclohexane dispersion of polyurea nanocapsules and the monomers cystamine and 2,4-TDI to examine their vibration spectra (Figure 4.8). The absorption peak at 2242 cm^{-1}, belonging to the stretching vibration of NCO, is very distinct for

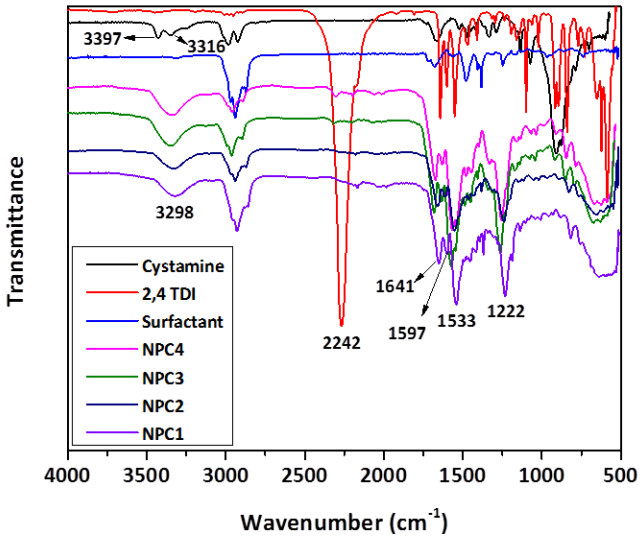

Figure 4.8. FTIR spectra of the cyclohexane dispersion of polyurea nanocapsules (NPC1-4), cystamine, 2,4 TDI, and the surfactant.

2,4-TDI but disappeared entirely for nanocapsules, implying that there was no detectable polyurea with isocyanate end groups after the synthesis (Figure 4.8). Furthermore, the presence of characteristic groups including C-N (at 1222 cm^{-1}), aromatic ring (at 1597 cm^{-1}), urea carbonyl (at 1641 cm^{-1}), and NH with the absorption peaks (at 1533 and 3298 cm^{-1}) were all confirmed.[160] FTIR analysis has clearly proved full conversion of the isocyanate groups after the formation of the nanocapsules the data about the polyurea formation but it cannot conclusively show whether cystamine has been completely incorporated into the nanocapsule shell.

To extract any free cystamine that has not been polymerized, freeze-dried nanocapsules were re-dispersed in DMSO-d_6 and stirred in a close vial at room temperature for 72 h. The incorporation of cystamine into the polyurea shell was examined by performing ^{1}H-NMR spectroscopy on the supernatant after centrifugation (Figure 4.9). The ethyl protons of the monomer cystamine, appearing as triplet at 2.7 and 2.78 ppm ($C_{1'}$ and $C_{2'}$), can also be found in the spectrum of the supernatant where they show a higher chemical shift of 2.83 and 3.4 ppm (C_8 and C_9) due to the influence of the phenylene and urea group.

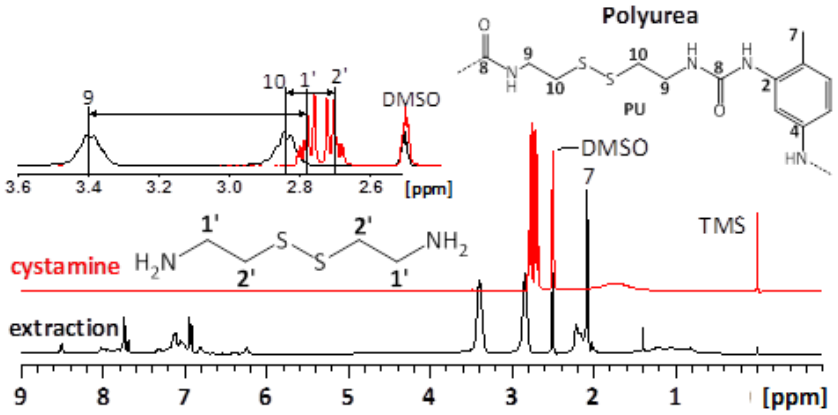

Figure 4.9. ^{1}H NMR spectra of cystamine and the extracted dispersion (*i.e.* supernatant) of sample NPC4.

Furthermore, the ethyl protons of the monomer cystamine cannot be differentiated from the noise in the NMR spectrum of the supernatant. The calculation of integration for the shifted cystamine resonances showed that more than 95% of cystamine reacted with TDI. Thus, the incorporation of responsive groups into the shell was achieved.

For a triggered release, it is essential to verify that the disulfide bonds of cystamine remains intact after polymerization. The shape of the S2p area in X-ray photoelectron spectroscopy (XPS) indicates the presence of dialkyl disulfide at ~ 164 eV. [162-165] The observed signal around 164 eV for NPC4 (Figure 4.10) could be therefore assigned to disulfide bonds of the polyurea shell. The results of FTIR, NMR, and XPS spectra proved that polyurea formation occurred as result of the reaction between cystamine and 2,4-TDI. The shell with the disulfide bonds of cystamine is promising for the stimulus-responsive release of payloads under reductive conditions.

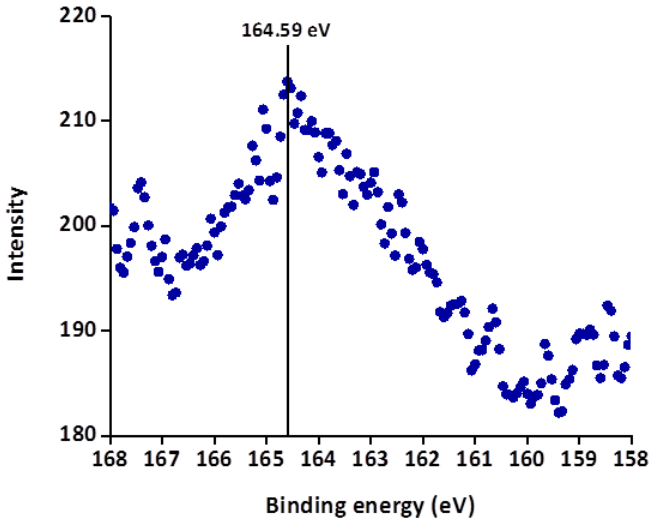

Figure 4.10. S2p region in the XPS spectrum of sample NPC4.

4.2.4. Reduction-responsive release of the payloads from the nanocapsules

The release performance of nanocapsules largely relies on their ability to suppress non-controlled leakage of the payload from the core and to release the payload selectively in response to an external stimulus. Non-controlled leakage of the payload is a major challenge for the efficient storage of the payload before site-selective delivery. Non-controlled leakage of a hydrophilic dye from the polyurea nanocapsules in aqueous dispersions was determined by centrifugation of the dispersion and by measuring the concentration of the dye in the supernatant by using UV-Vis spectroscopy. As shown in Figure 4.11a, the amount of non-controlled leakage of the dye in the dispersion of NPC1 was 30% of the initial dye concentration used for the preparation of the nanocapsules whereas this value decreased to4% for NPC4. This decrease was attributed to the increase in shell thickness as result of a four times increment in the amount of monomers used for the preparation of nanocapsules. Sample NPC4 was chosen for further study of the release profile because it displayed the lowest leakage among all samples.

As shown before, accessible disulfide bonds exist in the nanocapsules shell. This special feature can be exploited to release the payload in the core of the nanocapsules upon application of a reducing reagent. To study the reduction-induced release of the dye out of NPC4, its dispersion was diluted in an aqueous release medium at pH ~ 7.0 and samples were withdrawn from the reaction mixture at certain time intervals. The amount of dye in the supernatants after centrifugation of nanocapsules was then measured by UV-Vis spectroscopy to calculate the released amount of the dye. To trigger the responsive release, tris (2-carboxyethyl)phosphine hydrochloride (TCEP) was added to the release medium as reduction reagent. The released amount of the payload for the untreated sample reached ~ 14% at t = 24 h, which is indicative of a slow leaking of the dye from the nanocapsules. However, the reduction-responsive behavior of the release was evidenced by the large increase of the dye upon addition of the reducing agent, with a release reaching up to 62% at t = 24 h (Fig. 4.11b). The increase in the dye release was associated with the cleavage of the disulfide bonds inside the shell. The

occurrence of disulfide cleavage was supported by the quantification of remaining TCEP in release medium *via* ^{31}P-NMR spectroscopy.[166] In accordance with literature the signal for remaining TCEP signal appeared at 16.6 ppm, whereas oxidized TCEP shows up at 56.9 ppm (Figure 4.11c). By calculation and comparison of the integrals of the phosphate and the TCEP signals between the three samples the total amount of remaining TCEP can be determined.

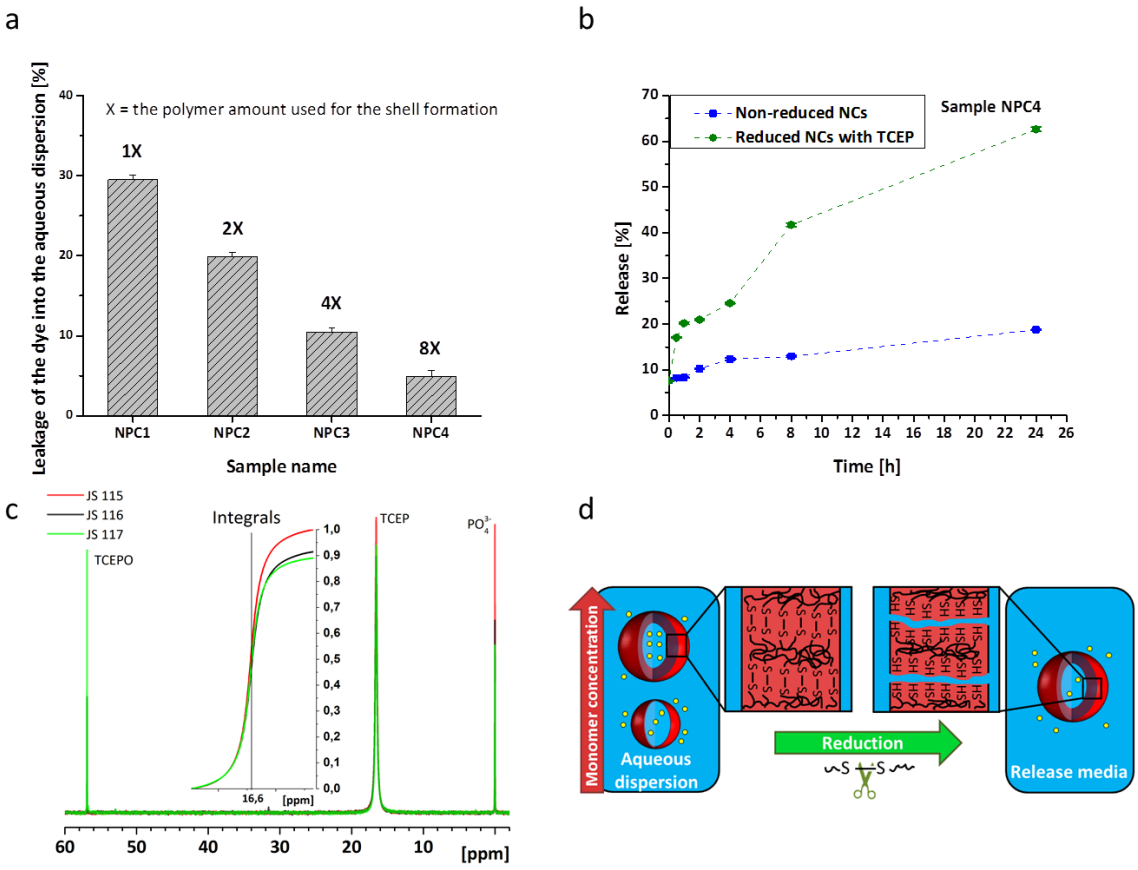

Figure 4.11. (a) Leakage of the dye into nanocapsule aqueous dispersions. (b) Release profiles of the dye for both reduced and non-reduced nanocapsules prepared with the highest amount of monomers (sample NPC4). (c) ^{31}P-NMR spectra for quantification of TCEP in sample NPC4 24 h after addition of TCEP. (d) Schematics depicting the release behavior from polyurea nanocapsules. At high concentration of monomers, the amount of dye in the aqueous dispersion decreases while release only occurs significantly upon reduction of disulfide bonds present in the shell.

Hence the consumption of TCEP can be calculated, which is equivalent to the number of disulfide bonds that were cleaved. Disulfide bond cleavage of the nanocapsules (NPC4) consumed 8.6% of TCEP which means that about 86 % of the disulfide bonds were cleaved. For JS 117 about 93 % of the disulfide bonds in pure cystamine were cleaved, consuming 11.1% of TCEP. About 86% of the disulfide bonds incorporated into the nanocapsules were cleaved at *t* = 24 h (Figure 4.11c and Table 4.5). This means that the kinetics of a selective release from nanocapsules containing hydrophilic payloads can be significantly improved by the combination of a larger shell thickness and the insertion of a responsive unit in the shell-forming materials (Fig. 4.11d).

Table 4.5. Preparation of samples for TCEP quantification via ^{31}P-NMR spectroscopy.

Entry	TCEP [g·L^{-1}]	Cystamine [g·L^{-1}]	K_3PO_4 [g·L^{-1}]	NCP4 -Dispersion [g·L^{-1}]
JS115	33.4	0	1.99	0
JS116	33.2	0	2.88	500
JS117	33.0	2.0	2.07	0

4.2.5. Conclusions and Outlook

In this project, the concept of stimulus-induced release of hydrophilic payloads from nanocapsules was demonstrated for redox-responsive nanocapsules. Polyurea nanocapsules were prepared by the inverse miniemulsion process. The cores were composed of water and the shells were responsive to redox reagent by the incorporation of disulfide bonds into the shells during the synthesis. The shell thickness was tuned by varying the monomers concentration used for the preparation of nanocapsules. Non-controlled leakage of the hydrophilic payload was hindered by increasing the shell thickness. The triggered-release of the payload was successfully achieved under reductive conditions. This novel concept of stimulus-responsive release of hydrophilic payloads from hydrophilic cores without non-controlled leakage of payloads represents a significant advancement in the synthesis of nanocapsules for applications in water such as drug-delivery and self-healing.

4.3. Triblock copolymers vs blends of diblock copolymers for nanocapsules addressed by three independent stimuli[3]

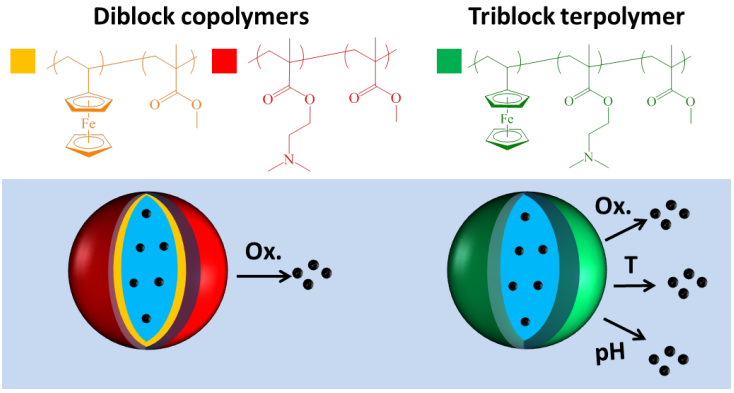

In previous sections, we presented two strategies to deal with the non-controlled leakage of payloads from nanocapsules consisting of a hydrophilic core (*e.g.* water). Nanocapsules with a hydrophobic core are another type of nanocapsules which have received widespread attention in recent years due to their projected applications. Hydrophobic payloads such as drugs or dyes can be loaded into their core and protected by the outer shell. The payload can also be released by triggering the responsive units of the shell with an external trigger such as pH, temperature, and redox potential. We report here novel triple stimuli-responsive nanocapsules that selectively respond to changes in temperature, pH value, and redox potential. The nanocapsules were prepared from either a triple responsive triblock terpolymer or a blend of the responsive diblock copolymers, both synthesized by sequential anionic polymerization. We then compare the release performance of the nanocapsules upon oxidative condition and changes of temperature or pH value. Our results reveal the close correlation between the release properties of stimuli-responsive nanocontainers and the microstructure of the polymer shell. In fact, the microphase separation between the responsive diblock copolymers across the shell significantly hinders the triggered release of the payload from the nanocapsules. These results demonstrate that fine morphology of the triblock

[3]Parts of this section are accepted by Polymer Chemistry under the title "Triblock copolymers versus blends of diblock copolymers for nanocapsules addressed by three independent stimuli".

terpolymers can be exploited to achieve the triggered release of payloads form polymer nanocontainers upon application of three different external triggers.

4.3.1. Motivation

Controlling the transport of molecules and ions through a membrane is crucial in release systems applied for biomedicine and anticorrosion. Nevertheless, artificial membranes are far less advanced compared to natural membranes and therefore research on controlled release of molecules through artificial membranes is necessary. The triggered release of payloads from containers in response to external stimuli has sparked considerable interest among researchers since they have the potential for many different applicatons.[96, 167-173] Tremendous efforts have been devoted to obtain a triggered release by modifying the physiochemical properties of the shell. These efforts include the use of stimuli-responsive functional groups that display sharp transitions of properties to certain stimuli from external environment. Miniature containers consisting of stimulus-responsive shells are promising for applications such as biomedicine[174-178], anticorrosion[17, 179], sensors[180], and water purification.[181] Most of these studies are focused on one trigger to release payloads. However, practical applications occur usually in complex environments. In some cases, containers responsive to multiple stimuli are necessary for selective release of several payloads. An example is combination therapy, where multiple medications are needed to fight one disease through the synergetic effect of drugs.[182, 183] In other cases, pulsatile release of payloads from miniature containers is required, namely for treating chronic diseases to relieve patients pains caused by frequent injections.

Block copolymers, consisting of two or more polymer segments that are covalently connected, feature the intrinsic capability to undergo microphase separation that yields fascinating structures in bulk or selective solvents.[7, 8] For example, multicompartmentalized vesicles, polygonal bilayer sheets and, wormlike micelles were synthesized from ABC triblock terpolymers and their self-assembled structures studied in water.[184-186] Furthermore, a variety of interesting stimuli-responsive containers have been generated by exploiting block

copolymers as shell-forming materials.[119, 187-198] For instance, pH/temperature- and pH/redox-responsive nanocapsules (NCs) were synthesized from diblock copolymers and the selective release of two different payloads from NCs has been studied.[195] Triple-responsive micelles synthesized from diblock copolymers are other successful examples for multi stimuli-responsive materials.[188, 194] A fascinating example for multi stimuli-responsive micelles is the micelle formation by triple-responsive disulfide linked diblock copolymers.[188] Another one are triple-stimuli micelles synthesized by self-assembly of amphiphilic diblock copolymer in water.[197] However in these examples, the micelles do not encapsulate a liquid core as it is the case for polymer NCs. Bearing in mind that at least one polymer needs to remain hydrophobic to hold the shape of the polymer nanocontainers, recently, vesicles of ferrocene-containing triblock terpolymer were synthesized and their redox-responsive release studied.[199] Although the hydrophobic segment of the triblock terpolymer guarantees the structural integrity of these vesicles after oxidation, there was only one addressable segment present, *i.e.* the ferrocene containing segment. Triple-responsive NCs can be in principle fabricated using three responsive homopolymers, two dual-responsive diblock copolymers, or a triple-responsive triblock terpolymer. We can anticipate that the preparation of triple-responsive containers with a blend of stimulus-responsive homopolymers will most probably result in phase separation inside the shell. The buried homopolymers will therefore not be addressable by one of the external stimuli applied to the nanocontainers. Another disadvantage of using a blend of stimulus-responsive homopolymers for the preparation of containers is the decrease of container stability due to absence of covalent linkage between different compartments. To overcome this issue, we propose to use a triple responsive triblock terpolymer to build the shell of nanocontainers. Alternatively, we compare the performance of such nanocontainers with nanocontainers prepared with a blend of responsive diblock copolymers. In both types of samples, we synthesized the polymer so that the shells have exactly the same chemical composition in term of molar amount of the block segments. To fulfill this goal, the triblock poly(vinylferrocene)-*b*-poly(methyl methacrylate)-*b*- poly(*N*,*N*-dimethylaminoethyl methacrylate) (PVFc-*b*-PMMA-*b*-PDMAEMA) and blends of the corresponding diblock copolymers of PVFc-*b*-PMMA and

PDMAEMA-*b*-PMMA were synthesized. The copolymers were used to fabricate nanocontainers and the triggered release of the encapsulated payload upon pH change, redox reagent, and temperature was investigated. A detailed insight on the correlation between the release properties and shells microstructure of the NCs was obtained using a combination of characterization methods.

4.3.2. Preparation and characterization triblock terpolymers nanocapsules

Triblock terpolymers were synthesized by the group of Dr. Markus Gallei (AK Rehahn) at the TU Darmstadt (Figure 4.12). The molecular weights of the used triblock terpolymers are summarized in Table. 4.6.

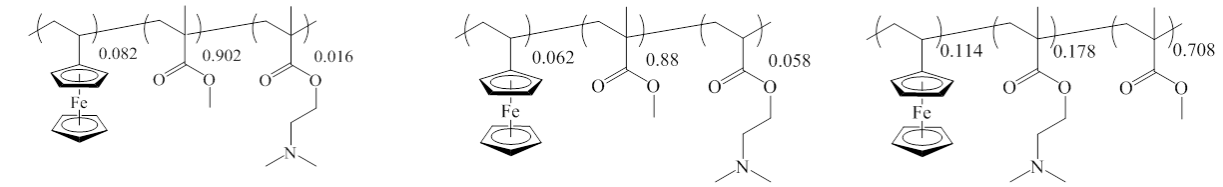

$PVFc_{8.2}$-*b*-$PMMA_{90.2}$-*b*-$PDMAEMA_{1.6}$ $PVFc_{6.2}$-*b*-$PMMA_{88}$-*b*-$PDMAEMA_{5.8}$ $PVFc_{11.4}$-*b*-$PDMAEMA_{17.8}$-*b*-$PMMA_{70.8}$

Figure 4.12. Chemical structure of the triblock terpolymers used for the preparation of the NCs.

Table 4.6. Molecular weights of the triblock terpolymers used in this study.

Entry	Apparent average molecular weight [g·mol^{-1}]			
	PVFc (M_n)[a]	PVFc (M_w)[a]	PMMA (M_w)[b]	PDMAEMA (M_w)[b]
$PVFc_{8.2}$-*b*-$PMMA_{90.2}$-*b*-$PDMAEMA_{1.6}$	17700	17800	88200	2500
$PVFc_{6.2}$-*b*-$PMMA_{88}$-*b*-$PDMAEMA_{5.8}$	8500	25800	173000	17900
$PVFc_{11.4}$-*b*-$PDMAEMA_{17.8}$-*b*-$PMMA_{70.8}$	8500	25800	75200	29600

[a] Determined by SEC-MALLS in THF; [b] Calculated from ^{1}H-NMR spectra.

The triblock terpolymers were used for the preparation of NCs by the solvent evaporation process from miniemulsion droplets.[200] This technique has been successfully applied for synthesis of NCs from different polymers including functional block copolymers[201] and for the encapsulation of various payloads.[39] The final morphology of a colloidal system consisting of different non-miscible phases strongly depends on the interfacial tensions between theses phases.[29]

Triblock terpolymer (Figure 4.13a) and hexadecane (a non-solvent for the copolymer) were dissolved in dichloromethane containing a small amount of Nile-Red (NR) and then mixed with a basic aqueous solution of cetyltrimethylammmonium chloride (CTMA-Cl) by stirring and ultrasonication to form a miniemulsion. After the evaporation of dichloromethane, the terpolymer precipitated at the droplet/water interface and formed a shell around the liquid core composed of hexadecane. These dispersions were later used for stimuli-responsive release experiments. The TEM images showed evidence of a core-shell structure for the NCs (Figure 4.13b-d). In the TEM images some NCs appeared to be collapsed inside the vacuum chamber of the electron microscope. The obtained NCs displayed hydrodynamic diameters between 190 and 225 nm while their polydispersity index were measured between 0.22 and 0.29 (Table 4.7) as determined by DLS measurements. The relatively high polydispersity index of the NCs is inherent to the preparation method used and not the result of droplet coalescence or aggregation.[202]

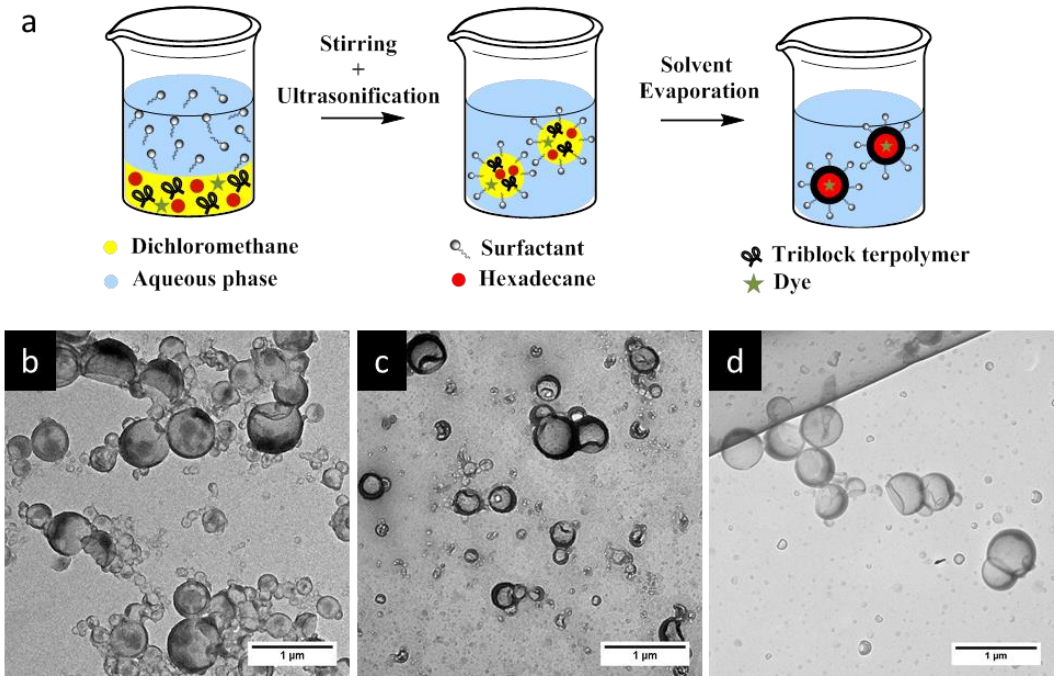

Figure 4.13. (a) Schematics for the preparation of the NCs by solvent evaporation miniemulsion. TEM images of NCs prepared with triblock terpolymers $PVFc_{8.2}$-*b*-$PMMA_{90.2}$-*b*-$PDMAEMA_{1.6}$ (b), $PVFc_{6.2}$-*b*-$PMMA_{88}$-*b*-$PDMAEMA_{5.8}$ (c), and $PVFc_{11.4}$-*b*-$PDMAEMA_{17.8}$-*b*-$PMMA_{70.8}$ (d).

Table 4.7 Sizes of NCs prepared from triblock terpolymers measured by DLS.

NCs shell	Hydrodynamic radius [nm] [a]	Polydispersity index [b]
$PVFc_{8.2}$-*b*-$PMMA_{90.2}$-*b*-$PDMAEMA_{1.6}$	225	0.29
$PVFc_{6.2}$-*b*-$PMMA_{88}$-*b*-$PDMAEMA_{5.8}$	193	0.22
$PVFc_{11.4}$-*b*-$PDMAEMA_{17.8}$-*b*-$PMMA_{70.8}$	190	0.29

[a] as measured by DLS; [b] determined at 90°

4.3.3. Stimuli-responsive release of the payload from triblock copolymers nanocapsules

The presence of a responsive unit in a shell is not a guarantee that the shell will allow for a release of payloads upon activation of the shell by an external stimulus. Therefore, we used different compositions of triblock terpolymers to achieve a significant triggered release of an encapsulated dye due to the presence of different morphologies. It is expected that an increase

in the length of a responsive block results in the increase of the shell responsivity to the stimuli. Therefore, triblock terpolymers with different block lengths were synthesized to determine the appropriate composition of the triblock terpolymer to yield an efficient stimulus-responsive release from the NCs. The stimuli-induced release of the payload was determined by monitoring the decrease of NR fluorescence with time in the aqueous release medium after application of the stimulus. We took the advantage of the fact that the fluorescence intensity of NR decreases largely in polar media.[203] The released amount of NR was calculated on the basis of that NR fluorescence intensity in an aqueous medium decreases upon application of stimuli due the opening of NCs.[204] The NCs dispersions were dialyzed before applying the pH change, redox agent, and temperature to remove any residual non-encapsulated dye. It is widely accepted that PVFc can be oxidized by a variety of oxidants.[205] The oxidation of the ferrocene complex to cationic iron species is associated with an increase of the polarity.[206, 207] This feature can be applied for the acceleration of payloads release. The response of NCs dispersions was determined by addition of H_2O_2 at various concentrations to the dispersions and monitoring the decrease of NR fluorescence in the aqueous release medium at *t* = 24 h. In general, the release of NR was more pronounced when H_2O_2 concentration increased from 4.4 to 35 wt. % (Figure 4.14a-b). Upon increasing of H_2O_2 concentration from 4.4 to 35 wt. %., there was an observable increment in the NR release up to 54%, 85%, and 91% from the NCs with 6.2, 8.2, and 11.4 mol% of PVFc, respectively (Figure 4.14a-b). At concentration of H_2O_2 equal 4.4 wt.%, there was a significant difference (30%) between the NR release from the NCs with 11.4 mol% PVFc and the NCs with 6.2 and 8.2 mol % of PVFc. This difference gradually decreased at intermediate concentrations of H_2O_2. Upon a further increase in H_2O_2 concentration to 35 wt.%, there was no significant difference between the release from the NCs with 8.2 and 11.4 mol% PVFc (Figure 4.14a and b). Therefore, the redox-responsive release from NCs largely depended on ratio oxidizing agent/responsive units in the copolymer. NCs with 11.4 mol% of PVFc displayed more response at the lowest concentration of H_2O_2. The significant increase in H_2O_2 concentration from 4.4 to 35 wt. % led to an excess of H_2O_2 and, therefore, the difference in mol% of PVFc between 8.2 and 11.4% was no longer a controlling parameter. This explains that the same

release from NCs with 8.2 and 11.4 mol% PVFc at 35 wt.% H_2O_2 concentration was observed. However, the increase in H_2O_2 concentration was effective until the amount of ferrocene moieties of PVFc remains sufficient for the oxidation reaction to ferrocenium. At a H_2O_2 concentration equal 35 wt.%, the released amount of NR from the NCs with 6.2 mol% of PVFc was 55% whereas it was 85% for the NCs with 8.2 mol% of PVFc. This significant difference implies that the small amount of ferrocene units of the NCs with 6.2 mol% of PVFc did not induce sufficient change in polarity to trigger release of the dye even if all ferrocene units of the NCs with 6.2 mol% of PVFc were oxidized. Therefore, increasing further the H_2O_2 concentration will not lead to a significant rise in the dye release.

PDMAEMA with tertiary amine groups in their side-chain can respond to pH and temperature.[51] Under acidic conditions, the tertiary amine groups are protonated and PDMAEMA (pK_a ~ 7.2) is water-soluble.[52] Furthermore, PDMAEMA display a hydrophilic-to-hydrophobic transition above its lower critical solution temperature (LCST) (~ 42 °C).[33] Therefore, the opening of the capsules can be triggered through change in the shell polarity upon application of pH value or temperature changes. Dispersions of the NCs were acidified to different pH values and the shell opening was correlated to the change of NR fluorescence intensity in the aqueous release medium. NCs shell containing 1.6 and 5.8 mol% of PDMAEMA did not respond significantly to acidification. Conversely, the NR fluorescence intensity for the NCs with 17.8 mol% of PDMAEMA decreased 50 and 95 at pH 2 and 1 compared to their control samples for release experiment, where pH value was measured 6.9, respectively (Figure. 4.14c). The temperature responsiveness of NCs was reported in term of NR fluorescence intensity changes. No effect of the temperature on the NR fluorescence intensity was also observed for NCs shell containing 1.6 and 5.8 mol% PDMAEMA. In the case of NCs shell containing 17.8 mol% PDMAEMA, NR fluorescence intensity increased upon the heating the dispersion above 75 °C. This is attributed to the PDMAEMA chains that undergo a molecular transition from a coiled to a dense globular structure. In other words, the environment of the dye was changed to hydrophobic, which resulted into an increase of fluorescence intensity at higher temperatures (Fig. 4.14d). Therefore, we selected for the studies in the ensuing section NCs which were prepared from

the triblock terpolymer containing PVFc and PDMEMA at molar percentage 11.4 and 17.8, respectively. Indeed, these polymers significantly responded to pH change, redox reagent, and temperature. In the rest of the section, the NCs prepared from the triblock copolymer $PVFc_{11.4}$-*b*-$PMMA_{70.8}$-*b*-$PDMAEMA_{17.8}$ is denominated as NC-TC.

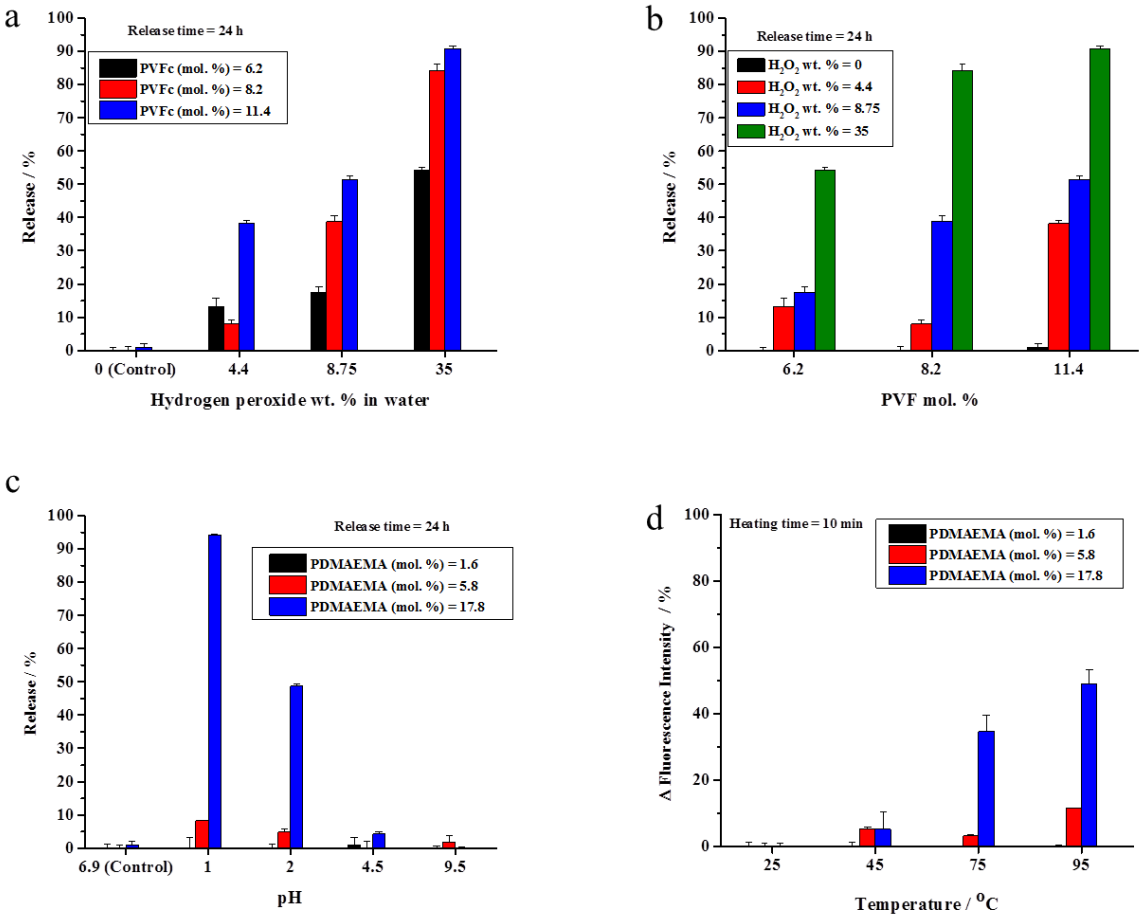

Figure 4.14. The released amount of NR out of the NCs prepared from triblock terpolymer with different compositions at different concentrations of H_2O_2 (a and b), different pH values (c). (d) The temperature responsiveness of the NCs at t = 10 min.

4.3.4. Stimuli-responsive release of the payload from nanocapsules consisting of blends of diblock copolymers

As mentioned in the introduction, triple stimuli-responsive release can also be in principle realized with a blend of two responsive diblock copolymers as shell material. Therefore, PVFc-*b*-PMMA and PDMAEMA-*b*-PMMA were synthesized to prepare NCs in order to gain additional insights into release profiles accompanied with changes on morphology. The molar percentage of PVFc and PDMAEMA were calculated so that it was possible to prepare polymer shells with the same concentration of shell. Furthermore, the molar amount of the different blocks was the same in the triblock terpolymer (NC-TC) and in the blend of diblock copolymers (NC-DC) (Table 4.6 and 4.8).

Table 4.8. Molecular weights of the diblock copolymers used in this study.

Entry	Apparent average molecular weight [g·mol^{-1}]			
	PVFc (M_n)[a]	PVFc (M_w)[a]	PMMA (M_w)[b]	PDMAEMA (M_w)[b]
$PVFc_{20}$-*b*-$PMMA_{80}$	9200	37400	70600	-
$PDMAEMA_{34}$-*b*-$PMMA_{66}$	-	-	89700	30500

[a] Determined by SEC-MALLS in THF; [b] Calculated from ^{1}H-NMR spectra.

TEM images of sample NC-DC showed evidence of core-shell structure (Figure 4.15b and c). The presence of small darker areas was observed on the surface of sample NC-DC in the TEM micrographs (Figure 4.15c) whereas they did not exist in TEM image of sample NC-TC (Figure 4.15d). The collapse of NCs due to the evaporation of the liquid core in the vacuum of SEM provides the opportunity to have a detailed insight to identify the observed small darker areas (Figure 4.15e and f). These small darker areas appeared as small domains and located on the interior surface of sample NC-DC (Figure 4.15ce). Therefore, microphase separation in sample NC-DC is evidenced by the presence of darker areas in TEM and the solid domains in SEM micrographs. The NC-TC displayed a patchy structure morphology consisting of very small grains

on the exterior surface of the NCs (Figure 4.15f), which revealed the presence of heterogeneities on the nanoscale on NC-TC surface.

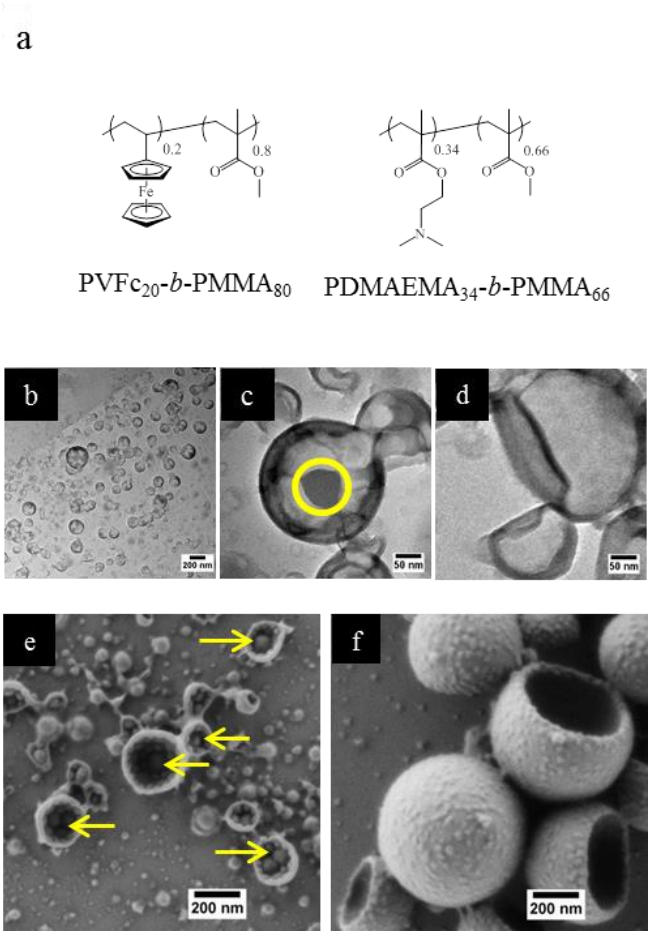

Figure 4.15. (a) Chemical structure of the diblock copolymers used for the preparation of sample NC-DC.TEM images (b and c) and SEM image (e) of the NCs prepared with the mixture of diblock copolymers, *i.e.* $PVFc_{20}$-*b*-$PMMA_{80}$ and $PDMAEMA_{34}$-*b*-$PMMA_{66}$. (d) TEM image and (f) SEM image of the NCs prepared from $PVFc_{11.4}$-*b*-$PDMAEMA_{17.8}$-*b*-$PMMA_{70.8}$. Yellow circle and arrows indicate small dark area and solid small domains in TEM and SEM images of the NCs prepared from $PVFc_{20}$-*b*-$PMMA_{80}$ and $PDMAEMA_{34}$-*b*-$PMMA_{66}$.

The response of NC-DC dispersions to oxidation, changes of pH and temperature, was investigated after removing the non-encapsulated dye by dialysis. The change of the NR

florescence intensity was followed to monitor the NCs opening (Figure 4.16). The overall release of the payload is the sum of two contributions - burst and (slow) diffusive release.[52] We studied pH and redox-induced release of NR from NC-DC and NC-TC at *t* = 10 and 1440 min (Figure 4.16).

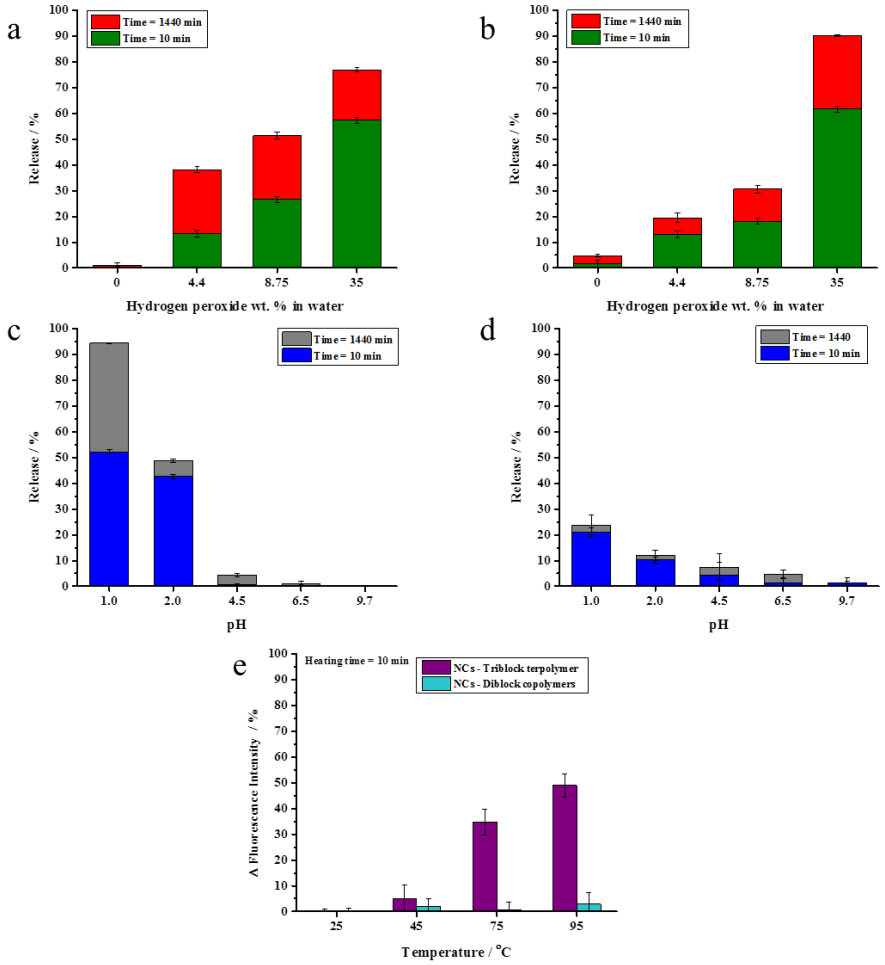

Figure 4.16. Released amount of NR at different H_2O_2 concentrations out of the NCs consisting of $PVFc_{11.4}$-*b*-$PDMAEMA_{17.8}$-*b*-$PMMA_{70.8}$ (a) and the mixture of $PVFc_{20}$-*b*-$PMMA_{80}$ and $PDMAEMA_{34}$-*b*-$PMMA_{66}$ (b) at *t* = 10 and 1440 min. The released amount of NR at different pH values for NCs prepared from the aforementioned triblock terpolymer (c) and the mixture of diblock copolymers (d) at *t* = 10 and 1440 min. (e) The temperature responsiveness of both types of NCs at *t* = 10 min.

There was a remarkable increase in NR release from 38 to 77% for sample NC-TC and from 20 to 90% for sample NC-DC upon increasing the concentration of H_2O_2 from 4.4 to 35 wt.% (Figure 4.16a-b). At a H_2O_2 concentration of 8.75 wt.%, the NR release out of NC - DC was 30% whereas the value for NC-TC reached 52%. Furthermore, the ratio between burst and diffusive release ($R_{b/d}$) for NC-TC and NCs-DC depended on the H_2O_2 concentration. $R_{b/d}$ increased from 0.5 to 3 for the NC-TC while it was almost constant (2.2) for sample NC-DC. The dispersions of NC-TC and NC-DC did not exhibit observable NR release at basic pH value whereas the release slightly increased at intermediate pH values (4.5 and 6.5) and reached 4% for NC-TC and 8% for NC-DC (Figure 4.16c-d).Upon further decrease of the pH value to 2 and below, the release reached 24% in the case of sample NC-DC, while about 95% of the encapsulated NR was released at pH 1.0 for sample NC-TC at t = 1440 min. Moreover, these results showed that diffusive release played a key role in the efficient release at pH 1.0. No effect of temperature on the release of NR was observed for sample NC-DC (Figure 4.16e). These results show that the NCs of a blend of diblock copolymers did not significantly respond to the pH change and temperature. In contrast, the NCs prepared from the triblock terpolymer exhibited a responsive behavior to pH change and temperature. Because the composition of the NCs is the same, the difference in release profile must be associated with differences in the microstructure of the polymer shell (Figure 4.15). Therefore, the samples NC-DC and NC-TC were analyzed in detail.

It is widely accepted that PDMAEMA accept protons under acidic conditions and thus the polymer chain tends to expand due to coulombic repulsion.[50] Thereby, one can expect an increase in the hydrodynamic radius of NCs due to gradual protonation and consequent swelling of the PDMEAMA block under acidification if this block is present on the surface of the NCs. The dispersions of both types of the NCs were subjected to different pH values and change of hydrodynamic radius was followed (Table 4.9). In the case of sample NC-TC, there was no observable change in hydrodynamic radius at pH 9.5 and 6.5 while an increase of 14 nm was observed at pH 4.5. The hydrodynamic radius of NC-DC exhibited a sharp increase (42 nm) when the pH value was decreased from 9.5 to 6.5. Upon further decrease to a pH value of 4.5, the hydrodynamic radius of NC-DC did not display a significant increase compared to their size

at pH 6.5 and reached 170 nm. The more pronounced increase in size for NC-DC (45 nm) than for NC-TC (15 nm) upon acidification suggests that a larger number of pH-responsive units is accessible in NC-DC. The non-responsive blocks ensured the structural integrity of the NCs by preventing dissolution of the block copolymers in the aqueous phase upon acidification. The zeta potential of the NCs dispersions were also measured at different pH values to monitor changes in the surface charge of the NCs caused by the protonation of PDMAEMA block segments on the NCs surface (Table 4.9). At pH 6.5, the zeta potential of sample NC-TC was 43 mV and it slightly increased to 48 mV upon the further decreasing the pH to 4.5. Moreover, there was no observable change in the zeta potential of sample NC-TC when the pH value increased from 6.5 to 9.5. The zeta potential of sample NC-DC was 36 mV at pH 9.5 while upon the further decreasing the pH to 6.5 and 4.5, it increased to 45 and 50 mV, respectively. The zeta potential results imply that PDMEAMA block segments were present on the surface of NC-TC and NC-DC since the NCs surface charge increased due to the PDMEAMA protonation upon acidification of the dispersions. It can be also concluded from the zeta potential measurements that the quantity of PDMEAMA block segments presenting on the surface of NC-TC was lower than of NC-DC since the latter displayed more significant change in its surface charge upon pH change. Although the increment in zeta potential for sample NC-TC upon acidification is not large, this slight increase can be correlated with the investigations reported above with electron microscopy.

Table 4.9. Hydrodynamic radius and zeta potential of NCs prepared from the triblock copolymer $PVFc_{11.4}$-*b*-$PDMAEMA_{17.8}$-*b*-$PMMA_{70.8}$ (NC-TC) and the mixture of the diblock copolymers $PVFc_{20}$-*b*-$PMMA_{80}$ and $PDMAEMA_{34}$-*b*-$PMMA_{66}$ (NC-DC) at different pH values.

Entry	Hydrodynamic radius [nm]			Zeta potential [mV]		
	pH = 4.5	pH = 6.5	pH = 9.5	pH = 4.5	pH = 6.5	pH = 9.5
NC-TC	204 ± 122	190 ± 102	191 ± 117	48 ± 11	43 ± 5	43 ± 6
NC-DC	169 ± 61	165 ± 69	123 ± 48	50 ± 8	45 ± 7	36 ± 7

In order to further prove that the microstructure was responsible for the difference in release profile for nanocapsules with the same chemical composition but different chemical structure (triblock terpolymer vs diblock), we carried out selective staining on the dried nanocapsules. Indeed, the reaction between selective agents and a polymer system leads can enhance the electron density contrast for TEM studies. In this study, iodomethane and chlorotrimethylsilane were utilized as staining agents to demonstrate whether the NCs surface contains PVFc and PDMAEMA segment blocks. Before that, PDMAEMA-*b*-PMMA NCs and PVFc-*b*-PMMA NCs were synthesized (Figure 4.17) and used to determine how iodomethane and chlorotrimethylsilane change TEM contrast of these NCs in reaction with PVFc and PDMAEMA block segments.

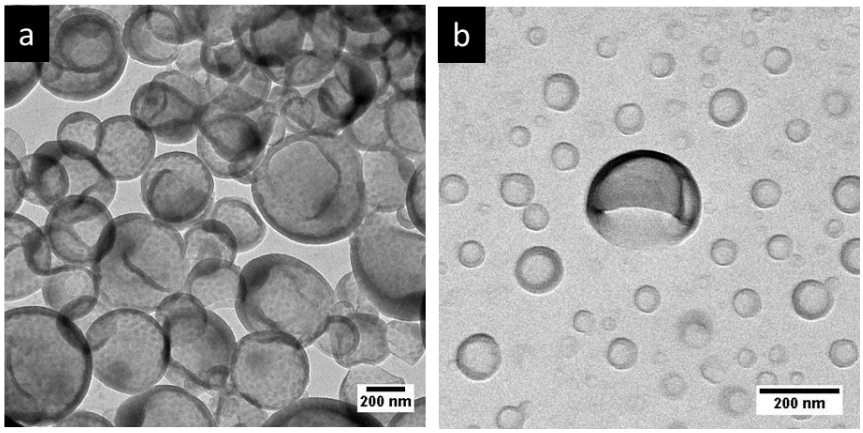

Figure 4.17 TEM images of NCs prepared from $PVFc_{20}$-*b*-$PMMA_{80}$ diblock copolymer (a) and from $PDMAEMA_{34}$-*b*-$PMMA_{66}$ diblock copolymer (b). In the case of first one, the presence of the iron in PVFc caused an inherent contrast between the two building blocks.

Upon utilization of iodomethane as staining agent, the surface of NC-TC became dark and exhibited some black spots (Figure 4.18a) whereas no significant change was observed for NC-DC (Figure 4.18b). Moreover, the surface of NCs prepared from PVFc-*b*-PMMA block copolymer became dark after staining with iodomethane (Figure 4.18c) while the TEM micrograph of NCs prepared from PDMAEMA-*b*-PMMA block copolymer did not display any contrast change (Figure 4.18d). These results imply that PVFc is present on the surface of NC-TC and not on the surface of NC-DC since iodomethane reacts with PVFc units by an oxidation reaction. Upon

application of chlorotrimethylsilane, a change in the TEM contrast and morphology of NC-TC, NC-DC, and NCs prepared from PDMAEMA-*b*-PMMA block copolymer were observed (Figure 4.18e-g). However, there was no observable difference in the TEM micrograph of NCs prepared from PVFc-*b*-PMMA block copolymer after staining with chlorotrimethylsilane (Figure 4.18h). Staining experiments with chlorotrimethylsilane suggest that PDMAEMA existed on the surface of NC-DC and NC-DC since chlorotrimethylsilane reacts with PDMAEMA units. One can conclude from the staining results that the shell of sample NC-DC contained two domains: PDMEAMA-*b*-PMMA diblock copolymer as the exterior layer and PVFc-*b*-PMMA block copolymer as the interior layer.

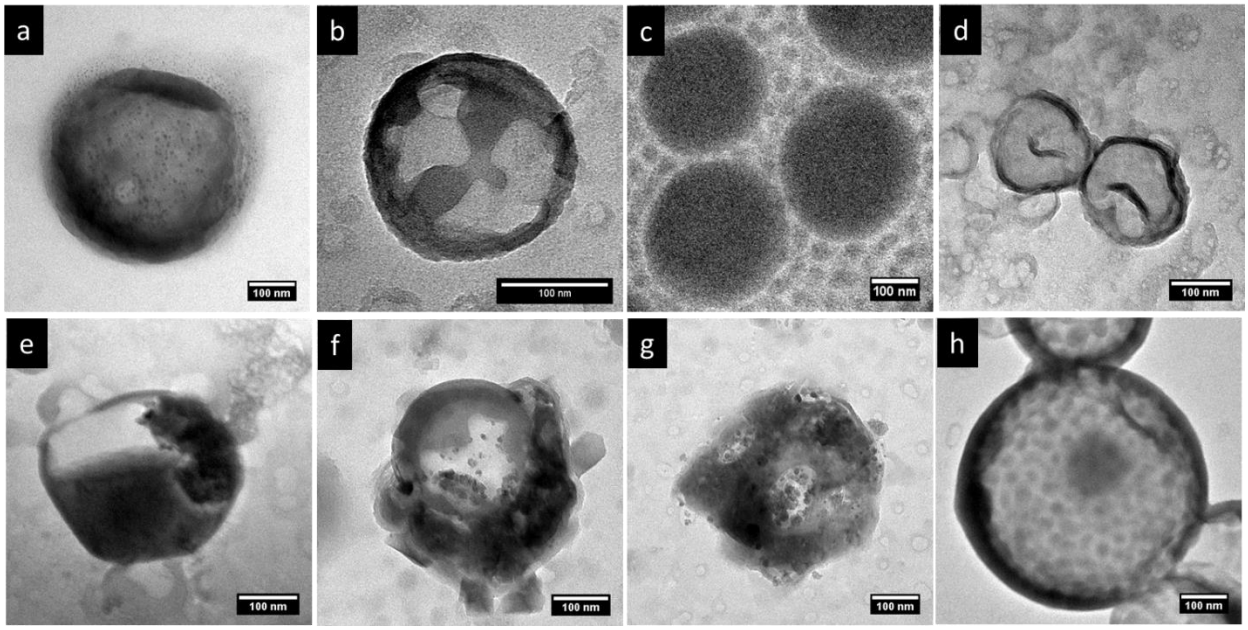

Figure 4.18. TEM images of NCs prepared from (a) $PVFc_{11.4}$-*b*-$PDMAEMA_{17.8}$-*b*-$PMMA_{70.8}$ block copolymer (sample NC-TC), (b) the mixture of $PVFc_{20}$-*b*-$PMMA_{80}$ and $PDMAEMA_{34}$-*b*-$PMMA_{66}$ block copolymers (sample NC-DC), (c) $PVFc_{20}$-*b*-$PMMA_{80}$ block copolymer, and (d) $PDMAEMA_{34}$-*b*-$PMMA_{66}$ block copolymer after selective staining experiment with iodomethane. TEM images of (e) sample NC-TC, (f) sample NC-DC, (g) NCs prepared from $PDMAEMA_{34}$-*b*-$PMMA_{66}$ block copolymer, and (h) NCs prepared from $PDMAEMA_{34}$-*b*-$PMMA_{66}$ block copolymer after selective staining experiment with chlorotrimethylsilane.

Microphase separation (Figure 4.15) between PVFc-*b*-PMMA and PDMAEMA-*b*-PMMA diblock copolymers in NC-DC shells can explain the observed differences in stimuli-induced release of the payload between NC-DC and NC-TC. In the case of NC-TC, the PVFc and PDMAEMA blocks were located on the NCs surface. The carefully designed triblock terpolymer precisely targeted the desired triple stimuli-responsive release of the payload as depicted in the Figure 4.19a. In the case of NC-DC, the phase separation occurred between PVFc-*b*-PMMA and PDMAEMA-*b*-PMMA diblock copolymers, with PDMAEMA-*b*-PMMA and PVFc-*b*-PMMA block copolymers forming the exterior and the interior layer of the shell, respectively. The interior layer played the role of a barrier that hinders the function of PDMAEMA as pH-responsive unit (Figure 4.19b). Furthermore, the presence of higher relative amount of PDMAEMA block segment on the shell surface of NC-DC resulted in the protonation and the subsequent swelling of PDMAEMA-*b*-PMMA diblock copolymer even at intermediate pH-values (pH 6.9) (Table 3). Therefore, the PDMAEMA-*b*-PMMA diblock copolymer, as the exterior layer, did not hinder the access of H_2O_2 to PVFc segment block and consequently the release of NR at pH 6.9.

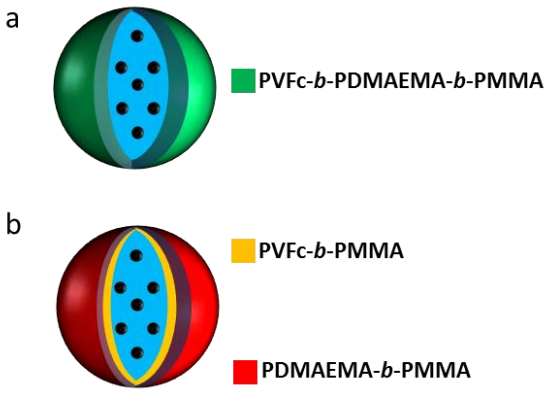

Figure 4.19. Schematic illustration of the configuration of shell-forming materials for (a) NCs prepared from $PVFc_{11.4}$-*b*-$PDMAEMA_{17.8}$-*b*-$PMMA_{70.8}$ triblock terpolymer and (b) NCs prepared from the mixture of $PVFc_{20}$-*b*-$PMMA_{80}$ and $PDMAEMA_{34}$-*b*-$PMMA_{66}$ block copolymers. Microphase separation inside the shell is the consequence of the latter one whereas a fine distribution of the segment blocks is achieved for the first one.

4.3.5. Conclusions and outlook

Triple stimuli-responsive NCs consisting of PVFc-*b*-PMMA-*b*-PDMAEMA triblock terpolymer were prepared by the solvent evaporation process from miniemulsion droplets. The NCs could encapsulate the dye in the core and protect it from leakage. The NCs dispersions exhibited high colloidal stability in aqueous release medium. The triggered release of the payload was achieved because the NCs shell was addressable by three different stimuli: pH change, oxidizing agent, and temperature. Alternatively, NCs prepared with a blend of responsive diblock copolymers, where their shells had exactly the same chemical composition in term of molar amount of blacks with NCs prepared from triblock copolymer. However, microphase separation occurred between the diblock copolymers in the NCs shell, which resulted in formation of shells with non-homogenous distribution of the diblock copolymers across the shell. Our results imply that PVFc-*b*-PMMA and PDMAEMA-*b*-PMMA diblock copolymers formed the interior and exterior layer across the shell, respectively. The exterior layer was not addressable more since its access to the core was hindered by the interior layer. This configuration of diblock block copolymers across the shell, therefore, made these NCs stimulus-responsive instead of triple stimuli-responsive. This study revealed how microstructure of containers shell dictates the release properties of payloads from polymer NCs and pave the way to precisely design NCs with addressable and high functional shell for applications in which selective delivery of one or several payloads upon application of different stimuli is necessary.

4.4. The pro-active payload strategy significantly increases selective release from mesoporous nanocapsules[4]

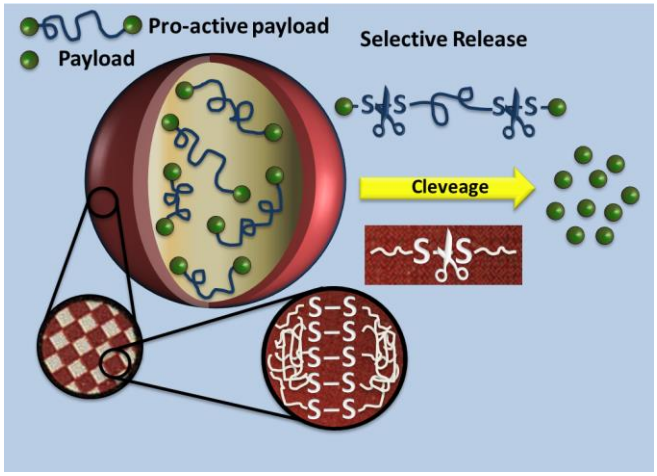

In previous sections, controlled-release systems mainly based on capsules with polymer shell were developed. Beside these polymer nanocapsules, nanocapsules consisting of a mesoporous shell (*e.g.* silica shell) have been widely highlighted as a versatile tool for the encapsulation of diverse molecules for different applications. The controlled release of payloads from mesoporous silica nanocapsules (SiNCs) consisting of stimulus-responsive shells is of considerable interest in applications such as self-healing and drug delivery materials. However, the release of payloads from SiNCs before the application of external triggers (*i.e*. non-selective release) remains a challenge. In fact, the non-selective release of payloads from SiNCs occurs because of the mesoporous nature of the silica shell that cannot trap payloads in the core of SiNCs perfectly. We establish an efficient and straightforward strategy based on the encapsulation of a pro-active payload to hinder the non-selective release of small payloads from mesoporous capsules. A pro-active payload is defined as a compound that is converted to an active functional molecule in the environment where it is needed. In this sense, it is a generalization of a prodrug. Encapsulating a pro-active payload instead of a payload allowed to hinder the non-selective release of the payload from SiNCs. A selective release of the payload could be achieved upon reduction of the encapsulated pro-active payload. Furthermore, the

[4] Parts of this section are submitted to Chemistry of Materials under the title "The pro-active payload strategy significantly increases selective release from mesoporous nanocapsules".

total amount of released substance is significantly enhanced by introducing responsive groups in the silica shell. These results show that the pro-active payload strategy combined with the use of stimulus-responsive materials can be successfully exploited to achieve selective release of cargo from mesoporous nanocapsules.

4.4.1. Motivation

As explained in previous sections, successful capsules for controlled-release applications should load/encapsulate molecules in large quantities and selectively deliver these molecules "just in time" upon the application of desired stimuli. Furthermore, they should be colloidally stable and remain intrinsically stable even after activation by external stimuli, especially for a pulsatile release of payloads which is interesting for applications such as corrosion monitoring and nanomedicine. Silica capsules have been widely highlighted as a versatile tool for the encapsulation of diverse molecules for drug delivery[168, 208-211] and anticorrosion[18, 212, 213] since they possess the aforementioned qualifications. The triggered release of payloads from silica capsules has been achieved by exploiting novel stimuli-responsive shell-forming materials sensitive to pH value, temperature, and redox reactions.[168, 213-217] Among possible reactions to trigger the release of payloads from capsules, oxidations and reductions have gained increasing attention because of the potential use in biomedical and anticorrosion applications. Glutathione-responsive capsules are good examples for a triggered intracellular drug and gen delivery because several intracellular compartments such as mitochondria, cytosol, and cell nucleus contain a high concentration of glutathione tripeptides compared to the extracellular fluids.[147, 149, 218, 219] It is widely accepted that reduction is the most reliable and selective trigger for sensing corrosion of metallic systems since the electrochemical potential of these systems decrease when corrosion occurs.[19, 220-222] The disulfide bond can be cleaved by reduction and this feature was exploited to synthesize materials containing disulfide bonds to achieve redox-responsive release from mesoporous silica.[18, 152, 213, 223-227] However, the development of silica systems capable of releasing the payload only in response to a specific external stimulus (*i.e.*, selective release) within a realistic timescale - few days for pharmaceutical applications[228] and

thousands of days for coatings[229] - remains a challenge. Nanocapsules consisting of silica shells are highly porous and this feature leads to non-controlled release of encapsulated (mainly low molecular weight) payloads, *i.e.* non-selective release. This non-selective release hampers the efficient storage of the payload before site-selective delivery by SiNCs upon application of external stimuli. Coatings containing capsules for the detection and hindrance of corrosion are good examples of applications with a considerable lag time between implementation of capsules and desired time for triggered release. Tremendous attempts have been devoted to overcome the non-selective release by tuning the pore size and geometry of silica carriers.[69, 230-233] In spite of these achievements, highly efficient and selective release from silica capsules have not been successfully achieved yet, especially for small molecules.

We aim here to significantly hinder non-selective release of low molecular weight payloads from silica NCs. To fulfill this goal, we first prepared a pro-active payload that is defined as a compound that is converted to an active functional molecule in the environment where it is needed. In this sense, it is a generalization of a prodrug. We then compared the release profiles of three SiNCs systems containing either payload or pro-active payload and non-responsive or redox-responsive silica shells. The strategy for hindering non-selective release of a payload by encapsulating a pro-active payload is depicted in Figure 4.20.

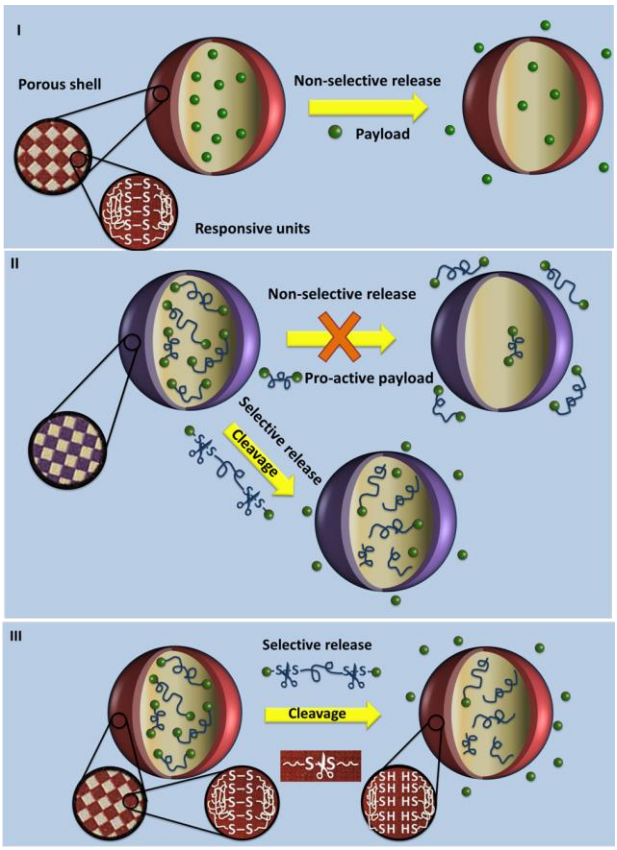

Figure 4.20. Schematic illustration of the release of a payload from SiNCs I: The porous shell of SiNCs cannot hinder non-selective release of the payload from the core II: Non-selective release is largely hindered by using the pro-active payload due to a significant increase in molecular size and due to a decrease in water solubility compared to the payload. The payload can be selectively delivered by cleavage from the encapsulated pro-active payload by reduction. III: The final released amount of the payload significantly enhances when the pro-active payload and the silica shell are responsive to reductive conditions.

4.4.2. Preparation of silica nanocapsules

The SiNCs were synthesized by miniemulsion polymerization following a previously reported procedure.[213] The miniemulsion droplets were used as templates for the hydrolysis and condensation of tetraethoxysilane (TEOS) at the droplets interface in order to achieve the encapsulation of m-xylene containing either the payload or the pro-active payload (*i.e.*

hydrophobic core). Bis[3-(triethoxysilyl)propyl] tetrasulfide (TESPT) was also introduced in the nanocapsule shell to allow a redox-responsive release of either the payload or the pro-active payload from the core (Figure 4.21a and Table 4.10). Tris(2-carboxyethyl)phosphine hydrochloride (TCEP), as reducing agent, is known to efficiently and selectively reduce disulfide bonds.[234, 235] Furthermore, it has been found to possess also advantageous effects against corrosion of galvanized steel[236], or as Hg^{2+} adsorbent.[237] SiNCs with average hydrodynamic diameters between 130 ± 56 and 175 ± 68 nm were obtained (Table 4.10). The TEM and SEM images presented evidence of a core-shell morphology (Figure 4.21b-c). The observed collapse of some SiNCs in SEM micrograph (Figure 4.21c) is due to their shrinkage caused by the vacuum of the electron microscope chamber.

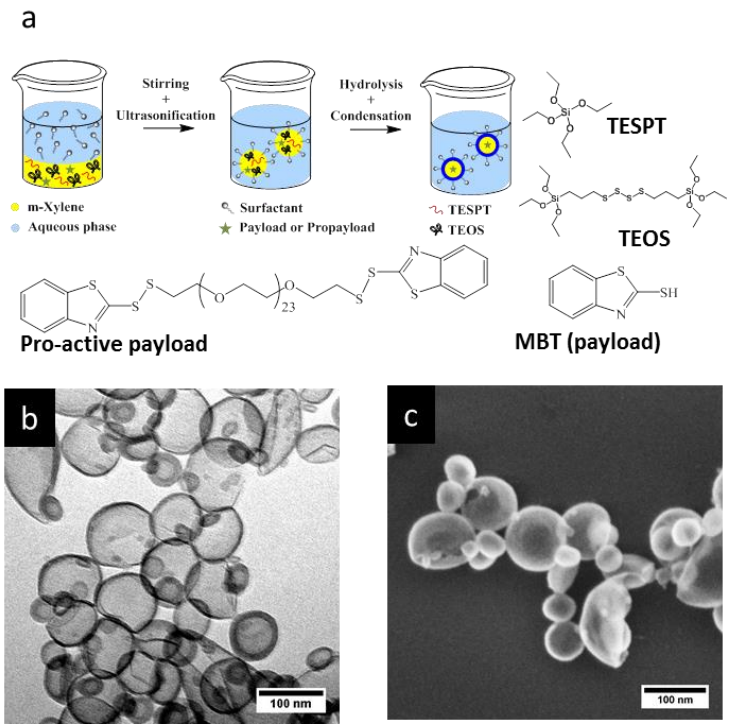

Figure 4.21. (a) Schematic illustration of the nanocapsule preparation by miniemulsion polymerization. (b) TEM and (c) SEM micrographs of SiNCs containing MBT (sample SiNCs-SSSS-(MBT), Table 4.10).

Table 4.10. Composition of the dispersed phase of SiNCs and average hydrodynamic diameters of the SiNCs used in the experiments.

Entry	TEOS [g]	TESPT [g]	Cargo [mg]		Average hydrodynamic diameter [nm]
SiNCs-SSSS-(MBT)	1.5	0.5	MBT	3	175 ± 68
SiNCs-(PEG-MBT)	2.0	-	PEG-MBT	12	130 ± 56
SiNCs-SSSS-(PEG-MBT)	1.5	0.5	PEG-MBT	12	162 ± 62

The SiNCs were loaded with either 2-mercaptobenzothiazole (MBT) (*i.e.* the payload) or α,ω-(2,2'dithio[benzothiazolyl])-poly(ethylene glycol) (PEG-MBT) (*i.e.* the pro-active payload) by dissolving MBT and PEG-MBT in *m*-xylene before emulsification. In both cases, the final concentrations of MBT in the dispersed phases of the samples were calculated to be identical. MBT was selected because of its excellent corrosion inhibiting properties.[19, 99] Moreover, the absorption of MBT can be well distinguished in an aqueous medium (Figure 5.5), the release behavior of MBT could therefore be determined by monitoring its concentration over time in the continuous phase of the dialyzed dispersions. The formation of the pro-active payload (PEG-MBT) was carried out by condensation of poly(ethylene glycol) dithiol (PEG dithiol) with 2,2'-dithiobis(benzothiazole) by a thiol-disulfide interchange reaction (Figure 4.22).[238]

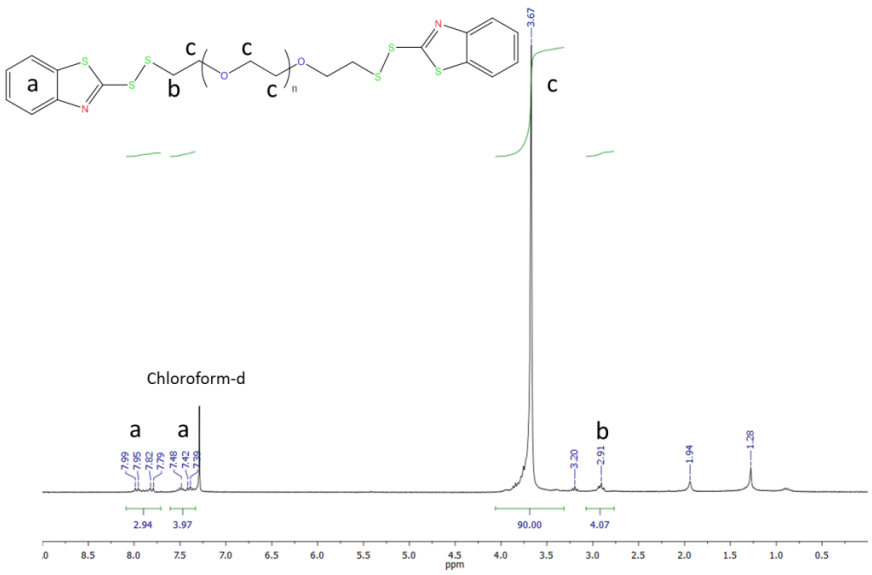

Figure 4.22. ^{1}H NMR spectrum of α,ω-(2,2'dithio[benzothiazolyl])-poly(ethylene glycol) (PEG-MBT) in chloroform-d.

The successful cleavage of MBT from the pro-active payload upon application of TCEP was proven (98%) by a preliminary experiment in which *m*-xylene containing the pro-active payload was stirred for 24 h with an aqueous phase containing of TCEP at room temperature (4.23). The encapsulation efficiency after emulsification, calculated by subtracting the total amount of the cargo in dispersion from the amount of cargo in the continuous phase, was determined by centrifugation of the dispersion and measuring the concentration of MBT and PEG-MBT in the supernatant. The amount of PEG-MBT in the supernatant was determined by reducing PEG-MBT at room temperature by TCEP and measuring the concentration of MBT after 24 h. The encapsulation efficiencies for SiNCs-SSSS-(MBT), SiNCs-(PEG-MBT), and SiNCs-SSSS-(PEG-MBT) were calculated to be 84%, 97%, and 100%, respectively. The observed increase in encapsulation efficiency for the SiNCs containing PEG-MBT is attributed to a lower water solubility of the pro-active payload (practically insoluble) than MBT (0.32 $g \cdot L^{-1}$).

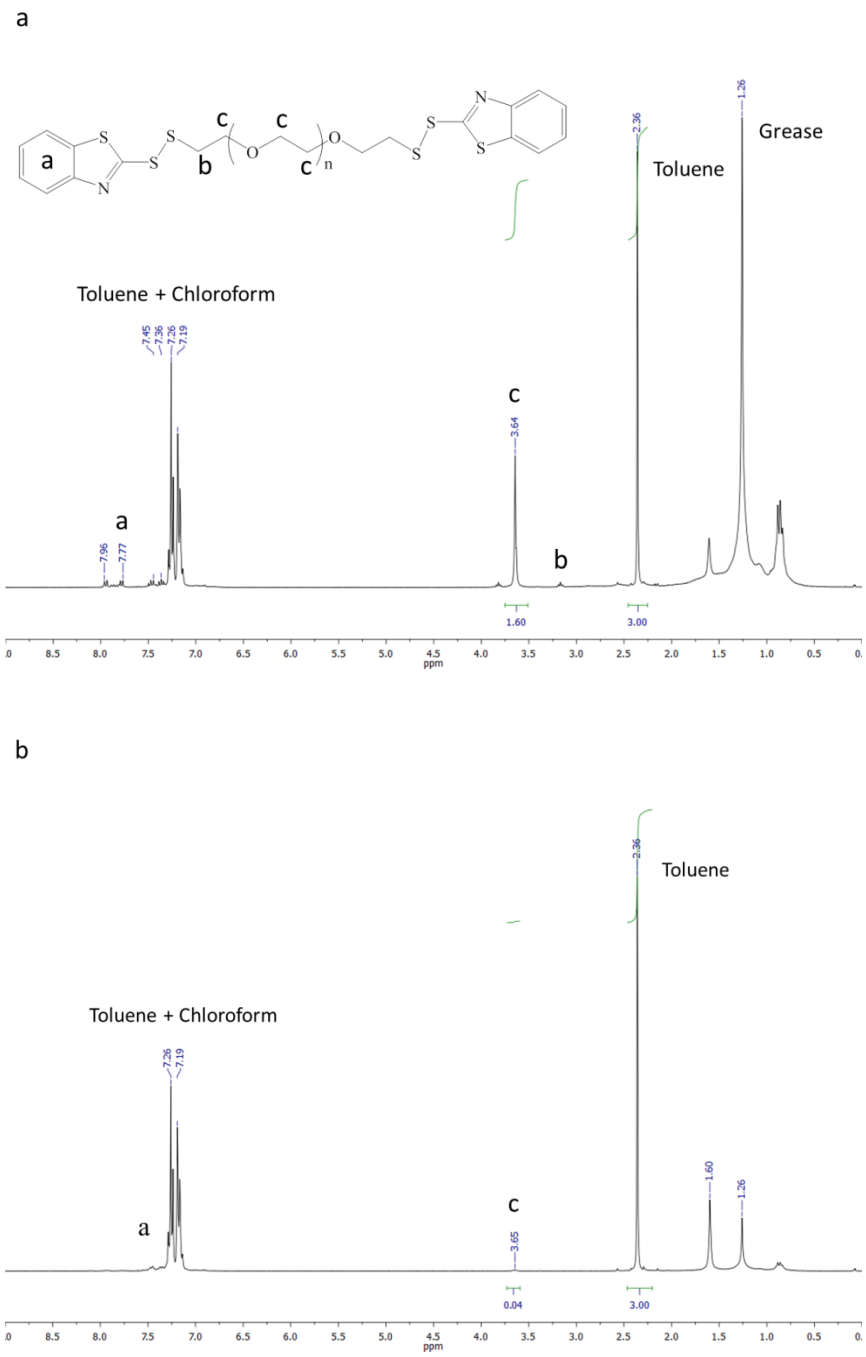

Figure 4.23. ^{1}H NMR spectra of *m*-xylene phases containing PEG-MBT after stirring with (a) distilled water and (b) and an aqueous solution containing TCEP.

4.4.3. Release of the payload and the pro-active payload

Insight into the release properties of SiNCs-SSSS-(MBT) was gained by monitoring the concentration of released MBT over time. The non-selective release of MBT from SiNCs-SSSS-(MBT) gradually increased with time and was measured to be 40% at *t* = 1440 min (Figure 4.24a) (see SI for the details of release experiments). The responsivity of SiNCs-SSSS-(MBT) was also investigated by addition of tris (2-carboxylethyl)phosphine (TCEP) in the aqueous release medium. Upon addition of TCEP to the release medium, the release profile of MBT displayed an initial release of 50% at *t* = 60 min and a released amount of 71% at *t* = 1440 min (Figure 4.24a). The change in the release profile of MBT after application of the reducing agent was attributed to the increase in the permeability of shells because the disulfide bonds were cleaved. According to these two values (*i.e.* 40 and 71%), 44% of the final released amount of MBT can be considered as selectively released at *t* = 1440 min. The high value for the non-selective release is mainly associated with the small size of MBT and the incapacity of porous silica shell to efficiently trap the payload in the core. However, these results imply that the disulfide bonds of the shell can successfully be cleaved upon application of the reducing agent and thereby trigger the release of MBT in the first 120 min (Figure 4.24a).

In order to examine whether the encapsulation of the pro-active payload effectively hinders the non-selective release of the payload from the mesoporous silica shell, the release profile of PEG-MBT from SiNCs-(PEG-MBT) in the aqueous release medium was measured over time. To determine the released amount of PEG-MBT over time, TCEP was added to samples which were withdrawn from the release medium at certain intervals of time and these reaction mixtures were kept at room temperature for 24 h before measuring the concentration of MBT (Figure 4.24b). These SiNCs were found to release a small amount of the pro-active payload (8%) after 1440 min, which corresponds to a 5 times decrease in the value of non-selective release of MBT compared to SiNCs-SSSS-(MBT) (40%). This significant decrease in the non-selective release of MBT from SiNCs-(PEG-MBT) can be explained by the facts that (i) the pro-active payload (M_w ~

1334 g·mol^{-1}) has larger molecular size than MBT (M_w = 167 g·mol^{-1}), and (ii) the pro-active payload has a much lower solubility in the aqueous release medium compared to MBT.

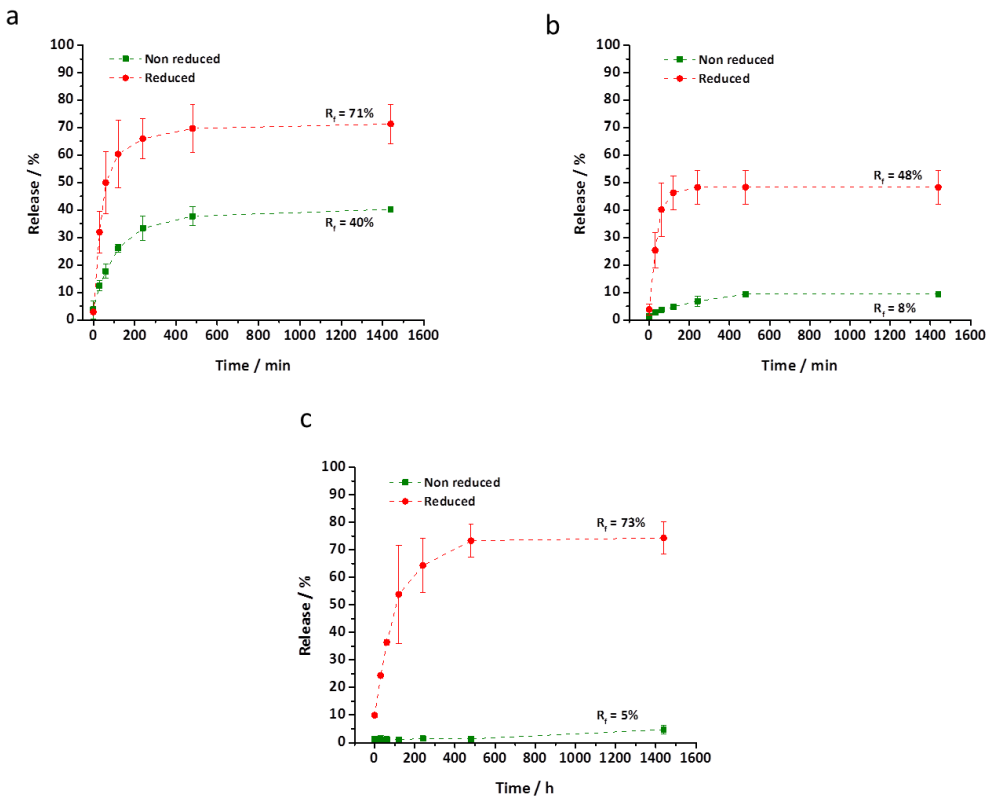

Figure 4.24. Temporal release profiles of**:** (a) MBT from non-reduced and reduced SiNCs consisting of TEOS and TESPT (sample SiNCs-SSSS-(MBT)), (b) PEG-MBT and MBT from SiNCs consisting of TEOS (sample SiNCs-(PEG-MBT)) before and after cleavage of MBT from PEG-MBT by TCEP, respectively, and (c) PEG-MBT from SiNCs consisting of TEOS and TESPT (sample SiNCs-SSSS-(PEG-MBT)), and MBT from these SiNCs upon reductive condition. R_f refers to the final released amount of the cargo at t = 1440 min.

In fact, larger molecules require larger pore sizes and need higher activation energies to diffuse through the shell. However, the reduction of non-selective release of the pro-active payload is not a guarantee that the SiNCs will allow for a selective-release of the payload. Therefore, we investigated the cleavage of MBT from the pro-active payload encapsulated in SiNCs by

measuring the released amount of MBT over time after the addition of the reducing agent in the aqueous release medium. The results showed that the addition of the reducing agent triggered the cleavage of MBT with a fast release (46%) in the first 120 min (Figure 4.24b). The selective release of MBT form SiNCs-(PEG-MBT) was calculated to be 83% of the final released amount of MBT (48%) after 1440 min.

As shown before, the cleavage of the disulfide bond introduced in the silica shell by the addition of TESPT triggered the delivery of MBT. Therefore, one can conclude that the final released amount of MBT would be maximized for reduction-responsive SiNCs containing PEG-MBT (sample SiNCs-SSSS-(PEG-MBT)). The cleavage of disulfide bonds across the silica shell upon reduction by TCEP is expected to increase the shell permeability. This facilitated the release of MBT molecules after cleavage of the pro-active payload in higher quantities compared to the non-reduced shell. The non-selective release of MBT for SiNCs-SSSS-(PEG-MBT) was 5% while the final released amount of MBT upon reduction by TCEP was 73% (Figure 4.24c). Therefore, the value of final release from SiNCs-SSSS-(PEG-MBT) increased by 52% in comparison with this value for SiNCs-(PEG-MBT). Additionally, the selective release of MBT from SiNCs-SSSS-(PEG-MBT) was calculated to be 93% of the final released amount, which represents 12% increase compared to this value for SiNCs-(PEG-MBT) (83%) (Figure 4.24b-c). The release values of the SiNCs contents are summarized in Table 4.11.

Table 4.11. The values of non-selective release, final released amount, and selective release of the cargo from the SiNCs at *t* = 1440 min.

Entry	Release value [%]			
	Non-selective release		Final released amount of MBT	Selective release of MBT [a]
	MBT	PEG-MBT		
SiNCs-SSSS-(MBT)	40	-	70	44
SiNCs-(PEG-MBT)	-	8	48	83
SiNCs-SSSS-(PEG-MBT)	-	5	73	93

[a] Selective release / % = $\frac{(\text{Final released amount }) - (\text{Non-selective release})}{\text{Final released amount}} \times 100$

4.4.4. Conclusions and outlook

The concept of utilizing pro-active payloads in order to significantly increase the selective release of small size payloads from mesoporous nanocapsules was demonstrated. Silica nanocapsules were successfully synthesized by hydrolysis and condensation of functional alkoxysilane in miniemulsion droplets. The tetrasulfide groups were used as shell-forming materials to achieve reduction-responsive shells. The non-selective release of 2-mercaptobenzothiazole (MBT) from silica nanocapsules were measured to be 40%. The release of MBT from the silica nanocapsules was triggered (71%) by reduction of the tetrasulfide groups of the shell upon addition of the reducing agent. However, the non-selective release of MBT (40%) largely decreased the efficiency of these silica nanocapsules for the precise delivery of the payload. To overcome the problem of non-selective release, a pro-active payload consisting of MBT molecules coupled to poly(ethylene glycol) dithiol (PEG dithiol) was synthesized. The pro-active payload could not diffuse through the silica shell due to its larger molecular size compared to MBT. Additionally, MBT molecules were selectively cleaved form the encapsulated pro-active payload upon the application of reducing agent and subsequently entered to release medium. The combination of the encapsulation of the pro-active payload and the responsive behavior of the silica nanocapsules resulted in increasing the final released amount of MBT up to 73% while 93% of MBT in the release medium could be selectivity delivered from the silica nanocapsules. This work presents a successful model to achieve selective release of the payload from the porous shell. This insight into the superior behavior of nanocapsules containing pro-active payloads will pave the way to design and synthesize controlled release systems with unique potential to selectively release payloads “just in time” upon specific environmental conditions.

5. Experimental part

5.1. Experimental details for section 4.1

5.1.1. Materials

2-Nitrophenol sodium salt was purchased from Santa Cruz Biotechnology, Inc. 1,4-diaminobutane (>98.0%) and phosphonoformic acid trisodium salt hexahydrate (Foscarnet) (>98.0%) were purchased from Alfa Aesar. Potassium chloride (KCl) (≥99.%), calcium chloride (CaCl2) (≥96.0%), and potassium thiocyanate (KSCN) (≥99.0%) were purchased from Sigma Aldrich. 2,4-toluene diisocyanate (TDI) and cyclohexane (≥99.9%) were purchased from Sigma Aldrich. The surfactant Lubrizol U was supplied from Lubrizol Ltd. The potassium, calcium, and phosphorous standard solutions for ICP-OES were purchased from AppliChem GmbH, Chem-Lab NV, and Fisher Scientific respectively. All chemicals or materials were used without further purification. Distilled water was used through all the experiments if not specifically mentioned.

5.1.2. Characterization Methods

The morphology of the NCs was examined with a transmission electron microscope (Jeol 1400) operating at an accelerating voltage of 120 kV and a Gemini 1530 (Carl Zeiss AG, Oberkochem, Germany) scanning electron microscope (SEM) operating at 0.35 kV. Droplets of 10 µL of the diluted dispersions were placed on a small silica wafer for scanning electron microscopy and on a carbon coated copper grid for TEM measurements. The UV-Vis absorption spectra were recorded with a Perkin Elmer Lambda 25 UV/VIS spectrometer. All dynamic light scattering (DLS) measurements were carried out on a commercially available instrument from ALV GmbH (Langen, Germany) consisting of a goniometer and an ALV-5000 multiple tau full-digital correlators with 320 channels. A helium-neon laser from JDS Uniphase (Milpitas, USA) with an operating intensity of 25 mW and a laser wavelength of λ = 632.8 nm was used as a light source. All solutions for the light scattering experiments were prepared in dust-free quartz cuvettes from Hellma (Müllheim, Germany) with an inner diameter of 18 mm, which were cleaned before with distilled acetone. For the measurements of NCs size, their dispersion was diluted

against an aqueous SDS solution, the same dilution condition with the release experiment). Samples were then withdrawn at two certain times, at t = 0 min and t = 240 min. The values of hydrodynamic diameters of the samples were determined by the extrapolation of value for q = 0. An Activa M spectrometer (Horiba Jobin Yvon, Bernsheim, Germany) equipped with a Meinhardt-type nebulizer and a cyclone chamber was used for ICP-OES measurements. The device was controlled by an ACTIVAnalyst 5.4 software. For the measurement the following conditions were chosen: 1250 W forward plasma power, 12 $L \cdot min^{-1}$ Ar flow, and 15 rpm pump flow. The Ar emission at 404.442 nm was employed as a reference line t. The emission lines chosen for calibration and quantification of potassium were 766.490 nm and 769.896 nm with a 5 s integration time. For calibration and quantification of calcium, the emission lines 373.690 and 422.673 with a 5 s integration time were chosen. The emission lines 213.618 and 253.560 were selected for calibration and quantification of phosphorus with a 5 s integration time. For the calibration 5 different standard concentrations were used, baseline correction, and a dynamic underground correction were provided by the software. Each measurement was an average of three repetitions and repeated two times.

5.1.3. Preparation of the nanocapsules

Polyurea nanocapsules (NCs) were synthesized via interfacial polyaddition reaction using the inverse miniemulsion technique according to the procedure explained previously[16] with slight changes as described in this section. Briefly, aqueous phases consisting of KCl, $CaCl_2$, 1,4-diaminobutane, and 2-nitrophenol sodium with a total volume of 1.3 g were prepared. 100 mg of the surfactant Lubrizol U was dissolved in 7.5 g of cyclohexane and mixed with the previously prepared aqueous solution. The obtained emulsion was stirred over 1 h at room temperature and then ultrasonicated for 180 s at 90% amplitude in a pulse regime (20 s sonication, 10 s pause) using a Branson Sonifier W-450-Digital and a 1/2” tip under ice cooling. A solution consisting of 2.5 g of cyclohexane and 262 mg of TDI was added dropwise to the previously prepared miniemulsion. The reaction proceeded for 24 h at room temperature under stirring. Afterwards, the nanocapsules were transferred into an aqueous phase using the following

procedure: 1 g of the nanocapsule dispersion in cyclohexane was mixed with 5 g of sodium dodecyl sulfate (SDS) aqueous solution (0.3 wt.%) under mechanical stirring for 24 h at room temperature. The same synthesis procedure was used for the preparation of NCs with different chemical compositions for the aqueous phases (see Table 4.1).

5.1.4. Release Experiments

The investigations on the release of polyurea NCs were carried out by dialysis. For each sample, dispersions of NCs (5 mL) were placed inside a dialysis bag (MWCO 14000) and then immersed into 195 mL of an aqueous medium with a pH value of 7.4. After a given time, 5 mL of the solution outside the dialysis bag was taken out followed by the addition of an equal amount of fresh solution to keep the amount constant. The amount of released 2-nitrophenol sodium salt was measured by UV-Vis spectroscopy. A calibration curve was also drawn by measuring a series of 2-nitrophenol sodium salt with known concentrations (Figure 5.1). The release of co-encapsulated potassium chloride and calcium chloride out of NCs were also quantified by ICP-OES (Figure 5.2). By measuring a series of potassium ion solution, calcium ion solution, and phosphorus ion solution with known concentrations, calibration curves for potassium chloride, calcium chloride, and Foscarnet were drawn.

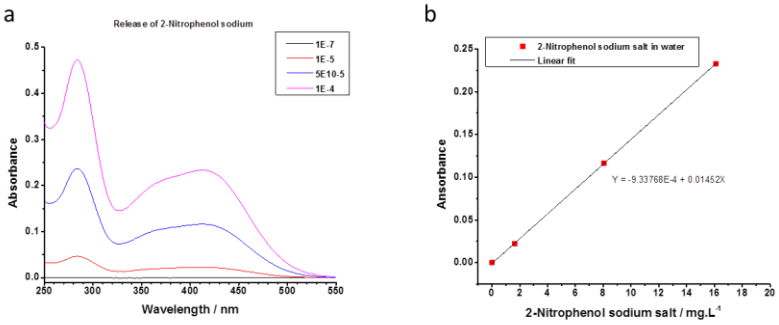

Figure 5.1. UV-Vis spectra of 2-nitrophenol sodium salt dissolved in water with different concentration (a). Calibration curve of 2-nitrophenol sodium salt in water for UV-Vis spectroscopy (b).

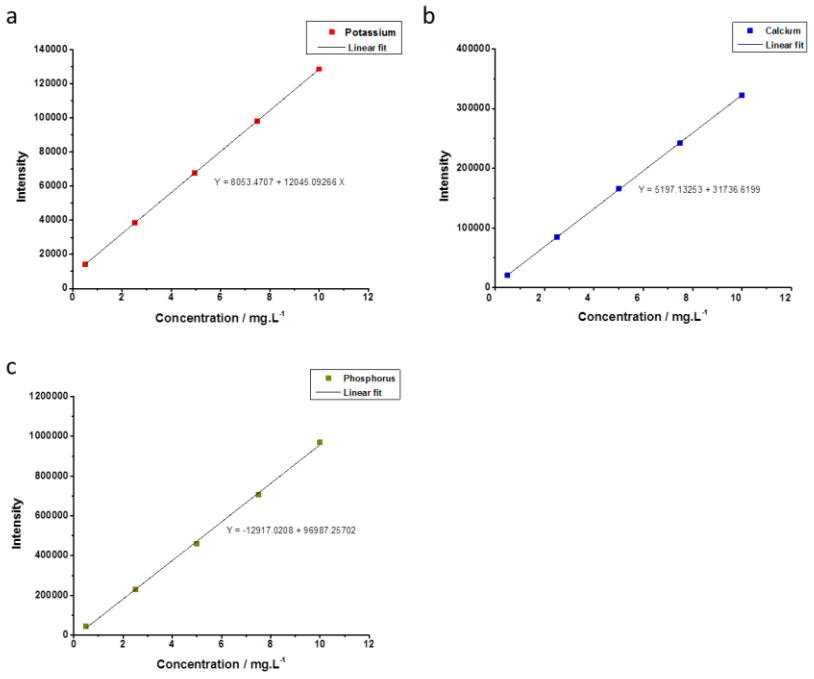

Figure 5.2. Calibration curves for potassium (a), calcium (b), and phosphorus (c) for ICP-OES.

5.2. Experimental details for section 4.2

5.2.1. Materials

Cystamine dihydrochloride (Sigma-Aldrich, 98%), 2,4-toluene diisocyanate (TDI, Sigma-Aldrich, 95%), Lubrizol U (Lubrizol Ltd.), sodium dodecyl sulfate (SDS, Alfa Aesar, 99%), rhodamine B (Sigma-Aldrich, 97%), tris(2-carboxyethyl)phosphine hydrochloride (TCEP, Sigma-Aldrich, 98%), cyclohexane (VWR, 99.5%), sodium hydroxide pellets (Sigma-Aldrich, 97%), hydrochloric acid (HCl) solution (Sigma-Aldrich, 37%), tris(hydroxymethyl)amino methane (Acros Organics, 99.8%), sodium chloride (NaCl, VWR, 99.9%), magnesium sulfate (Fisher), deuterium oxide (D_2O, ROTH, 99.8%), dimethyl sulfoxide-d_6 (DMSO- d_6, ROTH, 99.8%), trimethylsilane (Acros Organics, 99%), and dichloromethane (Sigma-Aldrich, 99.99%), were used as received. Distilled water was used for the preparation of all solutions.

5.2.2. Characterization methods

The morphology of the nanocapsules was examined with a transmission electron microscope (JEOL 1400) operating at an accelerating voltage of 120 kV and a Zeiss 1530 Gemini Leo scanning electron microscope operating at 0.35 kV. Droplets of 10 µL of the diluted cyclohexane dispersions were placed on copper grids for transmission electron microscopy (TEM) measurements. Dynamic light scattering (DLS) measurements were carried out on a commercially available instrument from ALV GmbH (Langen, Germany) consisting of a goniometer and an ALV-5000 multiple tau full-digital correlators with 320 channels. A helium-neon laser from JDS Uniphase (Milpitas, USA) with an operating intensity of 25 mW and a laser wavelength of λ = 632.8 nm was used as a light source. The values of hydrodynamic diameters of the nanocapsules in cyclohexane (as continuous phase) after dilution were determined by the extrapolation of value for q = 0 (zero angle). In all release experiments, the absorption intensity at the wavelength of 555 nm of the aqueous release medium was measured on a Tecan Plate Reader Infinite M1000 with 96 well microplates (Greiner Bio-One). ^{1}H NMR and ^{13}C nuclear magnetic resonance (NMR) spectra were recorded using a Bruker Avance 300. All

spectra were referenced internally to signals of the deuterated solvent. ^{31}P NMR spectra were recorded using a Bruker Avance 500. Fourier transform infrared spectroscopy (FTIR) analysis of the precursors and the cyclohexane dispersions of nanocapsules was done on a Nicolet 730 FTIR Spectrometer. X-ray photoelectron spectroscopy (XPS) was performed using a Kratos Axis Ultra spectrometer (Kratos, Manchester, England) using an Al Kα excitation source with a photon energy of 1487 eV. The data was acquired in the hybrid mode using a 0° take-off angle, defined as the angle between the surface normal and the axis of the analyzer lens. A charge neutralizer was always used during spectra collection to compensate charge build-up on the samples. The binding energy scale was calibrated using the main carbon peak at 284.8 eV in C1s region.

5.2.3. Deprotonation of cystamine dihydrochloride

A round dry flask was charged with 6.5 g cystamine dihydrochloride (28.875 mmol), 2.3 g sodium hydroxide (57.75 mmol), and 10 mL water. After 1 h stirring at room temperature, the mixture was freeze-dried to remove water and the residue was redissolved in 20 mL dichloromethane. After filtration, the liquid was dried over magnesium sulfate. The mixture was then filtered and the solvent was evaporated. Cystamine was obtained as yellow oil after drying in vacuum. The presence of the characteristic bonds of cystamine was confirmed in the Raman spectrum.

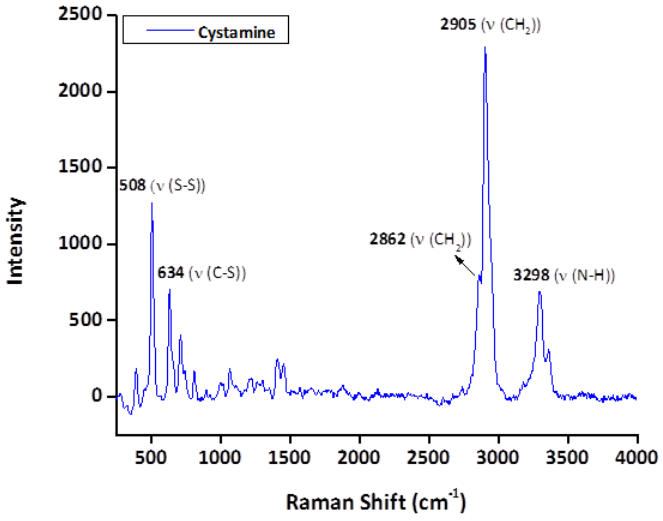

Figure 5.3. Raman spectrum of cystamine after deprotonation.

5.2.4. Preparation of the nanocapsules

Polyurea nanocapsules were synthesized via interfacial polyaddition reaction using the inverse miniemulsion technique according to a procedure reported previously[10] with slight changes described in this section. Briefly, cystamine dihydrochloride was deprotonated according to a procedure reported elsewhere42 (Fig. S1). Then, aqueous phases consisting of cystamine at known concentrations, rhodamine B (8 mg), and 1.3 g of water were prepared. 150 mg of the surfactant Lubrizol U was dissolved in 10 g of cyclohexane and mixed with the aforementioned aqueous solution. The obtained emulsion was stirred over 1 h at room temperature and then ultrasonicated for 180 s at 90% amplitude in a pulse regime (20 s sonication, 10 s pause) using a Branson Sonifier W-450-Digital and a 1/2" tip under ice cooling. A solution consisting of 5 g of cyclohexane and TDI at different concentrations was added dropwise to the previously prepared miniemulsion. The reaction proceeded for 24 h at room temperature under stirring. Afterwards, the nanocapsules were transferred into an aqueous phase using the following procedure: 1 g of the nanocapsule dispersion in cyclohexane was mixed with 5 g of a SDS

aqueous solution (0.5 wt. %) under mechanical stirring for 24 h at room temperature in an open vial to let evaporate the cyclohexane. The loss of evaporated water was compensated.

5.2.5. Release experiments

The investigations on the release of polyurea nanocapsules were carried out by dilution of 5 g of nanocapsules dispersions in 95 g of an aqueous solution with concentration of 5 mg mL^{-1} SDS, 6 mg mL^{-1} of tris(hydroxymethyl)amino methane, and 0.05 mol L^{-1} hydrogen chloride. The pH value of the aqueous release medium was 7. At certain time intervals, 2 mL of the release medium was taken out followed by a gently removal of supernatant after each centrifugation at 1467 g, 9168 g, and 36670 g. Each centrifugation step lasted for 20 min while temperature was set to 25 °C. The amount of rhodamine B was measured by absorbance microplate reader (Greiner Bio-One) at the wavelength of 555 nm. A calibration curve was also plotted by measuring a series of rhodamine B with known concentrations (Figure 5.4). In order to elucidate the redox responsiveness of the nanocapsules, TCEP was added to the release medium. The molar amount of TCEP in the release medium was calculated to be 10 times more than the molar amount of cystamine existing in nanocapsules shell.

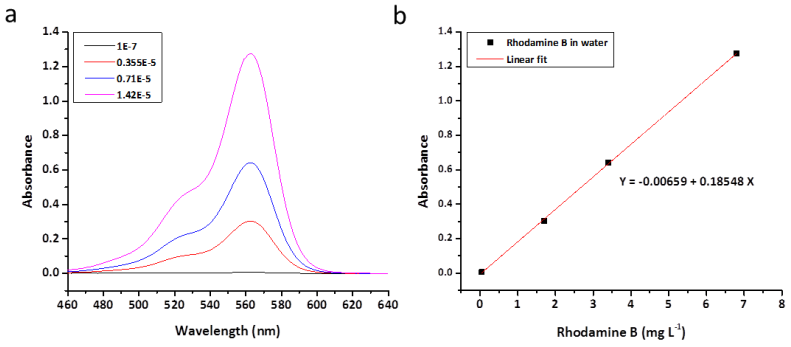

Figure. 5.4. (a) UV-Vis spectra of Rhodamine B dissolved in water at different concentrations. (b) Calibration curve of Rhodamine B in water for UV-Vis spectroscopy.

5.2.6. Cystamine extraction

To determine the residual cystamine monomer, nanocapsules with the same protocol as before but with D_2O as the liquid core instead of H_2O and without Rhodamine B were synthesized. After freeze drying the dispersions, the solid was redispersed in DMSO-d_6 and then stirred in close vial for 72 h at room temperature. After centrifugation, the amount of cystamine monomer in the supernatant was measured by ^{1}H NMR spectroscopy. A small amount of tetramethylsilane was added to the NMR tubes as internal standard.

5.2.7. Quantification of disulfide-bond cleavage

The consumption of TCEP, which was used as reducing agent for disulfide bonds cleavage in excess, was quantified with ^{31}P-NMR spectroscopy in aqueous solutions on a Bruker Avance 500 MHz spectrometer. All solutions and dispersions were degassed and samples were prepared under inert gas atmosphere to avoid any oxidation of TCEP by oxygen. K_3PO_4 was used as internal standard for reference and for quantification of the TCEP signal.

5.3. Experimental details for section 4.3

5.3.1. Materials

Dichloromethane (Sigma-Aldrich, 99.99%), hexadecane (HD, Sigma-Aldrich, 99%), Nile-red (Sigma-Aldrich), hexadecyltrimethylammonium chloride (CTMA-Cl, Alfa Aesar, 96%), sodium dodecyl sulfate (SDS, Alfa Aesar, 99%), hydrogen peroxide (H_2O_2, Sigma-Aldrich, 35%), sodium hydroxide pellets (Sigma-Aldrich, 97%), hydrochloric acid (HCl) solution (Sigma-Aldrich, 37%), iodomethane (Merck), and chlorotrimethylsilane (Alfa Aesar, 98%) were used as received. Demineralized water was used for the preparation of all dispersions. All other solvents and reagents were purchased from Fisher Scientific and used as received, unless otherwise stated. Tetrahydrofuran (THF) was distilled from sodium/benzophenone under reduced pressure (cryo-transfer) prior to the addition of 1,1-diphenylethylene (DPE) and *n*-BuLi as well as a second cryo-transfer. Methyl methacrylate and *N,N*-dimethylaminoethyl methacrylate (DMAEMA) were purified by 2-fold distillation over calcium hydride (CaH_2). In both cases, trioctyl aluminium (25 wt% in hexane) was subsequently added dropwise until a pale yellow color appeared. Prior to use in anionic polymerization protocols, the monomers were freshly distilled from these solutions. Vinylferrocene was synthesized and purified as reported elsewhere.[239]

5.3.2. Characterization methods

The morphology of the NCs was examined with a transmission electron microscope (TEM) (JEOL 1400) operating at an accelerating voltage of 120 kV and a Zeiss 1530 Gemini Leo scanning electron microscope (SEM) operating at 0.35 kV. 10 µL of the diluted dispersions were placed on small silica platelets for scanning electron microscopy and on copper grids for TEM measurements. For the vapor staining of NCs, iodomethane (300 µL) was dropped into a glass container which is included with the TEM grids within a small open glass vial. The container was left sealed at room temperature overnight. The same protocol was applied for staining with chlorotrimethylsilane. The evaporation of chlorotrimethylsilane in the sealed container was facilitated by using oil bath at 40 °C. All TEM samples were sputtered with carbon on a BALZERS

BAE 250 for 5 s to prevent beam damage during the transmission microscopy measurements. Dynamic light scattering (DLS) measurements were carried out on a commercially available instrument from ALV GmbH (Langen, Germany) consisting of a goniometer and an ALV-5000 multiple tau full-digital correlators with 320 channels. A helium-neon laser from JDS Uniphase (Milpitas, USA) with an operating intensity of 25 mW and a laser wavelength of λ = 632.8 nm was used as a light source. All solutions for the light scattering experiments were prepared in dust-free quartz cuvettes from Hellma (Müllheim, Germany) with an inner diameter of 18 mm, which were cleaned before with distilled acetone. For the measurements of NCs size, their dispersion was diluted against sodium hydroxide or hydrochloric solutions, which were prepared by dilution 1 mol L^{-1} solutions to the desired pH value, with concentration of 0.05 mg mL^{-1} of hexadecyltrimethylammonium chloride for 1 h before measurement. Hydrodynamic diameter and poly dispersity index (PDI) were an average of three times repetitions at an angle of 90°. Zeta potential of the NCs was measured on the dispersions were diluted in aqueous solutions at the desired pH value with concentration of 0.001 mol L^{-1} of potassium chloride (KCl) for 1 h before measurement. In all release experiments, the fluorescence intensity at the emission wavelength of 620 nm of the treated dispersion was measured on a Tecan Plate Reader Infinite M1000 at an excitation wavelength of 520 nm. Standard SEC was performed with THF as the mobile phase (flow rate 1 mL min^{-1}) on a SDV column set from PSS, Mainz (SDV 1000, SDV 10^5, SDV 10^6) at 30 °C. The calibration was carried out using PS standards from PSS (Mainz). For the SEC-MALLS experiments, a system composed of a Waters 515 pump (Waters, Milford, CT), a TSP AS100 autosampler, a Waters column oven, a Waters 486 UV-detector operating at 254 nm, a Waters 410 RI-detector, and a DAWN DSP light scattering detector (Wyatt Technology, Santa Barbara, CA) was used. The Astra version 4.73 (Wyatt Technology, Santa Barbara, CA) was used for data acquisition and the evaluation of the light-scattering experiments. The light scattering instrument was calibrated using pure toluene, assuming a Rayleigh ratio of $9.78 \cdot 10^{-6}$ cm^{-1} at 690 nm. An injection volume of 118 µL, a sample concentration of 1 $g \cdot L^{-1}$ to 2 $g \cdot L^{-1}$, a column temperature of 35 °C, and a THF flow rate of 1 mL min^{-1} were applied. Additional TEM images of the PVFc-*b*-PDMAEMA-*b*-PMMA bulk samples

were performed on a Zeiss EM10 with an operating voltage of 60 kV. The block copolymer was diluted in methylene chloride and the solvent was allowed to evaporate at room temperature. Thin films were heated at 150 °C in vacuum for 24 h. Ultrathin sections of the block copolymer film were cut into slices of 50-80 nm by using an ultramicrotome Ultracut UTC (Leica) equipped with a diamond knife. TEM images were recorded with a slow-scan CCD camera TRS (Tröndle).

5.3.3. Exemplary Synthesis of PVFc-*b*-PMMA-*b*-PDMAEMA

In an ampule equipped with a stirring bar 200 mg (1.89 mmol, 33 eq) VFc and 60 mg (1.41 mmol, 50 eq) LiCl is dissolved in dry 5 ml THF. The solution is cooled to -12 °C, and 34 µL (0.03 mmol, 1 eq) n-BuLi in hexane (1.6 M) is added quickly. After 16 h, an aliquot of the solution is taken from the ampule for characterization of the PVFc-block and terminated by adding methanol. Then, 20 mg (0.12 mmol, 4 eq) DPE and 6 mg (0.06 mmol, 2 eq) DMSB are added to the PVFc macro-anions. Meanwhile 1.1 g (11.2 mmol, 400 eq) MMA is dissolved in 45 mL dry THF and cooled to -78 °C. The polymerization of the MMA is started by fast addition of the PVFc-macroinitiator. After 1 h of reaction time, a sample of the solution is taken from the ampule for characterization of the diblock copolymer and terminated by adding methanol. Then, 130 mg (0.8 mmol, 27 eq) DMAEMA is added and after stirring at -78 °C for 1 h, 0.1 mL methanol is added to terminate the polymerization. The polymer solution is added to 250 ml water and stirred at 70 °C to precipitate the polymer. The polymer is collected by filtration and dried in vacuo. Yield: 1.3 g (90%).

The other polymers were synthesized by the same procedure in comparable yields. The amounts of the three monomers were varied according to the desired copolymer compositions. In the case of the triblock copolymer with a different block order ($PVFc_{11.4}$-b-$DMAEMA_{17.8}$-b-$PMMA_{70.8}$), DMAEMA was initiated with the PVFc-macroinitiator followed by addition of MMA. In the case of $PDMAEMA_{34}$-b-$PMMA_{66,}$ diphenylhexyl lithium was used instead of PVFc-macroinitiator (Table 4.6).

5.3.4. Preparation of the nanocapsules

50 mg of polymer and 50 mg of hexadecane were dissolved in 2.5 g of dichloromethane containing 1 mg of Nile-red (NR). The organic phase was added to 20 g of an aqueous solution with concentrations of 0.05 mg mL^{-1} and 0.1 mmol L^{-1} of hexadecyltrimethylammonium chloride (CTMA-Cl) and NaOH, respectively. The mixture was stirred at 1100 rpm for 1 h in a closed glass vial to obtain a macroemulsion. The emulsion was then subjected to ultrasonication under ice-cooling for 2 min in a 30 s pulse/10 s pause regimen (Branson W450-D sonifier with a 1/2 in. tip). Afterward, the dichloromethane was evaporated at room temperature while stirring at 500 rpm for 16 h. The dispersions were then dialyzed against their continuous phases for 1 day to remove the non-encapsulated dye. For the synthesis of NCs prepared from PVFc-*b*-PMMA block copolymer, an aqueous solution with a concentration of 0.05 mg mL^{-1} sodium dodecyl sulfate (SDS) was used.

5.3.5. Release experiments

To determine the responsiveness of the NCs, dispersions were mixed with aqueous solutions containing CTMA-Cl (0.05 mg mL^{-1}) and HCl at different concentrations (10^{-5} to 0.1 mol L^{-1}) with volume ratios 1:5 and stirred for 24 h. To measure the response of NCs to oxidation, the dispersions were mixed with hydrogen peroxide solutions at different concentrations (35 to 4.4 wt. %) containing CTMA-Cl (0.05 mg mL^{-1}) with volume ratios 1:5 and stirred for 24 h. The response of the NCs to temperature was measured by heating the dispersions at different temperature (45 to 95 °C) for 10 min. Control samples of the dispersions were also mixed with their continuous phase without addition of acid or oxidant at room temperature.

5.4. Experimental details for section 4.4

5.4.1. Materials

Tetraethoxysilane (TEOS) (Alfa Aesar, 98%), bis[3-(triethoxysilyl)propyl] tetrasulfide (TESPT) (Sigma Aldrich, 90%), hexadecyltrimethylammonium chloride (CTMA-Cl) (Alfa Aesar, 96%), hexadecane (HD) (Sigma Aldrich, 99%), tris(2-carboxyethyl)phosphine hydrochloride (TCEP) (Sigma Aldrich, 98%), m-xylene (Acros Organics, 99%), 2-mercaptobenzothiazole (MBT) (Sigma Aldrich, 97%), 2,2'-dithiobis(benzothiazole) (Sigma Aldrich, 99%), poly(ethylene glycol) dithiol (PEG dithiol) (M_n 1,000) (Sigma Aldrich), chloroform (Sigma Aldrich, 99%),chloroform-d (Acros Organics, 99%), and toluene (Acros Organics, 99%) were used as received. Demineralized water was used for the preparation of all dispersions.

5.4.2. Characterization methods

The morphology of the SiNCs was examined with a transmission electron microscope (TEM) (JEOL 1400) operating at an accelerating voltage of 120 kV and a Zeiss 1530 Gemini Leo scanning electron microscope (SEM) operating at 0.35 kV. Droplets of 10 µL of the diluted dispersions were placed on small silica platelets for scanning electron microscopy and on copper grids for TEM measurements. Dynamic light scattering (DLS) measurements were carried out on the dispersions of SiNCs with a Nicomp 380 Submicron Particle Sizer (PSS-Nicomp) at an angle of 90° for 300 s. In all release experiments, the absorbance of the treated dispersions was measured on a Tecan Plate Reader Infinite M1000 at wavelengths between 280 and 360 nm. ^{1}H NMR spectra were recorded using a Bruker Avance 300. All spectra were referenced internally to residual proton signals of the deuterated solvent.

5.4.3. Preparation of silica nanocapsules

TEOS and TESPT were first mixed with 125 mg of HD, 0.868 g of *m*-xylene, and either 3 mg of MBT or 12 mg of PEG-MBT. The mixture was then added to 30 g of an aqueous solution of 0.77 mg·mL^{-1} of CTMA-Cl. After emulsification under 1000 rpm for 1 h at room temperature, the

emulsion was sonicated under ice-cooling for 3 min at 70% amplitude in a pulse regime (30 s pulse/10 s pause) with Branson W450-D sonifier and a 1/2 inch tip. The miniemulsion was stirred under 1000 rpm at room temperature overnight to obtain the silica nanocapsules. The different compositions of the nanocapsules are summarized in Table 4.10.

5.4.4. Release experiments

The investigations on the release of SiNCs were carried out by dialysis. For each sample, dispersions of SiNCs (2 mL) were placed inside a dialysis bag (MWCO 14000) and then immersed into 10 mL of a tris(hydroxymethyl)amino methane buffer solution (pH ~ 7.1) containing of 0.77 mg·mL^{-1} CTMA-Cl. After a given time, 200 µL of the solution outside the dialysis bag was taken out followed by the addition of an equal amount of fresh solution to keep the amount constant. The released MBT was measured by UV-Vis spectroscopy. A calibration curve was also drawn by measuring a series of MBT with known concentrations (Figure 5.5).

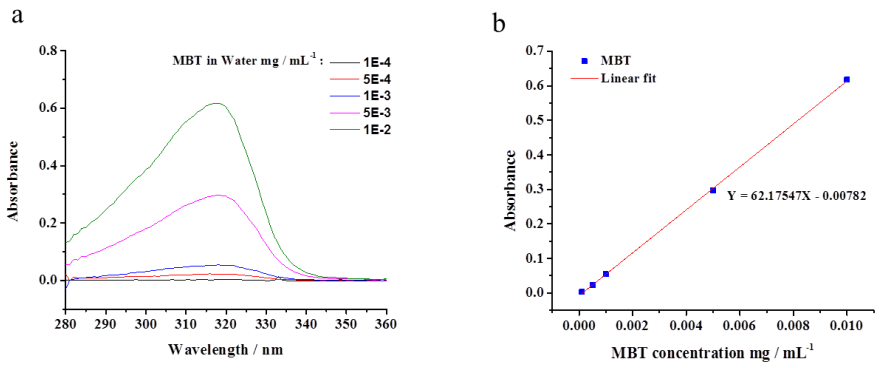

Figure 5.5. (a) UV-Vis spectra of MBT dissolved in water at different concentrations. (b) Calibration curve of MBT in water for UV-Vis spectroscopy.

5.4.5. Condensation of PEG dithiol with MBT

A mixture of 2,2'-dithiobis(benzothiazole) (66.4 mg, 0.2 mmol) and poly(ethylene glycol) dithiol (average M_n 1,000 g·mol^{-1}, 100 mg, 0.1 mmol) in chloroform (5 mL) was prepared. The resulting dispersion was stirred 16 h at room temperature until thin layer chromatography (TLC) did not show any of the starting reagent 2,2'-dithiobis(benzothiazole). Gradually the stirred dispersion became homogenous while the first hour. To remove the by-product benzothiazol-2-thiol, the chloroform phase was washed once with a 10% potassium hydroxide solution and brine. After drying over anhydrous sodium sulfate the solvent was removed at reduced pressure. The α,ω-(2,2'dithio[benzothiazolyl])-poly(ethylene glycol) (PEG-MBT) was obtained as yellowish solid residue (Yield: 95.5 mg, 0.071 mmol, 71%) (Figure 4.22).

5.4.6. Cleavage of MBT molecules from PEG-MBT

The cleavage of MBT molecules from PEG-MBT was carried out by mixing 2.5 mL of *m*-xylene containing of 5 mg of PEG-MBT (3.76 µmol, 1 eq) with 2.5 mL of aqueous solution containing 10.8 m of TCEP (37.6 µmol, 10 eq). A control sample was also prepared with the *m*-xylene phase and 2.5 mL of distilled water. Both emulsions were vigorously stirred for 24 h at room temperature. *m*-xylene phase was separated from the aqueous phase and then freeze dried. The precipitate was dissolved in chloroform-d containing small amount of toluene as internal standard for NMR measurement. No cleavage was observable in the control sample since no degradation to PEG-MBT occurred without TCEP (Figure 4.23a). In contrast, the results showed a significant decrease in the characteristic peak of poly(ethylene glycol) dithiol at 3.6 ppm in the presence of TCEP in the aqueous phase. This was attributed to the cleavage of disulfide-bonds and the subsequent transfer of PEG dithiol as hydrophilic monomer from *m*-xylene phase to aqueous phase (Figure 4.23b).

6. Summary and Outlook

The main objective of this thesis was to prepare polymer nanocapsules with improved capability for controlled-release of payloads. To fulfill this objective, new strategies were developed to (i) hinder non-controlled leakage and (ii) enhance controlled-release of payloads from these nanocapsules. Nanocapsules with either oily or aqueous core containing hydrophilic or hydrophobic payloads were prepared by miniemulsion technique.

In the first part (section 4.1), the release of hydrophilic payloads from polyurea nanocapsules was programmed by varying the osmotic pressure in the core of these nanocapsules. The results exhibited that the initial release of the payloads from the aqueous core was largely dependent on the concentration of osmotic pressure agents. The analysis showed that the correlation between the release of the dye and the concentration of the co-encapsulated salts (*i.e.* osmotic pressure agents) is non-linear. Further measurements displayed that the swelling of nanocapsules is the responsible mechanism for the observed differences between the release profiles of the dye from the nanocapsules loaded with osmotic pressure generating species and non-loaded ones. To diminish the burst release of the payload, nanocapsules with crosslinked shell were synthesized using crosslinker. Crosslinking had an influence on shell rigidity and, thus, decreased release kinetics by obstructing the swelling of nanocapsules despite of an osmotic pressure. Finally, we illustrated how this strategy can be utilized to induce triggered release or sustained release profiles through two different applications. This project has shown that osmotic pressure can be turned to an advantage for the acceleration of payloads release.

In the next set of experiments (section 4.2), the non-controlled leakage of hydrophilic payloads from the core due to osmotic pressure difference could be suppressed by varying the physicochemical properties of nanocapsule membranes thereby decreasing release kinetics. The shell thickness of polyurea nanocapsules was tuned by changing the monomer concentration used for the preparation of these nanocapsules. A significant increase of shell

thickness could largely decrease the non-controlled leakage of the hydrophilic payloads. In addition, this significant increment of shell thickness slowed down the release kinetics and thereby suppressed a precisely targeted delivery of the payload in desired time. Therefore, reduction-responsive unit were introduced into the thick shell to enable triggered release of the payload. Triggered-release of the payload was successfully upon application of reducing agent. In this work, the concept of stimulus-induced release of hydrophilic payloads from nanocapsules was demonstrated for redox-responsive nanocapsules.

The concept of using block copolymers responsive to one stimulus for the preparation of stimulus responsive capsules was extended to triblock terpolymers responsive to three independent stimuli (section 4.3). Novel triple stimuli-responsive nanocapsules consisting of PVFc-*b*-PDMAEMA-*b*-PMMA triblock terpolymer were prepared by the solvent evaporation process from miniemulsion droplets. The nanocapsules could encapsulate the dye in the core and perfectly protect it from non-controlled leakage. The triggered release of the payload was achieved because the nanocapsules shell was addressable by three different stimuli: pH change, oxidizing agent, and temperature. Alternatively, nanocapsules were synthesized with a mixture of responsive diblock copolymers, where their shell had the same chemical composition in terms of molar amount of blocks with nanocapsules synthesized from triblock terpolymer. However, the microphase separation between the responsive diblock copolymer across the shell hampers the release performance of the payloads from the nanocapsules. This configuration of diblock copolymers across the shell, thus, made these nanocapsules stimulus-responsive instead of triple stimuli-responsive. This study revealed how the fine morphology of triple responsive triblock terpolymer can be exploited to achieve nanocapsules addressed by three independent stimuli.

Finally, the concept of utilizing pro-active payloads in order to significantly increase the selective release of small size payloads from mesoporous nanocapsules was demonstrated (section 4.4). Silica nanocapsules were synthesized by the miniemulsion technique. The non-controlled release of payload largely decreased the efficiency of these silica nanocapsules for

the precise delivery of the payload. To overcome the problem of non-controlled release, a pro-active payload was synthesized. A pro-active payload is defined as a compound that is converted to an active functional molecule in the environment where it is needed. The pro-active payload could not diffuse through the silica shell due to its larger molecular size compared to the payload. The combination of the encapsulation of the pro-active payload and the responsive behavior of the silica nanocapsules led to significant increase in the final released amount of payload while almost the entire payload in the release medium could be selectivity delivered from the silica nanocapsules.

7. Zusammenfassung und Ausblick

Das Hauptaugenmerk dieser Dissertation lag auf der Herstellung von Polymer-Nanokapseln mit verbesserter Fähigkeit zur kontrollierten Freisetzung ihrer Beladung. Zur Erreichung dieses Ziels wurden neue Strategien entwickelt, um (i) unkontrolliertes Austreten zu verhindern und (ii) die kontrollierte Freisetzung des Inhaltes dieser Nanokapseln zu verbessern. Es wurden Nanokapseln, sowohl mit öligen als auch mit wässrigen Kernen, die hydrophile oder hydrophobe Beladungen enthalten, mithilfe der Miniemulsionstechnik hergestellt.

Im ersten Teil (section 4.1) wurde die Freisetzung von hydrophilen Beladungen aus Polyurea-Kapseln durch Variation des osmotischen Drucks im Inneren dieser Nanokapseln angepasst. Die Ergebnisse zeigten, dass die anfängliche Freisetzung der Beladungen aus dem wässrigen Kern stark von der Konzentration der osmotischen Druck-Agenzien abhängt. Die Analyse zeigte, dass die Korrelation zwischen der Freisetzung des Farbstoffs und der Konzentration des mit eingekapselten Salzes (i. e. des osmotischen Druck-Agens) nicht linear ist. Weitere Messungen wiesen darauf hin, dass das Anquellen der Nanokapseln der verantwortliche Mechanismus ist für die beobachteten Abweichungen zwischen dem Freisetzungsprofil des Farbstoffs aus den, mit osmotischen Druck generierenden Spezies geladenen, und den ungeladenen Kapseln. Um die Ladungs-Freisetzung durch Aufplatzen zu verringern, wurden Nanokapseln mit quer-vernetzten Schalen durch Einsatz eines Vernetzers hergestellt. Die Vernetzung hat Einfluss auf die Stabilität der Schale, was trotz des osmotischen Drucks zu einer Blockade des Anschwellens der Nanokapseln führt und damit eine reduzierte Freisetzungskinetik bewirkt. Abschließend haben wir anhand zwei verschiedener Anwendungen veranschaulicht, wie diese Strategie einsetzbar ist, um ein gesteuertes oder dauerhaftes Freisetzungsprofil zu erhalten. Dieses Projekt hat gezeigt, dass der osmotische Druck zum Vorteil für die Beschleunigung der Ladungsfreisetzung einsetzbar ist.

In der nächsten Reihe von Experimenten (section 4.2) konnte durch Veränderung der physikochemischen Eigenschaften der Nanokapselmembran das unkontrollierte Austreten der

hydrophilen Beladungen aus dem Kern wegen des osmotischen Druckunterschieds unterdrückt und dadurch die Freisetzungskinetik verringert werden. Die Schalendicke der Polyharnstoff-Nanokapseln wurde durch Veränderung der Monomer-Konzentration, die zu deren Herstellung verwendet wurden, eingestellt. Ein merklicher Anstieg der Schalendicke konnte die unkontrollierte Freisetzung der hydrophilen Beladungen deutlich senken. Außerdem reduzierte diese starke Erhöhung der Schalendicke die Freisetzungskinetik, wodurch die präzis-gezielte Abgabe der Beladung in gewünschter Zeit unterdrückt wurde. Deshalb wurden reduktionssensitive Einheiten in die dicke Schale eingebracht, um eine steuerbare Freisetzung der Beladung zu ermöglichen. Dies gelang erfolgreich nach Einsatz eines Reduktionsmittels. In dieser Arbeit wurde das Konzept der stimulus-induzierten Freisetzung von hydrophilen Beladungen aus Nanokapseln für Redox-sensitive Nanokapseln demonstriert.

Das Konzept des Einsatzes von Blockcopolymeren, die auf einen Stimulus reagieren, für die Herstellung von stimulus-responsiven Kapseln, wurde auf Triblockcopolymere, die sensitiv für drei unabhängige Stimuli sind, erweitert (section 4.3). Neuartige, dreifach stimuli-responsive Nanokapseln aus PVFc-*b*-PDMAEMA-*b*-PMMA Triblockterpolymer wurden mittels des Lösungsmittelverdampfungsverfahren aus Miniemulsionströpfchen hergestellt. Die Nanokapseln waren in der Lage den Farbstoff im Kern einzukapseln und ihn gegen unkontrolliertes Austreten zu sichern. Die steuerbare Freisetzung der Beladung wurde erzielt, weil die Nanokapsel durch drei unterschiedlichen Stimuli adressierbar war: durch Änderung des pH-Werts, durch Zugabe eines Oxidationsmittel und durch Variation der Temperatur. Als eine Alternative wurden Nanokapseln mit einer Mischung aus responsiven Diblockcopolymeren hergestellt, deren Schale dieselbe chemische Zusammensetzung, bezogen auf den molaren Anteil der Blöcke, besitzt wie die Nanokapseln aus Triblockcopolymeren. Allerdings hemmt die Mikrophasenseparation zwischen den responsiven Diblock-copolymeren die Freisetzung der Beladungen aus den Nanokapseln. Die Konfiguration der Diblockcopolymere innerhalb der Schale wiederum machte diese Nanokapseln stimulus-responsiv, im Gegensatz zu den dreifach stimuli-responsiven Kapseln. Diese Studie offenbart wie die feine Morphologie der dreifach

responsiven Triblock-terpolymere nutzbar ist, um Nanokapseln zu erzeugen, die durch drei unabhängige Stimuli adressierbar sind.

Zuletzt wurde das Konzept des Einsatzes von proaktiven Beladungen für einen signifikanten Anstieg der selektiven Freisetzung der kleinen Beladungen aus mesoporösen Nanokapseln demonstriert (section 4.4). Die Silika-Nanokapseln wurden mittels Miniemulsionstechnik hergestellt. Die unkontrollierte Ladungsfreisetzung verringerte die Effizienz dieser Silika-Nanokapseln für die präzise Abgabe der Beladungen erheblich. Um das Problem der unkontrollierten Freisetzung zu umgehen, wurde eine sogenannte proaktive Beladung hergestellt. Eine proaktive Beladung ist definiert als eine Verbindung, die erst in der entsprechenden Umgebung, wo es benötigt wird, in ein aktives, funktionelles Molekül umgesetzt wird. Dank der gewachsenen Größe, verglichen zur Beladung, konnte die proactive Beladung nicht mehr durch die Silika-schale diffundieren. Die Kombination aus der Einkapselung der proaktiven Beladung und des responsiven Verhalten der Silika-Nanokapseln führte zu einem signifikanten Anstieg des endgültig freigesetzten Anteils der Beladung, welches selektiv aus den Silika-Nanokapseln abgeben wurde.

References

1. Cosgrove, T., *Colloid Science: Principles, Methods, and Applications*. 2 ed.; Wiley-VCH: 2010.

2. Everett, D. H., *Basic Principles of Colloid Science*. RSC: 1988.

3. Napper, D. H., *Polymeric Stabilization of Colloidal Dispersions*. Academic Press: New York, 1983.

4. Becher, P., *Emulsions: Theory and Practice*. 3 ed.; Oxford University Press: New York, 2001.

5. Hubbell, J. A.; Chilkoti, A., *Science* **2012,** *337*, 303-305.

6. Saji, V. S.; Thomas, J., *Curr. Sci.* **2007,** *92*, 51-55.

7. Bates, F. S.; Fredrickson, G. H., *Annu. Rev. Phys. Chem.* **1990,** *41*, 525-557.

8. Matsen, M. W.; Bates, F. S., *Macromolecules* **1996,** *29*, 1091-1098.

9. Crank, J.; Park, G., *Diffusion in Polymer*. Academin Press: London, 1968.

10. Comyn, J., *Polymer permeability*. Springer Science & Business Media: 1985.

11. Andersson Trojer, M.; Nordstierna, L.; Nordin, M.; Nyden, M.; Holmberg, K., *Phys. Chem. Chem. Phys.* **2013,** *15*, 17727-17741.

12. Gaitzsch, J.; Huang, X.; Voit, B., *Chem. Rev.* **2015**.

13. Mora-Huertas, C.; Fessi, H.; Elaissari, A., *Int. J. Pharm.* **2010,** *385*, 113-142.

14. Sukhorukov, G. B.; Rogach, A. L.; Zebli, B.; Liedl, T.; Skirtach, A. G.; Köhler, K.; Antipov, A. A.; Gaponik, N.; Susha, A. S.; Winterhalter, M., *Small* **2005,** *1*, 194-200.

15. Landfester, K., *Annu. Rev. Mater. Res.* **2006,** *36*, 231-279.

16. Crespy, D.; Stark, M.; Hoffmann-Richter, C.; Ziener, U.; Landfester, K., *Macromolecules* **2007,** *40*, 3122-3135.

17. Lv, L.-P.; Zhao, Y.; Vilbrandt, N.; Gallei, M.; Vimalanandan, A.; Rohwerder, M.; Landfester, K.; Crespy, D., *J. Am. Chem. Soc.* **2013,** *135*, 14198-14205.

18. Fickert, J.; Rupper, P.; Graf, R.; Landfester, K.; Crespy, D., *J. Mater. Chem.* **2012,** *22*, 2286-2291.

19. Vimalanandan, A.; Lv, L. P.; Tran, T. H.; Landfester, K.; Crespy, D.; Rohwerder, M., *Adv. Mater.* **2013,** *25*, 6980-6984.

20. van den Dungen, E. T.; Klumperman, B., *J. Polym. Sci., Part A: Polym. Chem.* **2010,** *48*, 5215-5230.

21. Butt, H. J.; Graf, K.; Kappl, M., *Physics and chemistry of Interfaces*. Wiley-VCH: 2006.

22. Li, Q.; Jonas, U.; Zhao, X. S.; Kappl, M., *Asia Pac. J. Chem. Eng.* **2008,** *3*, 255-268.

23. Verwey, E. W.; Overbeek, J. T. G., *Theory of the Stability of Lyophobic Colloids*. Elsevier: Amsterdam, 1948.

24. Derjaguin, B. L. L., *Prog. Surf. Sci.* **1993,** *43*, 30-59.

25. Napper, D. H., *Ind. Eng. Chem. Prod. Res. Dev.* **1970,** *9*, 467-477.

26. Ugelstad, J.; Lervik, H.; Gardinovacki, B.; Sund, E., *Pure Appl. Chem.* **1971,** *26*, 121-152.

27. Chou, Y. J.; El-Aasser, M. S.; Vanderhoff, J. W., *J. Dispersion Sci. Technol.* **1980,** *1*, 129-150.

28. Landfester, K., *Macromol. Rapid Commun.* **2001,** *22*, 896-936.

29. Torza, S.; Mason, S. G., *J. Colloid Interface Sci.* **1970,** *33*, 67-83.

30. Sundberg, D. C.; Casassa, A. P.; Pantazopoulos, J.; Muscato, M. R.; Kronberg, B.; Berg, J., *J. Appl. Polym. Sci.* **1990,** *41*, 1425-1442.

31. Chen, Y. C.; Dimonie, V.; El-Aasser, M. S., *Macromolecules* **1991,** *24*, 3779-3787.

32. Tanaka, T.; Okayama, M.; Kitayama, Y.; Kagawa, Y.; Okubo, M., *Langmuir* **2010,** *26*, 7843-7847.

33. Romanski, F. S.; Winkler, J. S.; Riccobene, R. C.; Tomassone, M. S., *Langmuir* **2012,** *28*, 3756-3765.

34. Saito, N.; Kagari, Y.; Okubo, M., *Langmuir* **2006,** *22*, 9397-9402.

35. Lee, S.; Rudin, A., *J. Polym. Sci., Part A: Polym. Chem.* **1992,** *30*, 2211-2216.

36. Hong, Y.; Gao, C.; Shi, Y.; Shen, J., *Polym. Adv. Technol.* **2005,** *16*, 622-627.

37. Williams, R. J.; Rozenberg, B. A.; Pascault, J.-P., Reaction-induced phase separation in modified thermosetting polymers. In *Polymer Analysis Polymer Physics*, Springer: 1997; pp 95-156.

38. Vanderhoff, J. W.; El-Aasser, M. S.; Ugelstad, J., Polymer emulsification process. Google Patents: 1979.

39. Staff, R. H.; Landfester, K.; Crespy, D., Recent advances in the emulsion solvent evaporation technique for the preparation of nanoparticles and nanocapsules. In *Hierarchical Macromolecular Structures: 60 Years after the Staudinger Nobel Prize II*, Percec, V., Ed. Springer: 2013; pp 329-344.

40. O'Donnell, P. B.; McGinity, J. W., *Adv. Drug Deliv. Rev.* **1997,** *28*, 25-42.

41. Zhao, Y.; Fickert, J.; Landfester, K.; Crespy, D., *Small* **2012,** *8*, 2954-2958.

42. Wohnhaas, C.; Friedemann, K.; Busko, D.; Landfester, K.; Baluschev, S.; Crespy, D.; Turshatov, A., *ACS Macro Lett.* **2013,** *2*, 446-450.

43. Antonietti, M.; Landfester, K., *Prog. Polym. Sci.* **2002,** *27*, 689-757.

44. Tiarks, F.; Landfester, K.; Antonietti, M., *Langmuir* **2001,** *17*, 908-918.

45. Musyanovych, A.; Landfester, K., Synthesis of poly (butylcyanoacrylate) nanocapsules by interfacial polymerization in miniemulsions for the delivery of DNA molecules. In *Surface and Interfacial Forces–From Fundamentals to Applications*, Springer: 2008; pp 120-127.

46. Jagielski, N.; Sharma, S.; Hombach, V.; Mailänder, V.; Rasche, V.; Landfester, K., *Macromol. Chem. Phys.* **2007,** *208*, 2229-2241.

47. Torini, L.; Argillier, J.; Zydowicz, N., *Macromolecules* **2005,** *38*, 3225-3236.

48. Luo, Y.; Zhou, X., *J. Polym. Sci., Part A: Polym. Chem.* **2004,** *42*, 2145-2154.

49. Cao, Z.; Shan, G., *J. Polym. Sci., Part A: Polym. Chem.* **2009,** *47*, 1522-1534.

50. Utama, R. H.; Drechsler, M.; Förster, S.; Zetterlund, P. B.; Stenzel, M. H., *ACS Macro Lett.* **2014,** *3*, 935-939.

51. Utama, R. H.; Stenzel, M. H.; Zetterlund, P. B., *Macromolecules* **2013,** *46*, 2118-2127.

52. Zhang, Y.; Zhu, S.; Yin, L.; Qian, F.; Tang, C.; Yin, C., *Eur. Polym. J.* **2008,** *44*, 1654-1661.

53. Baier, G.; Friedemann, K.; Leuschner, E. M.; Musyanovych, A.; Landfester, K. In *pH Stability of Poly (urethane/urea) Capsules Synthesized from Different Hydrophilic Monomers via Interfacial Polyaddition in the Inverse Miniemulsion Process*, Macromolecular Symposia, Wiley Online Library: 2013; pp 71-80.

54. Rosenbauer, E.-M.; Landfester, K.; Musyanovych, A., *Langmuir* **2009,** *25*, 12084-12091.

55. Baier, G.; Musyanovych, A.; Dass, M.; Theisinger, S.; Landfester, K., *Biomacromolecules* **2010,** *11*, 960-968.

56. Crank, J.; Park, G., *Diffusion in Polymer*. Academin Press: London, 1968.

57. Cohen, M. H.; Turnbull, D., *J. Chem. Phys.* **1959,** *31*, 1164.

58. Chow, T., *Macromol. Theory Simul.* **1995,** *4*, 397-404.

59. Vrentas, J. S.; Vrentas, C. M., *J. Polym. Sci., Part B: Polym. Phys.* **1992,** *30*, 1005-1011.

60. Vallet-Regí, M.; Balas, F.; Arcos, D., *Angew. Chem. Int. Ed.* **2007,** *46*, 7548-7558.

61. Argyo, C.; Weiss, V.; Bräuchle, C.; Bein, T., *Chem. Mater.* **2013,** *26*, 435-451.

62. Wakao, N.; Smith, J. M., *Chem. Eng. Sci.* **1962,** *17*, 825-834.

63. Crank, J., *The mathematics of diffusion*. Clarendon press Oxford: 1975; Vol. 2.

64. Rogers, C., Structural and chemical factors controlling the permeability of organic molecules through a polymer matrix. 1977.

65. Lewis, D.; Cowsar, D. In *Principles of controlled release pesticides*, ACS Symposium Series American Chemical Society, 1977.

66. Trojer, M. A.; Somasundaran, P., Encyclopedia of Surface and Colloid Science. Taylor & Francis: 2013.

67. Anderson, J. L.; Quinn, J. A., *Biophys. J.* **1974,** *14*, 130.

68. Trojer, M. A.; Nordstierna, L.; Nordin, M.; Nydén, M.; Holmberg, K., *Phys. Chem. Chem. Phys.* **2013,** *15*, 17727-17741.

69. Wang, S., *Microporous Mesoporous Mater.* **2009,** *117*, 1-9.

70. Zhou, Y.; Chu, J. S.; Wu, X. Y., *Eur. J. Pharm. Sci.* **2004,** *22*, 251-259.

71. Zhou, Y.; Wu, X. Y., *J. Control. Release* **2003,** *90*, 23-36.

72. Langevin, P., *Compt. Rend* **1908,** *146*, 530-533.

73. Ermak, D. L.; McCammon, J. A., *J. Chem. Phys.* **1978,** *69*, 1352-1360.

74. Verberg, R.; Alexeev, A.; Balazs, A. C., *J. Chem. Phys.* **2006,** *125*, 224712.

75. Aïnaoui, A.; Vergnaud, J., *Comput. Theor. Polym. Sci.* **2000,** *10*, 383-390.

76. Lopac, S. K.; Torres, M. P.; Wilson-Welder, J. H.; Wannemuehler, M. J.; Narasimhan, B., *J. Biomed. Mater. Res. B App.l Biomater.* **2009,** *91*, 938-947.

77. Chlon, C.; Guédon, C.; Verhaagen, B.; Shi, W. T.; Hall, C. S.; Lub, J.; Böhmer, M. R., *Biomacromolecules* **2009,** *10*, 1025-1031.

78. Sosnowski, S., *Polymer* **2001,** *42*, 637-643.

79. Izumikawa, S.; Yoshioka, S.; Aso, Y.; Takeda, Y., *J. Control. Release* **1991,** *15*, 133-140.

80. Dowding, P. J.; Atkin, R.; Vincent, B.; Bouillot, P., *Langmuir* **2004,** *20*, 11374-11379.

81. Gross-Heitfeld, C.; Linders, J. r.; Appel, R.; Selbach, F.; Mayer, C., *J. Phys. Chem. B* **2014,** *118*, 4932-4939.

82. Dowding, P. J.; Atkin, R.; Vincent, B.; Bouillot, P., *Langmuir* **2005,** *21*, 5278-5284.

83. He, F.; Mei, L.; Ju, X.-J.; Xie, R.; Wang, W.; Liu, Z.; Wu, F.; Chu, L.-Y., *J. Memb. Sci.* **2015,** *474*, 233-243.

84. Lodish, H. F.; Berk, A.; Zipursky, S. L.; Matsudaira, P.; Baltimore, D.; Darnell, J., *Molecular cell biology*. Citeseer: 2000; Vol. 4, p 271.

85. Kramer, P. J.; Boyer, J. S., *Water relations of plants and soils*. Academic press: 1995; p 71.

86. Rapatz, G.; Sullivan, J. J.; Luyet, B., *Cryobiology* **1968,** *5*, 18-25.

87. Boen, S. T., *Medicine* **1961,** *40*, 243-288.

88. Raoult-Wack, A., *Trends Food Sc.i Technol.* **1994,** *5*, 255-260.

89. Klaysom, C.; Cath, T. Y.; Depuydt, T.; Vankelecom, I. F., *Chem. Soc. Rev.* **2013,** *42*, 6959-6989.

90. Lensen, D.; Vriezema, D. M.; van Hest, J. C. M., *Macromol. Biosci.* **2008,** *8*, 991-1005.

91. Huckins, J. N.; Manuweera, G. K.; Petty, J. D.; Mackay, D.; Lebo, J. A., *Environ. Sci. Technol.* **1993,** *27*, 2489-2496.

92. Becker, A. L.; Johnston, A. P.; Caruso, F., *Small* **2010,** *6*.

93. Bysell, H.; Månsson, R.; Hansson, P.; Malmsten, M., *Adv. Drug Deliv. Rev.* **2011,** *63*, 1172-1185.

94. Choi, T. M.; Park, J.-G.; Kim, Y.-S.; Manoharan, V. N.; Kim, S.-H., *Chem. Mater.* **2015,** *27*, 1014-1020.

95. Zasadzinski, J. A.; Wong, B.; Forbes, N.; Braun, G.; Wu, G., *Curr. Opin. Colloid Interface Sci.* **2011,** *16*, 203-214.

96. Esser-Kahn, A. P.; Odom, S. A.; Sottos, N. R.; White, S. R.; Moore, J. S., *Macromolecules* **2011,** *44*, 5539-5553.

97. De Koker, S.; Hoogenboom, R.; De Geest, B. G., *Chem. Soc. Rev.* **2012,** *41*, 2867-2884.

98. Kim, J.-K.; Lee, E.; Lim, Y.-b.; Lee, M., *Angew .Chem., Int. Ed.* **2008,** *47*, 4662-4666.

99. Lv, L.-P.; Landfester, K.; Crespy, D., *Chem. Mater.* **2014,** *26*, 3351-3353.

100. Staff, R. H.; Gallei, M.; Mazurowski, M.; Rehahn, M.; Berger, R. d.; Landfester, K.; Crespy, D., *ACS nano* **2012,** *6*, 9042-9049.

101. Stuart, M. A. C.; Huck, W. T. S.; Genzer, J.; Muller, M.; Ober, C.; Stamm, M.; Sukhorukov, G. B.; Szleifer, I.; Tsukruk, V. V.; Urban, M.; Winnik, F.; Zauscher, S.; Luzinov, I.; Minko, S., *Nat. Mater.* **2010,** *9*, 101-113.

102. Ma, Y.; Dong, W.-F.; Hempenius, M. A.; Mohwald, H.; Julius Vancso, G., *Nat. Mater.* **2006,** *5*, 724-729.

103. Parshuram, G. S., Microencapsulation of Liquid Active Agents. In *Functional coatings: by polymer microencapsulation*, Ghosh, S. K., Ed. John Wiley & Sons: 2006; pp 153-186.

104. Gallagher, K. M.; Corrigan, O. I., *J. Control. Release* **2000,** *69*, 261-272.

105. Huang, X.; Brazel, C. S., *J. Control. Release* **2001,** *73*, 121-136.

106. Wang, C.-Y.; Ho, H.-O.; Lin, L.-H.; Lin, Y.-K.; Sheu, M.-T., *Int. J. Pharm.* **2005,** *297*, 89-97.

107. Lin, Y.-K.; Ho, H.-O., *J. Control. Release* **2003,** *89*, 57-69.

108. Schmidt, S.; Fernandes, P. A.; De Geest, B. G.; Delcea, M.; Skirtach, A. G.; Möhwald, H.; Fery, A., *Adv. Funct. Mater.* **2011,** *21*, 1411-1418.

109. Suzuki, S.; Asoh, T. A.; Kikuchi, A., *J. Biomed. Mater. Res., Part A* **2013,** *101*, 1345-1352.

110. Vinogradova, O. I.; Lebedeva, O. V.; Kim, B.-S., *Annu. Rev. Mater. Res.* **2006,** *36*, 143-178.

111. De Geest, B. G.; Déjugnat, C.; Sukhorukov, G. B.; Braeckmans, K.; De Smedt, S. C.; Demeester, J., *Adv. Mater.* **2005,** *17*, 2357-2361.

112. Gordon, V. D.; Chen, X.; Hutchinson, J. W.; Bausch, A. R.; Marquez, M.; Weitz, D. A., *J. Am. Chem. Soc.* **2004,** *126*, 14117-14122.

113. Shum, H. C.; Kim, J.-W.; Weitz, D. A., *J. Am. Chem. Soc.* **2008,** *130*, 9543-9549.

114. Takeuchi, J.; Ohkubo, A.; Yuasa, H., *Chem. Asian J.* **2015,** *10*, 586-594.

115. Lorenceau, E.; Utada, A. S.; Link, D. R.; Cristobal, G.; Joanicot, M.; Weitz, D. A., *Langmuir* **2005,** *21*, 9183-9186.

116. Martino, C.; Kim, S.-H.; Horsfall, L.; Abbaspourrad, A.; Rosser, S. J.; Cooper, J.; Weitz, D. A., *Angew .Chem., Int. Ed.* **2012,** *51*, 6416-6420.

117. Wang, J.; Wang, B. M.; Schwendeman, S. P., *J. Control. Release* **2002,** *82*, 289-307.

118. Wang, J.; Wang, B. M.; Schwendeman, S. P., *Biomaterials* **2004,** *25*, 1919-1927.

119. Chu, L.-Y.; Park, S.-H.; Yamaguchi, T.; Nakao, S.-i., *Langmuir* **2002,** *18*, 1856-1864.

120. Jiang, G.; Thanoo, B.; DeLuca, P. P., *Pharm. Dev. Technol.* **2002,** *7*, 391-399.

121. McFarland, B.; Pojman, J. A., *J. Appl. Polym. Sci.* **2015,** *132*.

122. Gross-Heitfeld, C.; Linders, J.; Appel, R.; Selbach, F.; Mayer, C., *J. Phys. Chem. B* **2014,** *118*, 4932-4939.

123. Yadav, S. K.; Khilar, K. C.; Suresh, A. K., *J. Memb. Sci.* **1997,** *125*, 213-218.

124. Kuethe, D. O.; Augenstein, D. C.; Gresser, J. D.; Wise, D. L., *J. Control. Release* **1992,** *18*, 159-164.

125. Peppas, N. A.; Narasimhan, B., *J. Control. Release* **2014,** *190*, 75-81.

126. Zehl, T.; Wahab, M.; Mogel, H.-J.; Schiller, P., *Langmuir* **2009,** *25*, 7313-7319.

127. Kim, S.-H.; Lee, T. Y.; Lee, S. S., *Small* **2014,** *10*, 1155-1162.

128. Torza, S.; Mason, S., *J. Colloid Interface Sci.* **1970,** *33*, 67-83.

129. Vincent, B., Emulsions. In *Colloid Science: Principles, Methods, and Applications*, 2 ed.; Cosgrove, T., Ed. Wiley-VCH: 2010; pp 117-133.

130. Pitzer, K. S., *J. Phys. Chem.* **1973,** *77*, 268-277.

131. Vinogradova, O. I.; Andrienko, D.; Lulevich, V. V.; Nordschild, S.; Sukhorukov, G. B., *Macromolecules* **2004,** *37*, 1113-1117.

132. Vimalanandan, A.; Lv, L.-P.; Tran, T. H.; Landfester, K.; Crespy, D.; Rohwerder, M., *Adv. Mater.* **2013,** *25*, 6980-6984.

133. Tran, T. H.; Vimalanandan, A.; Genchev, G.; Fickert, J.; Landfester, K.; Crespy, D.; Rohwerder, M., *Adv. Mater.* **2015,** *27*, 3825-3830.

134. Bacigalupo, A.; Boyd, A.; Slipper, J.; Curtis, J.; Clissold, S., *Expert Rev. Anti Infect. Ther.* **2012,** *10*, 1249-1264.

135. Bundgaard, H.; Mørk, N., *Int. J. Pharm.* **1990,** *63*, 213-218.

136. Landfester, K.; Mailänder, V., *Expert. Opin. Drug. Deliv.* **2013,** *10*, 593-609.

137. Crespy, D.; Landfester, K., *Beilstein J. Org. Chem.* **2010,** *6*, 1132-1148.

138. Zetterlund, P. B.; Thickett, S. C.; Perrier, S.; Bourgeat-Lami, E.; Lansalot, M., *Chem. Rev.* **2015,** *115*, 9745-9800.

139. Siegwart, D. J.; Srinivasan, A.; Bencherif, S. A.; Karunanidhi, A.; Oh, J. K.; Vaidya, S.; Jin, R.; Hollinger, J. O.; Matyjaszewski, K., *Biomacromolecules* **2009,** *10*, 2300-2309.

140. Utama, R. H.; Jiang, Y.; Zetterlund, P. B.; Stenzel, M. H., *Biomacromolecules* **2015,** *16*, 2144-2156.

141. Yow, H. N.; Wu, X.; Routh, A. F.; Guy, R. H., *Eur. J. Pharm. Biopharm.* **2009,** *72*, 62-68.

142. Page, C. C.; Moser, C. C.; Chen, X.; Dutton, P. L., *Nature* **1999,** *402*, 47-52.

143. Dröge, W., *Physiol. Rev.* **2002,** *82*, 47-95.

144. Coyle, J. T.; Puttfarcken, P., *Science* **1993,** *262*, 689-695.

145. Genestra, M., *Cell. Signal.* **2007,** *19*, 1807-1819.

146. Klaunig, J. E.; Kamendulis, L. M., *Annu. Rev. Pharmacol. Toxicol.* **2004,** *44*, 239-267.

147. Cheng, R.; Feng, F.; Meng, F.; Deng, C.; Feijen, J.; Zhong, Z., *J. Control. Release* **2011,** *152*, 2-12.

148. Zelikin, A. N.; Li, Q.; Caruso, F., *Chem. Mater.* **2008,** *20*, 2655-2661.

149. Sexton, A.; Whitney, P. G.; Chong, S.-F.; Zelikin, A. N.; Johnston, A. P. R.; De Rose, R.; Brooks, A. G.; Caruso, F.; Kent, S. J., *ACS Nano* **2009,** *3*, 3391-3400.

150. Sun, Y.; Yan, X.; Yuan, T.; Liang, J.; Fan, Y.; Gu, Z.; Zhang, X., *Biomaterials* **2010,** *31*, 7124-7131.

151. Lallana, E.; Tirelli, N., *Macromol. Chem. Phys.* **2013,** *214*, 143-158.

152. Liu, R.; Zhao, X.; Wu, T.; Feng, P., *J. Am. Chem. Soc.* **2008,** *130*, 14418-14419.

153. Wu, J.; Zhao, L.; Xu, X.; Bertrand, N.; Choi, W. I.; Yameen, B.; Shi, J.; Shah, V.; Mulvale, M.; MacLean, J. L., *Angew. Chem. Int. Ed. Engl.* **2015,** *127*, 9350-9355.

154. Nuhn, L.; Braun, L.; Overhoff, I.; Kelsch, A.; Schaeffel, D.; Koynov, K.; Zentel, R., *Macromol. Rapid. Commun.* **2014,** *35*, 2057-2064.

155. Yameen, B.; Vilos, C.; Choi, W. I.; Whyte, A.; Huang, J.; Pollit, L.; Farokhzad, O. C., *Chemistry* **2015,** *21*, 11325-11329.

156. Walid, H. A.; Calistor, N.; Seogjun, K.; Robert, J. D.; Jeff, W. F.; Charles, A. W., Development of Polyurea Nanocomposites with Improved Fire Retardancy. In *Fire and Polymers V*, American Chemical Society: 2009; Vol. 1013, pp 102-117.

157. Restani, R. B.; Morgado, P. I.; Ribeiro, M. P.; Correia, I. J.; Aguiar-Ricardo, A.; Bonifácio, V. D. B., *Angew. Chem. Int. Ed. Engl.* **2012,** *51*, 5162-5165.

158. Ibrahim, A. M.; Mahadevan, V.; Srinivasan, M., *Eur. Polym. J.* **1989,** *25*, 427-429.

159. Chattopadhyay, D. K.; Raju, K. V. S. N., *Prog. Polym. Sci.* **2007,** *32*, 352-418.

160. Han, H.; Li, S.; Zhu, X.; Jiang, X.; Kong, X. Z., *RSC Advances* **2014,** *4*, 33520-33529.

161. Delwbwcq, E.; Pascault, J. P.; Boutevin, B.; Ganachaud, F., *Chem. Rev.* **2013**, *113*, 80-118.

162. Castner, D. G.; Hinds, K.; Grainger, D. W., *Langmuir* **1996,** *12*, 5083-5086.

163. Sun, F.; Castner, D. G.; Mao, G.; Wang, W.; McKeown, P.; Grainger, D. W., *J. Am. Chem. Soc.* **1996,** *118*, 1856-1866.

164. Evans, S. D.; Goppert-Berarducci, K. E.; Urankar, E.; Gerenser, L. J.; Ulman, A.; Snyder, R. G., *Langmuir* **1991,** *7*, 2700-2709.

165. Laibinis, P. E.; Whitesides, G. M.; Allara, D. L.; Tao, Y. T.; Parikh, A. N.; Nuzzo, R. G., *J. Am. Chem. Soc.* **1991,** *113*, 7152-7167.

166. Krężel, A.; Latajka, R.; Bujacz, G. D.; Bal, W., *Inorg. Chem.* **2003,** *42*, 1994-2003.

167. Chu, L. Y.; Yamaguchi, T.; Nakao, S.-i., *Adv. Mater.* **2002,** *14*, 386-389.

168. Zhu, Y.; Shi, J.; Shen, W.; Dong, X.; Feng, J.; Ruan, M.; Li, Y., *Angew. Chem. Int. Ed.* **2005,** *117*, 5213-5217.

169. Gillies, E. R.; Fréchet, J. M. J., *Bioconjug. Chem.* **2005,** *16*, 361-368.

170. Angelatos, A. S.; Radt, B.; Caruso, F., *J. Phys. Chem. B* **2005,** *109*, 3071-3076.

171. Giri, S.; Trewyn, B. G.; Stellmaker, M. P.; Lin, V. S. Y., *Angew .Chem., Int. Ed.* **2005,** *44*, 5038-5044.

172. Such, G. K.; Tjipto, E.; Postma, A.; Johnston, A. P.; Caruso, F., *Nano Lett.* **2007,** *7*, 1706-1710.

173. Johnston, A. P. R.; Such, G. K.; Caruso, F., *Angew .Chem., Int. Ed.* **2010,** *49*, 2664-2666.

174. Bae, Y.; Fukushima, S.; Harada, A.; Kataoka, K., *Angew. Chem. Int. Ed.* **2003,** *42*, 4640-4643.

175. Alarcon, C. d. l. H.; Pennadam, S.; Alexander, C., *Chem. Soc. Rev.* **2005,** *34*, 276-285.

176. Hendrickson, G. R.; Smith, M. H.; South, A. B.; Lyon, L. A., *Adv. Funct. Mater.* **2010,** *20*, 1697-1712.

177. Kim, J.; Yoon, J.; Hayward, R. C., *Nat. Mater.* **2010,** *9*, 159-164.

178. Mura, S.; Nicolas, J.; Couvreur, P., *Nat. Mater.* **2013,** *12*, 991-1003.

179. Shchukin, D.; Möhwald, H., *Science* **2013,** *341*, 1458-1459.

180. Sagara, Y.; Kato, T., *Nat. Chem.* **2009,** *1*, 605-610.

181. Kota, A. K.; Kwon, G.; Choi, W.; Mabry, J. M.; Tuteja, A., *Nat. Commun.* **2012,** *3*, 1025.

182. Jain, R. K., *Nat. Med.* **2001,** *7*, 987-989.

183. Fitzgerald, J. B.; Schoeberl, B.; Nielsen, U. B.; Sorger, P. K., *Nat. Chem. Biol.* **2006,** *2*, 458-466.

184. Li, Z.; Hillmyer, M. A.; Lodge, T. P., *Nano Lett.* **2006,** *6*, 1245-1249.

185. Chambon, P.; Blanazs, A.; Battaglia, G.; Armes, S. P., *Macromolecules* **2012,** *45*, 5081-5090.

186. Mable, C. J.; Warren, N. J.; Thompson, K.; Mykhaylyk, O.; Armes, S. P., *Chem. Sci.* **2015,** *6*, 6179-6188.

187. Berger, S.; Zhang, H.; Pich, A., *Adv. Funct. Mater.* **2009,** *19*, 554-559.

188. Klaikherd, A.; Nagamani, C.; Thayumanavan, S., *J. Am. Chem. Soc.* **2009,** *131*, 4830-4838.

189. Motornov, M.; Roiter, Y.; Tokarev, I.; Minko, S., *Prog. Polym. Sc.i* **2010,** *35*, 174-211.

190. Stuart, M. A. C.; Huck, W. T. S.; Genzer, J.; Muller, M.; Ober, C.; Stamm, M.; Sukhorukov, G. B.; Szleifer, I.; Tsukruk, V. V.; Urban, M.; Winnik, F.; Zauscher, S.; Luzinov, I.; Minko, S., *Nat Mater* **2010,** *9*, 101-113.

191. Robb, M. J.; Connal, L. A.; Lee, B. F.; Lynd, N. A.; Hawker, C. J., *Polym. Chem.* **2012,** *3*, 1618-1628.

192. Gröschel, A. H.; Schacher, F. H.; Schmalz, H.; Borisov, O. V.; Zhulina, E. B.; Walther, A.; Müller, A. H. E., *Nat. Commun.* **2012,** *3*, 710.

193. Huang, X.; Voit, B., *Polym. Chem.* **2013,** *4*, 435-443.

194. Dong, J.; Wang, Y.; Zhang, J.; Zhan, X.; Zhu, S.; Yang, H.; Wang, G., *Soft Matter* **2013,** *9*, 370-373.

195. Staff, R. H.; Gallei, M.; Landfester, K.; Crespy, D., *Macromolecules* **2014,** *47*, 4876-4883.

196. Fleischmann, C.; Gopez, J.; Lundberg, P.; Ritter, H.; Killops, K. L.; Hawker, C. J.; Klinger, D., *Polym. Chem.* **2015,** *6*, 2029-2037.

197. Wu, G.; Chen, S.-C.; Liu, C.-L.; Wang, Y.-Z., *ACS nano* **2015,** *9*, 4649-4659.

198. Zhao, Y.; Lv, L.-P.; Jiang, S.; Landfester, K.; Crespy, D., *Polym. Chem.* **2015,** *6*, 4197-4205.

199. Shi, P.; Qu, Y.; Liu, C.; Khan, H.; Sun, P.; Zhang, W., *ACS Macro Lett.* **2015,** *5*, 88-93.

200. Landfester, K., *Adv. Mater.* **2001,** *13*, 765-768.

201. Staff, R. H.; Gallei, M.; Mazurowski, M.; Rehahn, M.; Berger, R.; Landfester, K.; Crespy, D., *ACS Nano* **2012,** *6*, 9042-9049.

202. Staff, R. H.; Schaeffel, D.; Turshatov, A.; Donadio, D.; Butt, H. J.; Landfester, K.; Koynov, K.; Crespy, D., *Small* **2013,** *9*, 3514-3522.

203. Dutta, A. K.; Kamada, K.; Ohta, K., *J. Photochem. Photobiol. A Chem.* **1996,** *93*, 57-64.

204. Jiang, J.; Tong, X.; Zhao, Y., *J. Am. Chem. Soc.* **2005,** *127*, 8290-8291.

205. D'Silva, C.; Afeworki, S.; Parri, O. L.; Baker, P. K.; Underhill, A. E., *J. Mater. Chem.* **1992,** *2*, 225-230.

206. Elbert, J.; Gallei, M.; Rüttiger, C.; Brunsen, A.; Didzoleit, H.; Stühn, B.; Rehahn, M., *Organometallics* **2013,** *32*, 5873-5878.

207. Elbert, J.; Krohm, F.; Rüttiger, C.; Kienle, S.; Didzoleit, H.; Balzer, B. N.; Hugel, T.; Stühn, B.; Gallei, M.; Brunsen, A., *Adv. Funct. Mater.* **2014,** *24*, 1591-1601.

208. Barbe, C.; Bartlett, J.; Kong, L.; Finnie, K.; Lin, H. Q.; Larkin, M.; Calleja, S.; Bush, A.; Calleja, G., *Adv. Mater.* **2004,** *16*, 1959-1966.

209. Clifford, N. W.; Iyer, K. S.; Raston, C. L., *J. Mater. Chem.* **2008,** *18*, 162-165.

210. Chen, Y.; Chen, H.; Zeng, D.; Tian, Y.; Chen, F.; Feng, J.; Shi, J., *ACS Nano* **2010,** *4*, 6001-6013.

211. Tarn, D.; Ashley, C. E.; Xue, M.; Carnes, E. C.; Zink, J. I.; Brinker, C. J., *Acc. Chem. Res.* **2013,** *46*, 792-801.

212. Maia, F.; Tedim, J.; Lisenkov, A. D.; Salak, A. N.; Zheludkevich, M. L.; Ferreira, M. G., *Nanoscale* **2012,** *4*, 1287-1298.

213. Fickert, J.; Schaeffel, D.; Koynov, K.; Landfester, K.; Crespy, D., *Colloid Polym. Sci.* **2014,** *292*, 251-255.

214. Xing, Z.; Wang, C.; Yan, J.; Zhang, L.; Li, L.; Zha, L., *Colloid Polym. Sci.* **2010,** *288*, 1723-1729.

215. Schlossbauer, A.; Warncke, S.; Gramlich, P. M.; Kecht, J.; Manetto, A.; Carell, T.; Bein, T., *Angew. Chem. Int. Ed.* **2010,** *49*, 4734-4737.

216. Lin, C.; Zhu, W.; Yang, H.; An, Q.; Tao, C. a.; Li, W.; Cui, J.; Li, Z.; Li, G., *Angew. Chem. Int. Ed.* **2011,** *123*, 5049-5053.

217. Li, G. L.; Zheng, Z.; Möhwald, H.; Shchukin, D. G., *ACS Nano* **2013,** *7*, 2470-2478.

218. Zelikin, A. N.; Quinn, J. F.; Caruso, F., *Biomacromolecules* **2006,** *7*, 27-30.

219. Chong, S.-F.; Sexton, A.; De Rose, R.; Kent, S. J.; Zelikin, A. N.; Caruso, F., *Biomaterials* **2009,** *30*, 5178-5186.

220. Abu, Y. M.; Aoki, K., *J. Electroanal. Chem.* **2005,** *583*, 133-139.

221. Rohwerder, M.; Michalik, A., *Electrochim. Acta* **2007,** *53*, 1300-1313.

222. Rohwerder, M.; Duc, L. M.; Michalik, A., *Electrochim. Acta* **2009,** *54*, 6075-6081.

223. Wan, X.; Wang, D.; Liu, S., *Langmuir* **2010,** *26*, 15574-15579.

224. Luo, Z.; Cai, K.; Hu, Y.; Zhao, L.; Liu, P.; Duan, L.; Yang, W., *Angew. Chem. Int. Ed.* **2011,** *50*, 640-643.

225. Luo, Z.; Ding, X.; Hu, Y.; Wu, S.; Xiang, Y.; Zeng, Y.; Zhang, B.; Yan, H.; Zhang, H.; Zhu, L.; Liu, J.; Li, J.; Cai, K.; Zhao, Y., *ACS Nano* **2013,** *7*, 10271-10284.

226. Nadrah, P.; Maver, U.; Jemec, A.; Tišler, T.; Bele, M.; Dražić, G.; Benčina, M.; Pintar, A.; Planinšek, O.; Gaberšček, M., *ACS. Appl. Mater. Interfaces* **2013,** *5*, 3908-3915.

227. Xiao, D.; Jia, H. Z.; Zhang, J.; Liu, C. W.; Zhuo, R. X.; Zhang, X. Z., *Small* **2014,** *10*, 591-598.

228. Brannon-Peppas, L.; Blanchette, J. O., *Adv. Drug Deliv. Rev.* **2012,** *64, Supplement*, 206-212.

229. Parshuram, G. S., In *Functional coatings: by polymer microencapsulation*

Ghosh, S. K., Ed. John Wiley & Sons: 2006; p 153.

230. Vallet-Regí, M.; Balas, F.; Arcos, D., *Angew. Chem. Int. Ed.* **2007,** *46*, 7548-7558.

231. Yang, P.; Gai, S.; Lin, J., *Chem. Soc. Rev.* **2012,** *41*, 3679-3698.

232. Qu, F.; Zhu, G.; Huang, S.; Li, S.; Sun, J.; Zhang, D.; Qiu, S., *Microporous Mesoporous Mater.* **2006,** *92*, 1-9.

233. Jia, L.; Shen, J.; Li, Z.; Zhang, D.; Zhang, Q.; Liu, G.; Zheng, D.; Tian, X., *Int. J. Pharm.* **2013,** *445*, 12-19.

234. Dmitrenko, O.; Thorpe, C.; Bach, R. D., *J. Org. Chem.* **2007,** *72*, 8298-8307.

235. Burns, J. A.; Butler, J. C.; Moran, J.; Whitesides, G. M., *J. Org. Chem.* **1991,** *56*, 2648-2650.

236. Montemor, M. F.; Cabral, A. M.; Zheludkevich, M. L.; Ferreira, M. G. S., *Surf. Coat. Technol.* **2006,** *200*, 2875-2885.

237. Guo, L.; Li, J.; Zhang, L.; Li, J.; Li, Y.; Yu, C.; Shi, J.; Ruan, M.; Feng, J., *J. Mater. Chem.* **2008,** *18*, 2733-2738.

238. Szajewski, R. P.; Whitesides, G. M., *J. Am. Chem. Soc.* **1980,** *102*, 2011-2026.

239. Gallei, M.; Klein, R.; Rehahn, M., *Macromolecules* **2010,** *43*, 1844-1854.

Abbreviation and Characters

Abbreviations

^{13}C NMR	carbon-13 nuclear magnetic resonance
^{1}H NMR	proton nuclear magnetic resonance
^{31}P-NMR	phosphorus-31 nuclear magnetic resonance
$CaCl_2$	calcium chloride
CaH_2	calcium hydride
CH_2Cl_2	dichloromethane
$CHCl_3$	chloroform
CTMA-Cl	cetyltrimethylammmonium chloride
D_2O	deuterium oxide
DLS	dynamic light scattering
DMAEMA	*N,N*-dimethylaminoethyl methacrylate
DMSO	dimethyl sulfoxide
DPE	1,1-diphenylethylene
Foscarnet	phosphonoformic acid trisodium salt hexahydrate
FT-IR	fourier transform infrared spectroscopy
H_2O_2	hydrogen peroxide
HCl	hydrochloric acid
HD	hexadecane
KCl	potassium chloride
KSCN	potassium thiocyanate
MBT	2-mercaptobenzothiazole
MMA	methyl methacrylate
NaCl	sodium chloride
NCO	cyanate
NCs	nanocapsule

NR	Nile red
o/w	oil-in-water
PDMAEMA	poly(2-dimethylaminoethyl methacrylate)
PEG dithiol	poly(ethylene glycol) dithiol
PU	polyurea
PVFc	poly(vinylferrocene)
SDS	sodium dodecyl sulfate
SEC	size exclusion chromatography
SEM	scanning electron microscopy
SiNCs	silica nanocapsules
TCEP	tris(2-carboxyethyl)phosphine hydrochloride
2,4-TDI	2,4-toluene diisocyanate
TEM	transmission electron microscopy
TEOS	tetraethoxysilane
TESPT	bis[3-(triethoxysilyl)propyl] tetrasulfide
THF	tetrahydrofuran
TMS	trimethylsilyl
VFc	vinylferrocene
w/o	water-in-oil
XPS	X-ray photoelectron spectroscopy

Characters and Symbols

$A_{i,j,k}$	interfacial area between the components *i*, *j*, or *k*
c	concentration
D_h	hydrodynamic diameter
E	energy
η	dynamic viscosity
G	Gibbs energy
$g(t)$	auto-correlation function
I	intensity
K_B	Boltzmann constant

m	mass
M_n	number-averaged molecular weight
M_w	weight-averaged molecular weight
Δp	Laplace pressure
Π	osmotic pressure
R_h	hydrodynamic radius
ρ	density
$s_{i,j,k}$	spreading coefficient of component *I, j,* or *k*
T	temperature
t	time
V	volume

Acknowledgements

Though hard to express all appreciation, I try to show my gratitude with the following few lines to people who ever helped me during my PhD study in the past three years.

Firstly, I am very grateful to Prof. Dr. Katharina Landfester for offering me the opportunity to study as a PhD candidate. From her, kind support and helpful discussions are always there.

My special thanks also go to my project leader Dr. Daniel Crespy for giving me freedom in my research, for valuable meetings and support during three years. Indeed, he helped me to become a better scientific researcher.

I would also like to give my appreciation to my cooperation partners: Dr. Markus Galle, Dr. Kristin Mohr, and Jochen Stadler for their kind help with the experiments and helpful discussion for the projects. It's really a pleasant experience working with them. I wish them all the best.

Many thanks will be also dedicated to my technician colleagues: Gunnar Glasser, Beate Müller, and Christine Rosenauer. They are always enthusiastic, warm-hearted and they really supported me with my research.

I would also like to give appreciation to my office mates: Dr. Staffan Lindberg, Elisabeth Rieger, and Beatriz Ma for proof-reading parts of this thesis.

Additionally and of course, I would thank all the members in the group of Prof. Landfester and my friends in MPI-P. They made my life in Mainz joyful and happy.

At last, I would like to give my special appreciation to my family for their unconditional love and support whenever and wherever I need.

Appendix

List of publications during PhD study

1. **S. Behzadi,** V. Serpooshan, R. Sakhtianchi, B. Müller, K. Landfester, D. Crespy, M. Mahmoudi. Protein Corona Change the Drug Release Profile of Nanocarriers: The "Overlooked" Factor at the Nanobio Interface. *Colloids Surf. B Biointerfaces* **2014**, *123*, 143-149

2. **S. Behzadi**, M. Gallei, J. Elbert, M. Appold, G. Glasser, K. Landfester. D. Crespy. Triblock Terpolymer *vs* Blends of Diblock Copolymers for Nanocapsules Addressed by Three Independent Stimuli. *Poly. Chem*. **2016**, Accepted.

3. **S. Behzadi**, C. Rosenauer, M. Kappl, K. Mohr, K Landfester, D. Crespy. Osmotic Pressure-Dependent Release Profiles of Payloads from Nanocontainers by Co-encapsulation of Simple Salts. *Nanoscale* **2016**, Underrevision.

4. **S. Behzadi**, M. Steinmann, D. Estupiñán, K. Landfester, D. Crespy. The Pro-active payload Strategy Significantly Increases Selective Release from Mesoporous Nanocapsules. Submitted.

5. **S. Behzadi**, J. Stadler, S. Hosseinpour, K. Landfester, D. Crespy. Controlled-release of Hydrophilic Payloads from Reduction-responsive Nanocapsules. In preparation

6. **S. Behzadi**, K. Landfester, M. J. W. Povey. D Crespy. Determination of the Shell Thickness of Polymer Nanocapsules by Ultrasound Spectroscopy. In preparation

List of publications before PhD study

1. **S. Behzadi**, et al. Determination of Nanoparticles Using UV-Vis Spectra. *Nanoscale* **2015**, *7*, 5134-5139

2**.** S. Laurent, AA. Saei, **S. Behzadi**, A. Panahifar, M. Mahmoudi. Superparamagnetic Iron Oxide Nanoparticles for Delivery of Therapeutic Agents: Opportunities and Challenges. *Expert Opin. Drug Deliv.* **2014**, *11*, 1449-1470

3. M. Mahmoudi, M. A. Shokrgozar, **S. Behzadi**. Slight Temperature Changes Affect Protein Affinity and Cellular Uptake/Toxicity of Nanoparticles. *Nanoscale* **2013**, *5*, 3240-3244

4. M. Mahmoudi, A. M. Abdelmonem, **S. Behzadi**, et al. Temperature: The "Ignored" Factor at the Nanobio Interface. *ACS Nano*, **2013**, *7*, 6555-6562

5. S. Sharifi, **S. Behzadi**, L. Forrest, P. Stroeve, S. Laurent, and M. Mahmoudi. Toxicity of Nanomaterials. *Chem. Soc. Rev.* **2012**, *41*, 2323-2343

6. **S. Behzadi**, M. Imani, M. Yousefi, P. Galinetto, A. Simchi, H. Amiri, P. Stroeve, M. Mahmoudi. Pyrolytic Carbon Coating for Biocompatibility of Titanium Oxide Nanoparticles: A Promising Candidate for Medical Applications. *Nanotecnology*, **2012**, *23*, 045102

Conferences

1. Oral presentation "Release of Payloads from Nanocontainers via Osmosis and Swelling" in the 29th conference of the European Colloid and Interface Society (**ECIS 2015**)

Curriculum Vitae

Personal information

Surname: Behzadi

Name: Shahed

Year of Birth: 1984

Place of Birth: Tehran, Iran

EDUCATION:

05/2013 – 05/2016 *PhD Candidate*, Max Planck Institute for Polymer Research, Mainz, Germany; 06/2013-06/2016

09/2009 – 01/2012 *Master***,** Materials Science and Engineering Dept., Sharif University of Technology; 2009-2012

09/2007 – 06/2012 *Bachelor***,** Materials Science and Engineering Dept., Sharif University of Technology; 2009-2012

POSITIONS:

01/2012 – 05/2013 Senior research assistant in laboratory of Nano-Bio Interactions, Pasture Institute of Iran

Fall Semester 2011-12 Teacher assistant, Microscopic Methods for Characterization of Nanoparticles, Nanotechnology Research Centre, Faculty of Pharmacy, Tehran University of Medical Sciences;

AWARDS AND HONORS:

Grant Award for M.Sc. thesis from Iran Nanotechnology Initiative Council; 2010